AMMONIA TOXICITY IN BACTERIA AND ITS IMPLICATIONS FOR TREATMENT OF AND RESOURCE RECOVERY FROM HIGHLY NITROGENOUS ORGANIC WASTES

By

AMANDA KAY LUTHER

A dissertation submitted to the Graduate School-New Brunswick

Rutgers, The State University of New Jersey

In partial fulfillment of the requirements for the degree of Doctor of Philosophy

Graduate Program in Environmental Science

Written under the direction of

Donna E. Fennell

And approved by

_____

_____

_____

_____

New Brunswick, NJ

October, 2015

ABSTRACT OF THE DISSERTATION

Ammonia toxicity in bacteria and its implications for treatment of and resource recovery from highly nitrogenous organic wastes

By AMANDA KAY LUTHER

Dissertation director:

Donna E. Fennell

Treatment of highly nitrogenous organic wastes (HNOWs) by anaerobic digestion (AD) results in the release of ammonia that can become inhibitory to methanogenesis as total ammonia nitrogen (TAN) concentration increases above 0.2 M (~3 g N L^{-1}). This inhibition reduces potential energy recovery (as biogas) from AD systems. Toxicity/inhibition has been attributed specifically to the un-ionized species of ammonia (NH_3), which increases with increasing pH and temperature. Protein degrading, amino acid fermenting bacteria play a key role in AD—liberating ammonia, and providing precursors (H_2, CO^2, and fatty acids) to downstream processes. The amino acid fermenting bacterium *Peptostreptococcus russellii* exhibits rapid growth on proteins, peptides, and amino acids, and can tolerate TAN concentrations up to 0.4 M at pH 8.5. Differential expression analysis of the *P. russellii* transcriptome comparing ammonia stressed (0.29 M NH_4^+, 74 mM NH_3) and sodium stressed (0.05 M sodium chloride) growth against unstressed growth, revealed a unique transcriptional response under ammonia stress, with 680

putative genes significantly, differentially, and uniquely expressed under ammonia stress. Specifically, exposure to high ammonia resulted in downregulation of major amino acid fermentation pathways, a shift in the energy conservation systems utilized by this bacterium, and the upregulation of a pathway for glycogen synthesis. Anaerobic digestion of HNOWs produces abundant ammonia that can be recovered as a resource. Electrochemical membrane electrolysis systems show promise for resource recovery from mixed wastewaters, permitting selective recovery of NH_4^+ as a high purity chemical. Here we demonstrated high rates of ammonia recovery from concentrated urine using an electrochemical cell (EC). EC processing of real urine sustained high flux of NH_4^+ at 275 ± 5 g N m^{-2} d^{-1} over ten days of operation, with a current efficiency of 55 ± 1% and an electrical cost of 13 kWh kg^{-1} N transferred.

Acknowledgements

I would like to first thank my mentor and advisor, Dr. Donna Fennell for her dedication and patience these past five years. Her careful guidance, support, and positive attitude made this experience both possible and enjoyable. Second I would like to thank Dr. Peter Strom, who served as a secondary advisor for much of my research. You are an excellent teacher, and I cannot thank you enough for welcoming me to Rutgers, and for your continued guidance throughout my studies. Thank you Lily and Korneel for critically reviewing my dissertation, and serving as committee members. Ms. Getson, "teacher", you were responsible for my education from grade 2 through 8, thanks for preparing me, I am so happy we have kept in touch. Thanks too to my supporters and friends at Ohio State University who encouraged me to go down this path, and believed in my capabilities.

Many people helped me find my way through challenges in the lab involving either technique, equipment, or data analysis, for this I would like to especially thank Val, Maria, Yun, Udi, Lee, Sunirat, Sarat, Laura, Weimin, Huajun, and Joachim. To the whole LabMET team in Gent, thanks for guiding me through the labs and your city, and thanks for the many Chimays. Dr. Rabaey, thank you for taking a chance on me and inviting me to Belgium to work in your lab, it changed my life. Joachim, my mentor in Gent, thanks for explaining the EC stuff so well, and for guiding me through the project and the manuscript.

Sunirat, thanks for the company and support, we found our way through this tunnel (sewer?) to this light at the end, together, and I am happy to have had a good friend in the lab. Sarah and Allyson, thanks for the good times, good debates, good hikes, and good meals; for introducing me to broiling, and to the delicious yet simple dish of green beans and black beans. Ed, you were there for me through some of the toughest parts of this degree, and I am grateful for your support. Thanks to my cats Peaches (RIP) and Pele, for being so cute and funny, and for keeping me warm at night. To Gio, also cute, funny, and warm, thanks for believing in me, and for helping me through the writing.

Finally, to my loving and supportive family, I thank you all. Mom and Dad thanks for your trust, love, and support throughout my life, and through this Ph.D. I owe you some time and attention. To my stepmoms, Connie and Robin, I appreciate your kindness and support too. Ryan, brother, thanks for your tough love and critical eye, most of my "coolness" I got from you, and I am grateful. To my little sibs Danny and Tayja, thanks for coming to my defense, it made me so happy to see you (and the rest of the family) in that audience. Ted, Linda, Lydia, and Tom (and kids), thanks for making your homes my home, and for all your support as well these past five years. It's been wonderful to be so close. Grandma and Grandpa, I am grateful for all your love and support always, and especially throughout this Ph.D. I love you, and must I loved living so close to you in these years. My visits with you in Cheshire were always so comfortable, and so calming. I will miss those weekends in your home dearly.

I am very grateful for the financial support I received from Rutgers first through a teaching assistantship in the Division of Life Sciences, and later through an NSF funded renewable fuels related Integrative Graduate Education and Research Traineeship (Fuels IGERT). The latter also provided the support to study abroad at the University of Gent as a visiting Ph.D researcher. This research was funded by a grant from the New Jersey Water Resource Research Institute and a grant from the New Jersey Agricultural Extension Station.

Table of Contents

List of Tables

List of Illustrations

Chapter 1: Introduction

1.1 Rationale

Release of reactive nitrogen species (e.g., ammonia, nitrate, nitrite, nitrous oxide, and NOx) into the environment can have negative consequences on ecosystems and human health. Sources of nitrogen pollution include direct losses from agricultural fertilizer application, treatment and handling operations of highly nitrogenous organic wastes (HNOWs), fossil fuel production and combustion, and industrial activities (Galloway *et al.*, 2010). HNOWs include various animal manures, food wastes, industrial food processing wastes, some wastewater treatment sludges, effluents from anaerobic digesters, landfill leachates, and source separated (human) urine. In addition to nitrogen, these wastes have high biochemical oxygen demand (BOD), which also imposes treatment requirements. Anaerobic digestion (AD) is often applied primarily to reduce the volume and BOD of these wastes. In this process, nitrogen is released mainly as ammonia. This ammonia accumulates in the effluent such that further treatment is then necessary to remove, transform, or recover the nitrogen.

AD is attractive due to its relatively low cost and potential for energy recovery but the accumulated ammonia nitrogen is inhibitory to the basic process, and can lead to complete failure of these systems (for extensive reviews see McCarty and McKinney, 1961; Kugelman and McCarty, 1965; Rajagopal et al., 2013; Yenigün and Demirel, 2013). For this reason, AD application to HNOWs as single feedstocks is limited. Addition of low nitrogen organic wastes for co-digestion is commonly

employed to alleviate toxicity and recover biogas. While this toxicity has been extensively documented, we have very little evidence of the genetic response to ammonia toxicity in microorganisms. Improving our understanding of the microbial behavior and response to ammonia in these environments is an essential step towards developing and improving AD technology.

In addition to understanding fundamental responses of microorganisms to ammonia, additional technologies are necessary to remove or recover the ammonia that is released during AD of HNOWs. Established technologies include nitrification/denitrification, anammox, stripping, and struvite precipitation (for reviews see Doyle and Parsons, 2002; Schmidt et al., 2003; Maurer et al., 2006). An emerging topic of research is focusing on developing membrane electrolysis systems (MES) for selective recovery of nutrients (such as ammonia) from complex waste streams. These can be bioelectrochemical systems (BESs) or strictly electrochemical systems (ESs). To date, various BESs have been investigated for nitrogen recovery from urine (Kuntke et al., 2012; Kuntke et al., 2014), while both BES and ES have been investigated for treating waste effluents (such as AD effluent) containing high levels of ammonia (Kuntke *et al.*, 2011; Desloover *et al.*, 2012, 2015; Gildemyn *et al.*, 2015). No studies have been reported investigating the effectiveness of an ES for treating source-separated urine.

Human urine contains high levels of nitrogen and accounts for approximately 75% (v/v) of the nitrogen in municipal wastewaters, yet only 1% of the wastewater volume. Human urine is an ideal concentrated waste stream for nitrogen and

phosphorus recovery. Source separation of this material with removal and recovery of the nitrogen closer to the source could greatly reduce the nitrogen load (and thus treatment costs) on WWTPs, and provide additional revenue through the recovery of ammonia and hydrogen through the application of an EC system.

1.2 Goal and Objectives

The overall goal of this work is to improve methods for treatment of HNOWs by 1, investigating the specific effect of ammonia on fermentative bacteria active in anaerobic digestion, and 2, assessing an electrochemical system for direct ammonia recovery from urine.

The specific objectives were to:

1. Outline the effect of ammonia release from hydrolysis and fermentation of a model protein to test the sensitivity of fermentative populations in a batch digestion system;
2. Develop a metabolic model for amino acid fermentation in *Peptostreptococcus russellii*, an ammonia tolerant bacterium with a high growth rate on peptides;
3. Understand the specific genetic response of *P. russellii* that allows its growth at high concentrations of free and ionized ammonia; and
4. Test the performance of an electrochemical system for ammonia recovery from undiluted human urine under different operational parameters.

1.3 Organization of the Dissertation

Chapter 1 states the rationale and goals of this work. Chapter 2 summarizes the literature relevant to ammonia inhibition in AD and toxicity to specific microorganisms and nitrogen recovery systems. Chapter 3 describes research to assess ammonia inhibition to fermentative populations during batch digestion of a model protein, and describes possible thermodynamic limitations imposed by excess ammonia. Chapters 4 and 5 present the protein fermenting bacterium *Peptostreptococcus russellii* as a model organism to study the physiological mechanism behind ammonia tolerance by describing *P. russellii*'s metabolism (Chapter 4) and analyzing the full transcriptional response of this bacterium under ammonia stressed growth (Chapter 5). Transcriptional analysis provides evidence to support or refute current models of ammonia toxicity for the organism, and may lead to the discovery of novel genes involved specifically in an ammonia stress response. Identification of these genes could provide means for monitoring ammonia stressed systems. Chapter 6 examines the feasibility and efficiency of ammonia extraction and recovery from undiluted human urine using a strictly electrochemically driven membrane electrolysis cell coupled to ammonia stripping and absorption. Performance of this ES is compared against previous studies of this system applied to anaerobic digestate, and also compared against the performance of the BESs studied to date that have been applied to urine.

Chapter 2: Literature Review

2.1 Nitrogen in the environment

2.1.1 Nitrogen cycling

The greatest available reservoir of nitrogen on this planet is the nitrogen gas (N_2) that is 78% (by volume) of the atmosphere. This elemental form is highly stable and unavailable to most life. Aside from a small contribution from abiotic processes, nitrogen gas is made bioavailable only through the activity of a limited number of species of bacteria and archaea (for a recent review see, Vitousek et al., 1997). These microbes transform N_2 to a more reactive form, ammonia (NH_3), through the process of biological nitrogen fixation (BNR). For this reason, nitrogen is a limiting nutrient in many environments. Once fixed, this ammonia is incorporated into organic compounds by a number of bacteria, archaea and plants, and can be oxidized to nitrite (NO_2^-) and nitrate (NO_3^{2-}), forms often preferred by many plants. These two forms can be reduced back to nitrogen gas through denitrification, also forming gaseous byproducts nitrous oxide (N_2O) and nitric oxide (NO). Abiotic processes, including the combustion of fossil fuels, can also oxidize nitrogen gas to N_2O, NO and nitrogen dioxide (NO_2). Thus, once fixed as ammonia a number of transformations can take place to distribute the various forms nitrogen across the land, water and air (Figure 2.1).

In the past century, the introduction of anthropogenic nitrogen fixation via the Haber-Bosch process (described in section 2.5.1) has now more than doubled the rate of nitrogen fixation, contributing to a net increase in the amount of reactive

nitrogen in the environment (Vitousek *et al.*, 1997; Galloway *et al.*, 2008; Gruber and Galloway, 2008), as illustrated in Figure 2.1. An estimated 121 Tg N yr^{-1} are produced globally through the Haber-Bosch process, with approximately 80% going towards fertilizer production and 20% towards other industrial processes (Galloway *et al.*, 2008). The fertilizer is applied to agricultural lands where the nitrogen is transferred through the food chain to crops, livestock and humans, with losses at each step along the way (Figure 2.2). This nitrogen is further redistributed across continents through global trade of fertilizer, crops, and animal products. The losses along the food chain are substantial, with the greatest losses seen during application of the fertilizer, and through the digestive track of livestock (Braun et al. 2007). In the first case, fertilizer applied but not taken up by the plants is lost immediately to the environment. The nitrogen loss through livestock production may be partially recovered (mainly from manure), but treatment and handling of the manure present opportunities for reentry to the environment. Most manures can be considered as HNOWs, thus improved recovery of ammonia from manure could reduce losses substantially. While recovery from human waste (as urine) appears a minor fraction of the total losses, its treatment is a necessary effort that can have substantial implications on human health and the environment.

2.1.2 Nitrogen as a pollutant

Different forms of reactive nitrogen can pose different risks to the environment and human health. Eutrophication occurs when otherwise limiting nutrients (e.g., nitrogen and phosphorus) are discharged to aquatic ecosystems (for a review see

Carpenter et al., 1998). This results in rapid biological growth with depletion of oxygen, which can lead to fish kills and disruption of aquatic ecosystems. Excess nitrogen discharge to terrestrial ecosystems can be disruptive by disturbing soil pH (Erisman *et al.*, 2013), which in turn effects soil ecosystems and plants. Accumulation of nitrate and nitrite in drinking water poses a direct risk to human health, especially to infants, because they are more susceptible to methemoglobinemia (Shibata *et al.*, 2014). Nitrogen released as ammonia into an aerobic environment will quickly be oxidized to nitrate (NO_3^{2-}) and nitrite (NO_2^-). Both NH_3 and NO_2^- are highly toxic to many aquatic organisms. For all these reasons, release of nitrogen from point sources is often strictly regulated in the US, and many countries around the world. Wastewater treatment plants (WWTPs) must often incorporate advanced treatment systems for nitrogen removal in their processing systems to meet strict National (and state) Pollution Discharge Elimination System and Total Maximum Daily Load limits for nitrogen and phosphorus (US EPA, 2010). Agricultural operations must also meet discharge requirements and these directly affect waste management options (US EPA, 2003).

2.2 Generation of HNOWs

2.2.1 Sources of nitrogen pollution

The work described in this dissertation will focus on HNOWs derived from agriculture; including animal manures, food waste, and source separated human urine. Typical nitrogen content for these HNOWs is given in Table 2.1. Loss of nitrogen can occur during generation, handling, and treatment of these different

HNOWs. Nitrogen flow through a typical industrial swine production system (Braun et al., 2007) is presented in Figure 2.2, and can result in 80% of nitrogen lost, despite direct manure recycling. Just in the application of the fertilizer, 24- 70% may be lost directly to the environment, depending on the crop and form of fertilizer (Galloway *et al.*, 2010). The fraction of nitrogen excreted varies by animal and will depend on the animal's life stage, and this loss, mainly manure, represents a significant proportion of HNOWs. Nitrogen from manure produced in animal feeding operations in the US alone is estimated to be 6×10^6 metric tons yr^{-1} (Mueller and Gronberg).

Crops and animal products designated for human food contribute to food waste generation. Food waste generation in the US alone is estimated at 31 million tons (US short tons) annually (US EPA, 2012). Here, food waste has the lowest recovery of all waste materials, and represents the largest fraction (21.1%) of total materials discarded in landfills (US EPA, 2012). In landfills, the nitrogen is released as ammonia and concentrated in the liquid that collects in the bottom of the landfill (leachate) (Reinhart and Townsend, 1998). This liquid can be considered an HNOW, with total ammonia nitrogen in excess of 1 g L^{-1} and decreasing carbon content as the leachate ages within the landfill (Pohland and Harper, 1985). Food waste itself has sufficient carbon content to be considered amenable to anaerobic digestion, but performance is limited often by ammonia inhibition (Zhang *et al.*, 2007, 2012; Banks *et al.*, 2011). Many recent studies are showing co-digestion to be a very promising solution for AD of food waste (Murto *et al.*, 2004; Gray *et al.*, 2008; Zhang *et al.*,

2011). This would be a viable option for treating certain HNOWs, depending mainly on the cost and availability of co-substrates.

2.2.2 Wastewater treatment pipeline in the US

The fraction of nitrogen consumed through plant and animal products by humans is largely excreted, mostly in urine. Human waste in the US is collected and transported through sewers by dilution with potable water. While this dilution eliminates any issues with ammonia toxicity to the biological treatment processes downstream, it limits the potential for resource recovery from this waste stream, making it more expensive to recover this nitrogen. Human urine contains high levels of nitrogen and accounts for approximately 75% of the nitrogen in municipal wastewaters yet only 1% of the volume (Larsen and Gujer, 1996). Wastewater treatment plants are designed to remove biochemical oxygen demand (BOD), pathogens and sometimes nutrients from wastewater. After removal of BOD during secondary wastewater treatment, much of the nitrogen remains in the effluent, but some of it is concentrated in the sludge, which is commonly treated by anaerobic digestion (AD). Although the concentrations at this stage are typically not high enough to impose any toxicity on the AD process here, the ammonia that is released to the effluent in this process must be recycled back through treatment, and can represent 20-40% of the plant's total nitrogen load (Locke and Laquidara, 2006; Stinson, 2006). The nitrogen is often treated through nitrification/denitrification (if required by permit), a biological process that releases the nitrogen as nitrogen gas

to the atmosphere. This recycles the nitrogen "over the atmosphere" (much of it initially fixed through the Haber-Bosch process) back to the environment.

2.3 Anaerobic digestion and limitations for treating HNOW

Anaerobic digestion refers to the engineered process designed to optimize the anaerobic decomposition of organic matter for treatment of, and recovery of energy from, organic wastes. Volume reduction and BOD removal is accomplished through the mineralization of organic compounds to methane, carbon dioxide, and hydrogen gas. Compared with other treatment methods, AD has the advantages of being relatively low cost (no aeration is necessary) and producing usable energy (methane). The process can be optimized so that a wastewater treatment facility could fully cover their energy costs and in some cases produce energy above their needs from this source (Gray *et al.*, 2008).

AD applied to HNOWs is problematic. First, as the C:N ratio of the digester feedstock decreases, the maximum potential methane production per kg of biomass decreases (Babson *et al.*, 2013). Second, the nitrogen is released as ammonia, which can accumulate to high concentrations (Babson *et al.*, 2013) that become toxic to various microbial populations within the reactor. This leads to reduced total biogas production, reactor upset, or complete failure of the digester (further detailed below). Third, the ammonia is not removed or treated in the process, and together with phosphorus accumulates in the effluent necessitating further treatment. In effect, anaerobic digestion serves to extract these nutrients from the organics, and concentrate them in the liquid phase.

2.3.1 Overview of process microbiology

AD is driven by a synergistic process to maximize energy capture within a complex microbial community. Anaerobic digestion can be divided into three sequential stages: hydrolysis, acidogenesis, and methanogenesis, as outlined in Figure 2.3. Complex polymers (e.g., proteins) are hydrolyzed to respective monomers (e.g., amino acids) then converted to short chain fatty acids (e.g., acetate, propionate, and butyrate), CO_2, and hydrogen through fermentation reactions. Acetate and hydrogen serve as the major precursors to methanogenesis. Acidogenesis (production of short-chain fatty acids) must be carefully balanced with methanogenesis because the accumulation of these acids can be inhibitory to microorganisms, depress pH, and lead to process failure.

The microbial dynamics in AD are highly complex, and the specific biochemical processes carried out by fermenting populations can shift according to the consumption rates of hydrogen and acetate (Worm *et al.*, 2011). For example many fermentations provide very little energy, or may not even provide enough energy to sustain growth under standard conditions. In the latter case, they can become thermodynamically favorable only if very low concentrations of end products (e.g., hydrogen) are maintained in the reactor. Thus hydrogen-consuming reactions help drive these fermentations. This interdependence has been termed interspecies hydrogen transfer and has been well documented (Stams, 1994; Worm *et al.*, 2011). For example, an important process that appears to play an important role in adaptation in ammonia-stressed AD is that of the syntrophic acetate oxidizing

bacteria (SAOB), which are dependent on consumption of hydrogen by syntrophic partners (e.g., hydrogenotrophic methanogens) in order to grow (Zinder and Koch, 1984; Schnürer *et al.*, 1994).

Under typical anaerobic digestion conditions, acetate is the major intermediate of AD with 2/3 of the methane produced from acetate, while the remaining 1/3 comes from hydrogenotrophic methanogenesis (Worm *et al.*, 2011). Relative to the fermenters, acetoclastic methanogens grow slowly with doubling times in the range 0.5-12 d (Jetten *et al.*, 1992). In contrast, syntrophic enrichments of SAOB with hydrogenotrophic methanogens have even slower growth rates, with doubling times up to 28 d (Schnürer *et al.*, 1994), although co-cultures have been reported with doubling times of 30-40 h (Zinder and Koch, 1984).

2.3.2 Effect of ammonia toxicity on the AD process

Ammonia toxicity in anaerobic digestion has been well studied and a number of reviews have been written on the subject (Chen *et al.*, 2008; Rajagopal *et al.*, 2013; Yenigün and Demirel, 2013). These reviews stress that ammonia toxicity is mainly caused by free ammonia (NH_3), the distribution of which is dependent on temperature, pH, total ammonia nitrogen (i.e., ammonia plus ammonium) concentrations, and ionic strength. Acclimation of the reactor communities can alleviate the inhibition. For these reasons, there is a wide range of reported inhibitory ammonia thresholds from various reactor and enrichment studies, summarized in Table 2.2. NH_3 is difficult to measure *in situ*, and therefore must be calculated. These calculations typically do not take into account the ionic strength

and the effect of total solids, which may lead to an overestimation of NH_3 concentration (Hafner and Bisogni Jr., 2009). Acclimation to incremental increases in ammonia over time have been most successful in developing robust methanogenic communities, but still result in an inhibited (lower methane yield) steady state operation (Angelidaki and Ahring, 1993; Hansen *et al.*, 1998; Schnürer and Nordberg, 2008). Two extensive studies from the 1960s looking at salt toxicity in anaerobic digestion (McCarty and McKinney, 1961; Kugelman and McCarty, 1965) compared the singular and combined effects of calcium, potassium, magnesium, sodium and ammonium salts on methane production. In these experiments ammonium salts had the most severe effect on growth; and the inhibition displayed a different pattern than that caused by the other salts. This finding suggested that the toxicity of ammonia is somehow unique, likely due to its dissociation to NH_3.

On the community level, methane inhibition in reactors that have acclimated to high ammonia concentrations induces a shift in the dominant methanogenic species. Schnürer and Nordberg (2008) have studied the relationship between hydrogenotrophic methanogens and syntrophic acetate oxidizing bacteria (SAOB) extensively and suggest that free ammonia acts as a selective agent for this pair by inhibiting the more sensitive aceticlastic methanogens, thus allowing the slower growing hydrogenotrophic methanogens to dominate, which in turn promotes the growth of SAOB. They further showed that this shift was observed specifically under stress from ammonia as opposed to sodium, potassium, or propionic acid stress, demonstrating a specific toxicity effect from ammonia on aceticlastic methanogens.

This higher sensitivity of aceticlastic methanogens to ammonia was also demonstrated by Angelidaki and Ahring (1993); however, they showed the sensitivity of both groups of methanogens such that 6 g TAN L^{-1} induced a 74% drop in specific activity of aceticlastic enrichments and a 52% drop in hydrogenotrophic enrichments. Furthermore, they observed a differential pattern of inhibition of the two groups with exposure to increasing ammonia (sigmoidal in acetoclastic, linear in hydrogenotrophic) suggesting there were two mechanisms of inhibition occurring; that is acetoclastic methanogens may be inhibited by both forms of ammonia, while hydrogenotrophic methanogens are sensitive to only one form.

The hydrolysis and fermentation stages of AD are typically considered non-limiting under ammonia stress (Hansen *et al.*, 1998) suggesting these populations have a higher tolerance for ammonia. Little attention has been paid to population dynamics within the fermenting communities under ammonia stress. In general, bacteria have been shown generally to have a high ammonium tolerance (Müller et al., 2006). Some bacteria appear also to have a high tolerance for free ammonia, as demonstrated by the isolation of a number of *Bacillus spp*. that can withstand >0.8M TAN (0.3 M FAN) at elevated pH. Ammonia inhibition thresholds described for pure cultures of bacteria are listed in Table 2.3.

2.4 Mechanics of ammonia toxicity

2.4.1 Ammonia chemistry

Ammonia is commonly used as a general term referring to both free ammonia (NH_3) and ionized ammonium (NH_4^+). As a weak acid, NH_4^+ dissociates into hydrogen ions

(H^+) and NH_3 to reach an equilibrium that is dependent on pH and temperature (Eq. 2.1). Likewise, NH_3 is a weak base and will consume protons to reach this equilibrium.

$$NH_4^+ \leftrightharpoons NH_{3(g)} + H^+ \quad \text{Eq. 2.1}$$

At 25°C, in dilute aqueous solution, the acid dissociation constant (K_a) of ammonium is 5.01×10^{-10} (pKa = 9.3) indicating that the molar concentration of the two species will be equal at pH = 9.3. This means that in neutral to acidic solutions NH_4^+ is predominant and NH_3 concentrations will remain at or below 1% of TAN, while at alkaline pH (>9.3) NH_3 is predominant. An increase in temperature will shift the equilibrium towards NH_3, while a decrease in temperature will shift the equilibrium towards NH_4^+. The term total ammonia nitrogen (TAN) refers specifically to the mass or concentration of nitrogen from both combined species. Free ammonia nitrogen (FAN) is used specifically to refer to the nitrogen present from free ammonia only, represented as NH_3-N.

As a gas, NH_3 will also partition to the gas phase. In dilute, aqueous solution, this equilibrium is governed by Henry's law according to the following equation:

$$K_H = \frac{pNH_{3(g)}}{[NH_3]_{(aq)}} = 1.5 \times 10^{-5} atm\, m^3\, mol^{-1} \quad \text{Eq. 2.2}$$

The K_H value shown in Eq. 2.2 was taken from a compilation of measured values (Sander, 1999) and applies at standard pressure (1 atm) and temperature (25 °C). K_H is the Henry's coefficient, which reflects the solubility of a gas in dilute aqueous

solution relative to its partial pressure (pNH_3) in the gas phase. The low K_H value for ammonia reflects its high solubility in water. Solubility is also affected by the ionic strength of the solution, such that solubility of ammonia decreases with increasing ionic strength.

2.4.2 Observed toxicity in plants, animals, and bacteria

Ammonia toxicity is likely a general phenomenon affecting all biological cells to varying degrees (Martinelle and Häggström, 1993; Britto and Kronzucker, 2002; Müller *et al.*, 2006). Plants are known to have a relatively low tolerance for increasing levels of NH_4^+ in soils where toxicity can occur above 10 mM TAN (Britto and Kronzucker, 2002). The mechanism of toxicity induces displacement of essential cations (mainly potassium) and likely places high energy demands on the cell for active efflux of NH_4^+ to maintain homeostasis (for review see Britto and Kronzucker 2002). In one study an overall increase in NH_4^+ flux (both inward and outward) between root cells and external media was observed in both ammonia sensitive and ammonia tolerant plant species exposed to increasing external TAN. Rates of efflux were much higher in the sensitive species, corresponded to a higher proportion of incoming ammonium, and corresponded to higher respiration rates yet lower growth (Britto *et al.*, 2001).

Ammonia toxicity in animal cells has also been proposed to act by increasing the energy burden on the cell. A decrease in viability during ammonia exposure was linked to inward transport of NH_4^+ via a sodium/potassium/chloride co-transporter (Martinelle *et al.*, 1996) followed by passive outward diffusion of NH_3. This cycling

of ammonia across the membrane leads to a decrease in pH inside the cell, which could lead to even greater energy burden to reestablish a physiological pH gradient. (Martinelle and Häggström, 1993). This futile cycling of ammonia across the cell membrane whereby inward active transport of ammonium is followed by passive outward transport of NH_3, can thus lower the internal pH and waste energy.

Experiments with *Corynebacterium glutamicum* (Müller *et al.*, 2006) revealed no evidence for such a futile cycle in bacteria. In this study *C. glutamicum* and other bacteria including *Escherichia coli* and *Bacillus subtilis* were shown to tolerate NH_4^+ in the range of 1 to 2 M. Here the authors concluded that the decrease in growth with increasing ammonium concentrations was likely due to an increase in ionic strength or osmolarity of the medium, rather than any specific ammonium toxicity (Müller *et al.*, 2006). The conclusion from this study was that unlike in animal and plant cells, which have a relatively low tolerance for NH_4^+, bacteria have a relatively high resistance to NH_4^+ that is likely a general phenomenon in bacteria.

2.4.3 Models of ammonia toxicity in bacteria and archaea

The speciation of ammonia into ionized and unionized species presents two possible routes of toxicity. NH_4^+ alone might act in the same manner as other salts studied; inducing a hyper osmotic stress effect at very high external salt concentrations (Csonka, 1989). This could be the dominant mechanism in neutral to acidic environments where NH_3 concentrations are low. Additionally, NH_4^+ was proposed to have a specific inhibitory effect on methanogens by way of interfering with Mg^{2+}

and Ca^{2+} binding to specific methanogenic proteins on the outer membrane of the cells of *Methanospirillum hungatei* (Sprott and Patel, 1986).

The typical response to hyperosmotic shock has been understood through extensive studies in *E. coli* (for review see Csonka, 1989). Briefly, as the concentration of a non-permeable solute (e.g., ammonium, sodium) increases or decreases outside the cell, osmotic pressure will drive water out of or into the cell, respectively. Cells must maintain osmotic homeostasis in order to maintain internal turgor pressures necessary for cell growth. In response to high osmolarity outside, cells maintain homeostasis temporarily by pumping in potassium ions via a potassium/proton symporter. Potassium ions accumulate internally to offset the difference in osmotic potential across the cell membrane. Cells eventually import or produce osmolytes to replace potassium. Osmolytes can include glycine betaine, carnitine, choline, or proline (Sleator and Hill, 2002).

As a small uncharged molecule, NH_3 can permeate the lipid bilayer that forms the cell membrane (for a review see, Kleiner, 1981). Under conditions where free ammonia concentrations are high (e.g., high TAN, high pH) influx of NH_3 consumes protons inside the cell, leading to an increase in the internal pH. To reestablish pH homeostasis, a potassium/proton antiporter can import protons with concurrent export of potassium ions (Figure 2.4). This model is supported by experiments with pure cultures of methanogens where cells were exposed briefly to high NH_3-N concentration (Sprott *et al.*, 1984). In some methanogens they observed an influx of free ammonia coinciding with a rapid efflux of potassium (K^+) ions. Depletion of

cytosolic potassium up to 98% was observed in some methanogens (*Methanospirillum hungatei*, *Methanosarcina barkeri*) as well as two bacteria (*Escherichia coli*, *Bacillus polymyxa*) but not at all in other methanogens (*Methanobacter thermoautotrophicum*, *Methanobacter bryantii*). In *M. hungatei* exposure to high external TAN at alkaline pH caused a steady decrease in the proton motive force (pmf) as K^+ was depleted (Sprott *et al*., 1984). Furthermore, external K^+ concentration influences the exchange, since the addition of KCl to the growth medium to intracellular concentrations reduced the K^+ efflux effect, and prevented influx of ammonia (up to 79% less than observed under low K^+). The reasoning for this is that without inward flux of protons, ammonia exchange slows due to increasing pH of the cytoplasm from equilibration of NH_3. Interestingly, Na^+ exposure also induced a substantial efflux of K^+ in some methanogens (*M. hungatei*, *M. barkeri*, *Methanobacterium formicicum*) leading to accumulation of sodium within the cell in an apparent direct exchange of the cations.

Studies documenting the genetic response underlying ammonia tolerance or stress response are sparse. Two studies by de Macario and Macario (reviewed in de Macario and Macario, 2003) showed that ammonia toxicity induced a dose dependent expression of *hsp70* (*dnaK*) and *trkA* in both *Methanosarcina mazeii* and *Methanosarcina thermophile*. In these archaea, the *trkA* gene, encoding a protein involved in regulation of the TrkH K^+/H^+ symporter, is co-located with the heat shock genes *grpE*, *dnaK*, and *dnaJ*. In *M. mazeii* expression of the heat shock genes was observed under 30, 60, and 180 minutes of exposure to 2 or 6 g TAN L^{-1}, but *trkA* expression was only observed at the higher TAN dose (Hofman-Bang *et al.*,

1999). The expression of *trkA* under increasing ammonia concentrations links the TrkH type K^+/H^+ transporter to ammonia shock in methanogens, and by extension this transporter might be responsible for the potassium efflux observed in so many other methanogens. One suggested outcome of the study was that additional information on the genetic response to ammonia toxicity is needed to eventually lead to identification of specific biomarker genes that would enable better monitoring of bioreactor populations under ammonia stress.

2.5 Emerging technologies for nitrogen treatment or recovery

2.5.1 Current technologies

Additional treatment is necessary to remove or recover soluble forms of nitrogen from HNOW streams. The current technologies applied at large scale include nitrification/denitrification, direct stripping of the ammonia, and precipitation of ammonia together with magnesium and phosphate as struvite (Verstraete and Philips, 1998; Doyle and Parsons, 2002; Maurer *et al.*, 2006; Ferraz *et al.*, 2013). The most common method utilized at wastewater treatment facilities in the US is nitrification/denitrification, which is relatively inexpensive compared to other methods (Maurer *et al.*, 2006). Nitrogen recovery for resale must compete with the primary current technology for ammonia production from raw materials, which is the Haber-Bosch process. One way of assessing nitrogen removal/recovery technologies is to compare their energetic costs relative to ammonia production via the Haber-Bosch process (Table 2.4). The Haber-Bosch process utilizes natural gas or oil directly, but the cost is represented as electricity for sake of comparing these

technologies with other systems. It is important to note that the energy source utilized for any technology will have additional costs to consider. For example, if electricity is required, the primary energy input will be greater due to inefficiencies in converting that primary source to electricity. This is not considered in the costs presented here. Additional considerations should be made for external costs associated with a particular primary energy source, such as carbon emissions, that are not reflected in the energetic costs. During the Haber-Bosch process, hydrogen derived from oil or natural gas is combined with nitrogen to produce ammonia (Eq 2.3) at an approximate energy cost of 28 to 40 GJ tonne^{-1} (primary energy).

$$N_2 + 3H_2 \longrightarrow 2NH_3 \qquad \text{Eq. 2.3}$$

The energy of the reaction is -92 kJ mol^{-1} (-46 kJ mol^{-1} NH_3). Most of the energy use (39.3 GJ tonne^{-1}) is supplied by natural gas or oil. When comparing energy requirements for different technologies, the source of power (electric, oil, gas, etc.) will have an effect on the cost.

2.5.2 Emerging technologies for recovery of nutrients from source separated human excreted waste streams

Source separation of human wastes consisting of yellow water (urine) and black water (feces), could be a critical system component for reducing the need to treat/recover nitrogen in wastewater. The nitrogen in urine accounts for approximately 75% of the total nitrogen load to a typical wastewater treatment plant, yet constitutes only 1% of the total liquid volume. Separating the urine and

minimizing the dilution (e.g., through waterless or low dilution toilets) would produce a waste stream with concentrations of ammonia between 4 and 8 g L^{-1}. At a typical US WWTP, a portion of this nitrogen is incorporated into the biomass produced during secondary biological treatment (e.g., activated sludge). Waste secondary treatment biomass may be treated by AD for mass/volume reduction and energy recovery. Leachate from the digested sludge is generally recycled back to the front of the treatment facility, in some cases accounting for 30% of the total nitrogen load on the plant (Stinson, 2006), where it would then be converted to nitrogen gas through biological nitrification-denitrification. In underdeveloped countries where wastewater treatment is unregulated or unavailable, or, in developed countries during storm events and facility overload, these wastes may end up in the environment with little or no treatment, posing negative consequences to both human health and environment. In places where no central treatment facilities exist, small scale decentralized solutions may be more readily deployed.

Bioelectrochemical systems (BESs) have gained attention in recent years for their potential application in wastewater treatment (Pham *et al.*, 2006; Logan and Rabaey, 2012). BESs couple the oxidation or reduction of organics by microbial processes to an electrochemical cell whereby biomass either transfers electrons to the anode (bioanode type reactor), or biomass at the cathode accepts electrons from the cathode (biocathode type reactor). A BES can be operated as a microbial fuel cell (MFC) that produces a current or as a microbial electrochemical cell MEC that requires minimal electrical power input; the latter enables water reduction at the cathode to produce hydroxyl ions and hydrogen gas (Logan and Rabaey, 2012). In

both systems, the current production is driven by microbial oxidation of organic carbon. This electron transfer creates a current that can drive the translocation of ions from anode to cathode across an ion permeable membrane. Ammonia can be removed from the cathode and recovered as ammonium sulfate through incorporation of a stripping/absorption column. In the case of the MEC and EC, hydroxyl production at the cathode can serve to produce the base necessary to efficiently strip NH_3 from this stream, while also producing hydrogen gas, a high value fuel.

BESs for ammonia recovery has been demonstrated in wastewater effluents (Clauwaert *et al.*, 2008; Mook *et al.*, 2012) and source separated urine (Kuntke et al., 2012,2014). A strictly electrochemical cell was demonstrated to recover ammonia from anaerobic digestate in situ while also reducing ammonia toxicity on the digester process (Desloover *et al.*, 2012, 2015).

2.6 Chapter 2 tables

Table 2.1 Nitrogen content representative of some highly nitrogenous organic wastes

Waste	**C:N ratio (w:w)**	**% N (dry weight)**	**Reference**
Municipal food waste	14-16	2-3	NRAES, 1992
Sewage sludge	5-16	2-7	NRAES, 1992
Swine manure	9-19	2-4	NRAES, 1992
Cattle manure	11-30	2-4	NRAES, 1992
Laying hen manure	3-10	4-10	NRAES, 1992
Mixed slaughterhouse	2-4	7-10	NRAES, 1992
Urine (no dilution)	0.5	Not available	Udert et al., 2006

Table 2.2 Examples of ammonia nitrogen inhibition threshold levels in anaerobic digesters and enrichment cultures

Description	TAN, (mM) (FAN, mM) limit	[a]Reactor configuration	pH	Temp. °C	Definition of inhibition threshold	Reference
Swine manure digestion	300 (79)	CSTR	8	55	50% decrease in apparent specific activity	Hansen et al., 1998
Mixed cultures in standard medium fed acetate	600 (5.7-7.4)	Semi continuous flow through reactor,	7.0-7.2	30-35	50% reduction in biogas production	de Baere et al., 1984
Synthetic wastewater feed, different seed materials tested	430 (57)	4.5L UASB	8.1	35	Up to this conc., 78-90% COD removal	Calli et al., 2005
Enrichment cultures from cattle manure	430 (n.r.)	Batch culture	7.2-7.3	55	Methane yield reduced aceticlastic enrichment by 73%, hydrogenotrophic by 53%	Angelidaki and Ahring, 1993
Acetic acid in media, NH_4Cl added to bring up ammonia in enrichment cultures	357-429 (9-11)	Enrichment transfers, batch	7.3	37	Induced a shift from aceticlastic dominant to hydrogenotrophic dominant methanogenesis	Schnürer and Nordberg, 2008
Organic fraction municipal waste, egg albumin as N source	393-493 (n.r.)	4.5L, semi continuous	8		Gas yield reduced by half, shift from aceticlastic to hydrogenotrophic	
Potato juice	130-140 (5.7)	4.5 L, CSTR, Granulated sludge	7.6-7.8	30	Failure of methanogenesis	Koster, 1986
Acetate feed, NH_4Cl and NH_4Ac salts tested on	214 (11)	¾ L digesters	7.9	35	Complete inhibition of	McCarty and McKinney, 1961

enrichment cultures	methanogenesis

[a]*CSTR, Completely mixed stirred tank reactor; UASB, upflow anaerobic sludge blanket*
n.r, not reported

Table 2.3 Ammonia inhibition in pure cultures of bacteria and archaea

Description	Species	TAN, (mM) (FAN, mM) limit	pH	Temp. °C	Definition of inhibition threshold	Reference
EHG Medium, mixed carbon source	*Bacillus* spp.	982 (50)	8 or 9	37	Minimum inhibitory FAN	Leejeerajumnean et al., 2000
	Bacillus spp.	858 (300)				
	Bacillus spp.	>1432 (500)				
TAN added as ammonium sulfate, minimal media (mops, urea carbon sources)	*Corynebacterium glutamicum*	2000 (n.r)	7	30	3h lag phase, decreased growth	Müller et al., 2006
TAN added as ammonium sulfate, glucose carbon source	*Escherichia coli* MG1655	750	n.r	37	Growth rate decreased by ~1/2	
TAN added as ammonium sulfate, peptone carbon source	*Bacillus subtilis* 168	750	7.5	30	Growth rate decreased by ~1/2	

n.r., not reported

Table 2.4 Comparison of energy costs of technologies available for nitrogen treatment or recovery

Technology	**Energy cost[a] (kWh kg^{-1} N)**	**Final product**
Nitrification/denitrification[b]	4	N_2
Struvite precipitation for quantitative nitrogen recovery[c]	23	Struvite ($MgNH_3PO_4$-$6H_2O$),
Stripping[d]	9	Ammonium sulfate
Haber-Bosch[e]	10[b]	Ammonia (NH_3)

[a]*source* (Maurer *et al.*, 2003)
[b]*includes electrical costs (aeration), WWTP = wastewater treatment plant*
[c]*includes chemical costs (magnesium oxide and phosphoric acid)*
[d]*includes chemical costs (calcium oxide and sulfuric acid) and electrical costs (aeration)*
[e]*energy derived from natural gas, converted to kWh units*

2.7 Chapter 2 figures

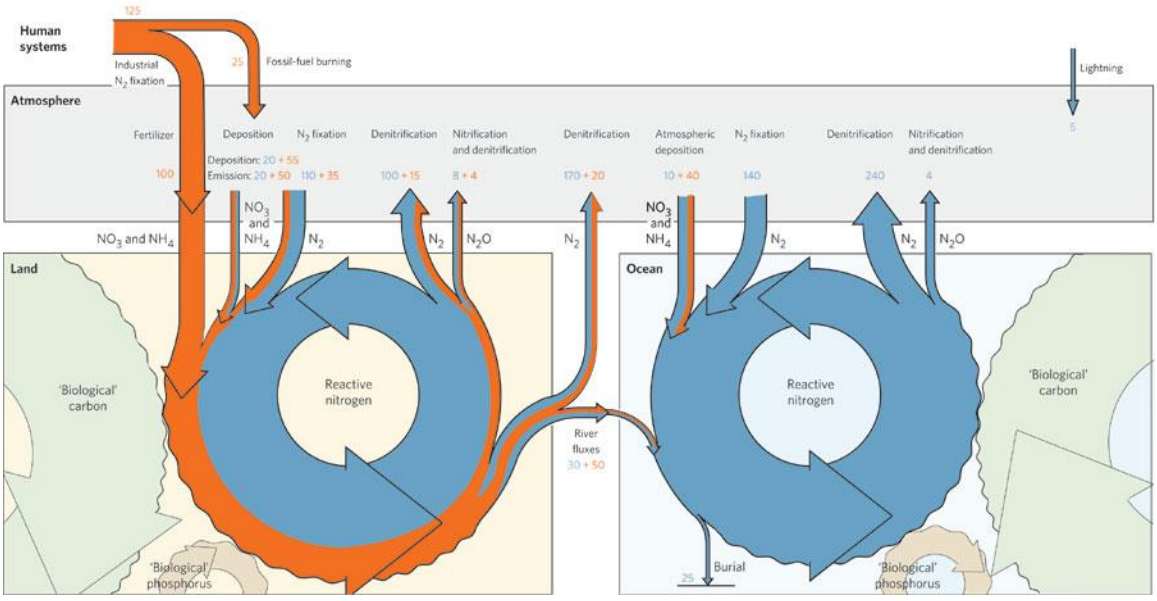

Figure 2.1 Nitrogen cycling in the environment. Taken from Gruber and Galloway, 2008. Blue fluxes denote natural transformations, orange depicts anthropogenic contributions. Values are in Tg N per year based on 1990s values, and have uncertainties from 20 to 50%.

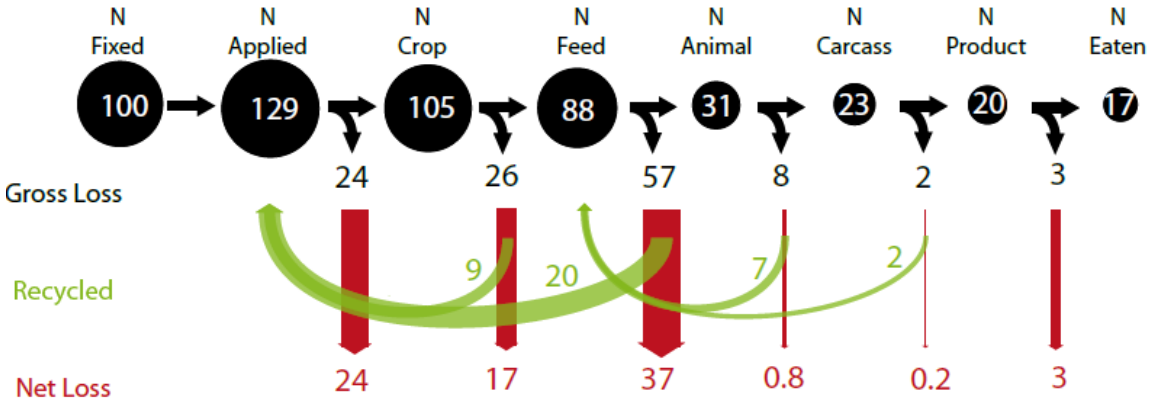

Figure 2.2 Nitrogen losses through a typical industrial swine production system where numbers shown are percentages. Taken from Braun et al., 2007.

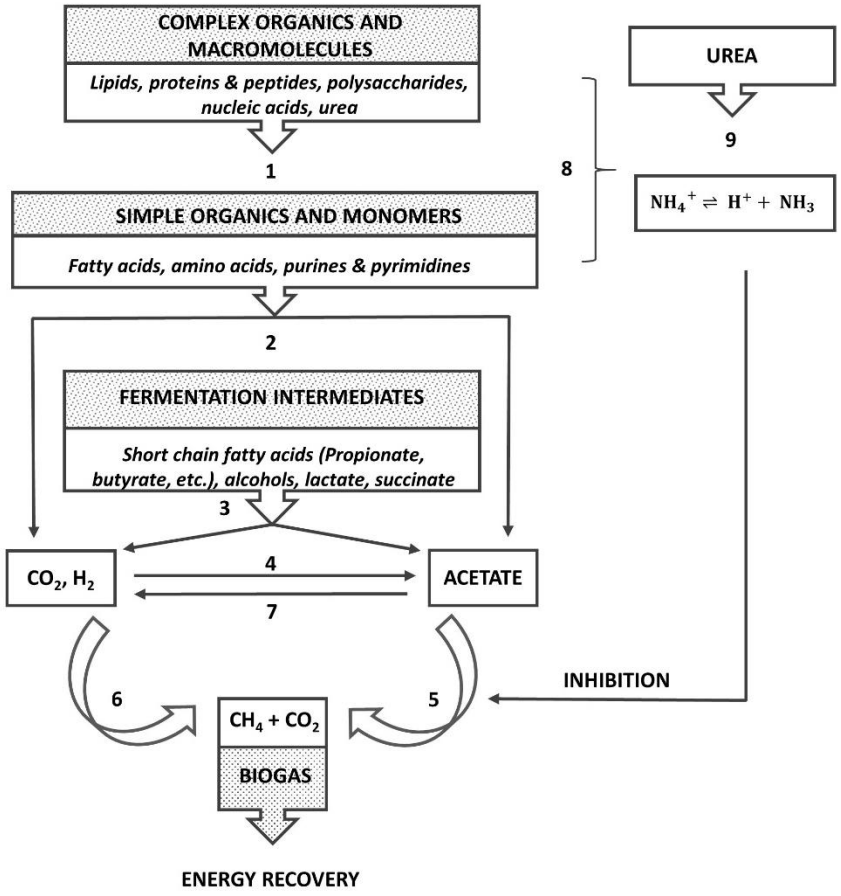

Figure 2.3 Anaerobic digestion process. Hydrolytic bacteria and primary fermenters, 1; primary fermenters, 2; secondary fermenters, 3; acetogenic bacteria, 4; acetoclastic methanogens, 5; hydrogenotrophic methanogens, 6; syntrophic acetate oxidizing bacteria, 7. Ammonia is released through fermentation of amino acids and nucleic acids, 8; and ureolytic bacteria, 9. Modified from Worm et al. (Worm *et al.*, 2011)

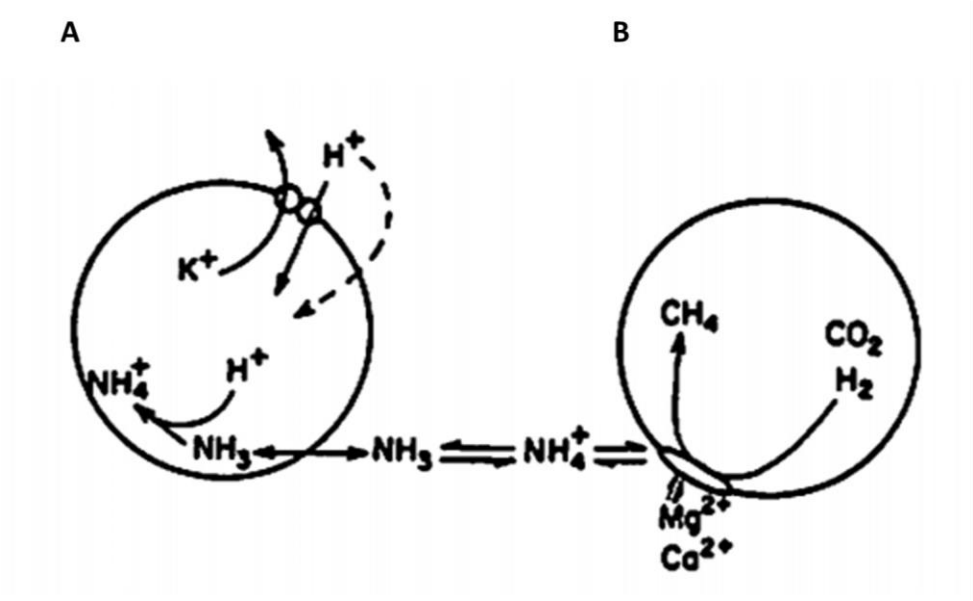

Figure 2.4 Proposed mechanisms of ammonia toxicity in methanogens through free ammonia (NH_3) toxicity (A), or NH_4^+ (B). Taken from Sprott and Patel, 1986.

Chapter 3: Model digestion of a protein substrate

3.1 Introduction

Protein and urea are the major sources of nitrogen in organic wastes (Larsen and Gujer, 1996; Nahm, 2003; Abouelenien *et al.*, 2010). Hydrolysis of urea occurs almost immediately during the collection and transport of urine through the activity of ubiquitous ureolytic bacteria (Udert *et al.*, 2003) and results in the release of ammonia (NH_3) and carbonic acid (H_2CO_3). Wastewaters from the dairy industry vary widely in BOD (500-5000 mg BOD L^{-1}), but protein can account for up to 60% of the BOD content (Demirel *et al.*, 2005). Protein must first be hydrolyzed before the individual amino acids can be used for carbon and energy by fermentative organisms, which releases ammonia. It is the fermentation rather than the hydrolysis step that releases ammonia. The inhibitory effect of both free and ionized ammonia on methane production in AD has been well documented (for reviews see Rajagopal et al., 2013; Yenigün and Demirel, 2013), and it is generally understood that there is little or no inhibitory effect on the (previously occurring) fermentation reactions, suggesting these populations already have a high tolerance for ammonia.

In a recent study Oh and Martin (2014) used a theoretical electrochemical model approach to investigate thermodynamic limitations from increasing ammonium concentration and pH on a consortium of syntrophic ammonia oxidizing bacteria (AOB) and methanogens. They concluded that carbonate concentration was driving thermodynamics in this system. An increase in carbonate speciation at high pH was

inhibitory to aceticlastic methanogens, while consumption of carbonate by AOB limited the hydrogenotrophic methanogens.

In this study we examined the rate of ammonia release and the effect of final ammonia concentration on methane and volatile fatty acid production by a mixed culture methanogenic biomass fermenting casein. To investigate whether ammonia accumulation could be thermodynamically limiting, we examined Gibb's free energies for select amino acid fermentation reactions at different prevailing reactor ammonium and volatile fatty acids concentrations.

3.2 Materials and Methods

3.2.1 Experimental and reactor design

Anaerobic digestion of the milk protein, casein, was performed in 160 mL serum bottle reactors (Wheaton, Millville) containing 100 mL liquid volume, sealed with 0.5 in chlorobutyl stoppers and aluminum crimp caps. Three live treatments were established in triplicate in which casein was provided as the sole substrate at 10, 30, or 60 g L^{-1}, respectively. Three different control treatments were also established in triplicate: a killed control provided 10 g casein L^{-1} and autoclaved (3 min, 121 °C) three times over three days; a live inoculum control, provided no casein substrate; and a live buffered control provided 10 g casein L^{-1}, and amended with 30 mM sodium bicarbonate. Reactors were established under a nitrogen atmosphere (100% high purity grade), or in the case of the buffered control a 30% CO_2/70% N_2 (v/v) atmosphere. The inoculum (10% v/v) was effluent digestate from an active anaerobic digester treating wastewater solids obtained from the Joint Meeting of

Essex and Union Counties Edward P. Decher Secondary Wastewater Treatment Facility located in Elizabeth, NJ, USA. Reactors were incubated at 30 °C and the following parameters were monitored over 58 days: biogas volume and methane content; fatty acid concentration, including formic, acetic, propionic, iso-butyric, butyric, iso-valeric, valeric, iso-caproic, caproic, and heptanoic acids; total ammonia nitrogen (TAN) and pH. A seventh treatment was set up after these experiments were carried out, referred to as the "no inoculum control". In this treatment 10 g L^{-1} casein was added to the medium as substrate, inoculum was omitted, and triplicate reactors were autoclaved three times over three days.

3.2.2 Medium preparation

Anaerobic minimal medium (Zinder, 1998) was prepared according to Table 3.1, except that sodium bicarbonate was omitted in all but the buffer control. Casein (Acros Organics, now Thermo Fisher Scientific, Waltham, MA, USA, 92% purity) was the primary carbon and energy source. The amino acid composition of casein (MP Biomedicals, Santa Ana CA, USA, technical data sheet for CAS # 9000-71-9) is shown in Table 3.2.

3.2.3 Biogas and methane

The volume of biogas produced from the digesters was measured by water displacement through a burette every 1-2 days. The methane content of the biogas was determined using headspace analysis of a 0.25 mL sample of the biogas at atmospheric pressure. The biogas sample was obtained from bottle headspaces

using a gastight Pressure-Lok® precision analytical syringe (VICI Precision Sampling, Inc., Baton Rouge). The biogas sample was analyzed using an Agilent 6890N gas chromatograph (GC) equipped with a flame ionization detector (Agilent Technologies, Santa Clara, CA, USA) and a GS GasPro column (Agilent Technologies, Santa Clara, CA, USA). Helium was used as the carrier gas at a constant pressure of 131 kPa (19 psi); oven temperature was held at 150°C. Methane content (%) was determined by comparing integrated chromatographic peak areas from the samples to an eight-point standard (9.5 to 95 % methane) curve obtained by diluting and analyzing 0.25 mL aliquots of a 95% methane standard (Matheson Tri-Gas, Basking Ridge, NJ, USA). Biogas and methane production for all reactors with casein addition are reported on a per gram casein basis normalized for substrate loading by dividing the volume measurements for the 40 and 60 g L^{-1} reactors by four and six, respectively, since the reactor volume was 0.1 L.

3.2.4 Chemical analyses

Liquid samples (1.5 mL) for both total ammonia nitrogen (TAN) and volatile fatty acids (VFAs) determinations were removed from the reactors using a sterile plastic 3 mL syringe with an 18 gauge sterile needle that had been flushed with sterile N_2. The slurry sample was adjusted to pH < 3 by addition of 10 N sulfuric acid, then centrifuged for 5 minutes at 13000 rotations per minute (rpm) (14000 x g) by a 5424 series desktop centrifuge (Eppendorf, Hamburg, Germany). The supernatant was transferred to a clean 1.5 mL microcentrifuge tube and stored for up to 30 d at

4 °C , according to standard method 4500-NH3 (Clesceri *et al.*, 1998) for ammonium samples.

TAN concentrations were determined using a Dionex ICS 1000 ion chromatograph equipped with a Dionex IonPac™ CS12A column and CSRS™300 4 mm suppressor (all Thermo Scientific, Waltham, MA). A solution of 20 mN methanosulfonic acid was used as the mobile phase, and samples were quantified against standard concentrations (0.325 to 100 mg TAN L^{-1}) of NH_4Cl. TAN accumulation and production rates are also reported on a per gram casein basis for all treatments where casein was added.

Free ammonia (NH_3-N) concentrations were calculated from TAN and pH measurements for each time point using Eq. 3.1.

$$NH_3\text{-}N = TAN \times \frac{10^{pH}}{\left(\frac{Kb}{Kw}\right)\times 10^{pH}} \qquad \text{Eq. 3.1}$$

where K_b is the base dissociation constant for ammonia, 1.82×10^{-5} at 30 °C (Bates and Pinching, 1950) and K_w is the water dissociation constant, 1.46×10^{-14} [5] at 30 °C (Marshall and Franck, 1981).

VFA concentrations were determined using a Beckman Coulter® System Gold™ HPLC (Beckman-Coulter, Inc., Fullerton, CA) equipped with an Aminex HPX-87H column (Bio-Rad Laboratories, Hercules, CA). A 5 mM solution of H_2SO_4 was used as the mobile phase, and samples were quantified against a volatile acid standard mix (Supelco Analytical, Bellefonte, PA, cat#46975U) over a concentration range of 62.5

mg L^{-1} to 1000 mg L^{-1}. Total VFAs were reported in units of "mg as acetate L^{-1}" by summing the molar concentrations of all fatty acids detected, then converting to a mass concentration on an as acetate basis. VFA accumulation and production rates are also reported as per gram casein fed for all treatments where casein is added.

The pH was determined directly from 1.5 mL reactor liquid slurry samples using a Symphony calomel glass micro combination pH electrode (VWR International, Radnor, PA) which was calibrated against standard solutions of pH 4.0 and 7.0 (Oaklon, Vernon Hills, CA) at 25 °C.

3.2.5 Gibbs free energy calculations

Gibb's free energies for fermentation reactions listed in Table 3.5 were calculated according to Eq. 3.2.

$$\Delta G°_r = \sum n\Delta G°_f(products) - \sum n\Delta G°_f(reactants) \quad \text{Eq. 3.2}$$

where $\Delta G°_r$ is the standard Gibb's free energy for the reaction, $\Delta G°_f$ is the free energy of formation for specific chemical species, and n is the molar coefficient for the product or reactant species. Corrections for temperature and physiological concentration (as obtained from experimental results) were made using Eq. 3.3

$$\Delta G = \Delta G° + RT ln\, Q \quad \text{Eq. 3.3}$$

where R is the ideal gas constant (8.314 J mol^{-1} K^{-1}) and T is the absolute temperature (°K). Q was determined using Eq. 3.4.

$$Q = \frac{[A]^a[B]^b}{[C]^c[D]^d} \quad \text{Eq. 3.4}$$

where A and B correspond to the molar concentration of reactants, and C and D to the molar concentration of products, each raised to their respective molar coefficient (a, b, c, d). All calculations were performed for 30 °C.

3.2.6 Statistical methods

One-way ANOVA was performed on acetate concentrations and TAN concentrations for each reactor at day 11 to determine if there were any significant differences in these data sets. There were nine total treatment conditions, set up in triplicate for a total of 27 data points. A Tukeys highly significant difference test was then performed to test if there were significant differences between pairs of treatments.

3.3 Results and Discussion

3.3.1 Biogas production during casein digestion

The biogas production rate and methane content from different experimental treatments is shown in Figure 3.1. Total biogas production, which is the sum of methane, carbon dioxide, and hydrogen, peaked at day 4 in all live bottles (Figure 3.1A). The methane content was below 20 % in all treatments for the first 10 days of the experiment (Figure 3.1B). Methane production rates for the buffered and non-buffered reactors were 0.3 and 0.2 mL d^{-1} from day 8 to 11, and methane was just reaching 10% of the biogas mixture. Methane production in the 40 and 60 g L^{-1} casein loading during the first 11 days were 10 fold lower and constituted < 1% of

the biogas. Peak biogas production rates for the buffered and non-buffered reactors were 19 and 20 mL d^{-1} from day 3 to 4, with methane accounting for < 1% of the biogas mixture. Peak biogas production rates for the buffered and non-buffered reactors were 19 and 20 mL d^{-1} from day 0 to 3. Peak biogas production rates for the buffered and non-buffered reactors were 11 and 17 mL d^{-1} from day 3 to 4. Methane was < 1% of the biogas mixture for all reactor treatments over the first 4 days. The biogas produced under the higher casein loadings through day 11 likely contained (mostly) CO_2 and (some) H_2, since these are the expected major gaseous products of fermentation; however, these constituents were not measured. By day 5, corresponding closely with peak biogas production, TAN had accumulated to 1.2 ± 0, 3 ± 0.2, and 4.8 ± 0 g L^{-1} in the 10, 40 and 60 g L^{-1} casein treatments, respectively (Figure 3.2B). Methane production in the buffered and non-buffered reactors began after day 11, reaching 3 and 2 mL d^{-1} (or 179 and 151 mL cumulatively) in each, respectively, by day 58. Methane production in the higher casein loadings began to increase, reaching 0.3 and 0.5 mL d^{-1} (or 6 and 9 mL cumulatively) for the 40 and 60 g L^{-1} casein treatments by day 58, respectively. Cumulative methane production for each treatment is shown in Figure 3.2C. No methane was detected in the killed control throughout the entirety of the run. No biogas production was observed in the no inoculum control (results not shown) over 41 days of incubation.

3.3.2 Inhibition of ammonia production from fermentation of amino acids

To determine if ammonia was inhibitory to fermentation in these reactors, we compared the accumulation of TAN and total VFAs on a per gram casein loaded

basis. At the two higher casein loadings (40 and 60 g L^{-1}), TAN and VFA production rates over the first 11 days and final accumulations were lower than that of the buffered and non-buffered low loading rate (10 g L^{-1}) reactors (Figure 3.2 B,D). Maximum production rates are reported for each treatment along with the day of peak production in Table 3.3. The rate of ammonia production was nearly twice as high at ~2 g TAN per day for the lower casein loads and peaked early at day 1. The higher casein loaded treatments experienced lower ammonia production rates near 1 g TAN per day which did not peak until day 3. This indicates that there is some inhibition of ammonia production in the higher casein loaded bottles.

Values for all parameters measured at day 11 are given in Table 3.4 while values for day 58 are given in Table 3.5. Higher casein loads led to higher concentrations of ammonia as this fermentation product accumulated, reaching 4.1 and 6.2 g TAN L^{-1} in the 40 and 60 g L^{-1} casein loads, respectively, of the casein protein with little inhibition to the ammonia producing (protein fermenting) process.

TAN for each reactor treatment was further assessed by a one-way ANOVA and highly significant difference tests. Only VFA accumulation in the background control (no casein) was found to be statistically different than all other treatments ($p < .01$). TAN accumulation in the killed control (10 g L^{-1} casein), 40 g L^{-1}, and 60 g L^{-1} casein loads were found to be significantly different than the 10 g L^{-1} casein treatments ($p < .01$), but not statistically different than each other. Finally, TAN accumulation was significantly different in all treatments compared with the background control. TAN concentration in the 40 g L^{-1} and 60 g L^{-1} casein loaded reactors reached 3.5 g L^{-1}

(0.2 M) and 5.3 g L^{-1} (0.4 M), respectively by day 11 (Table 3.4). TAN concentrations well within the range reported as inhibitory to methanogens were reached through fermentation of the casein substrate. In the 10 g L^{-1} casein loads TAN levels do not reach the reported inhibitory levels and stay below 2 g TAN L^{-1} through the end of the run. Over the course of these runs, the maximal ammonia production rate was lower under the two higher casein loaded reactors, and these reactors experiences a lag in ammonia production (Table 3.3). These results suggest that fermentation reactions, as measured by ammonia and VFA production, were inhibited at higher casein loading, and likely a result of higher TAN accumulation (or by pH drop as discussed in section 3.3.3). The killed controls experienced a 6 day lag before VFA and TAN production was observed. Ammonia accumulation in the no inoculum control (results not shown) reached only 4 mg L^{-1} after 41 days of incubation (<1% N release from casein). Therefore, it is likely that the biomass present in the digester sludge was not completely deactivated by the three successive days of autoclave treatment in the killed control, and ammonia release from casein is due to biological activity in these tests.

3.3.3 pH stability

Reactors with higher casein loading experienced lower pH over the run (Figure 3.2A). An initial drop in pH during the first two days was observed in all non-buffered reactors. The greatest drop was observed at 60 g L^{-1} casein load, where the pH decreased to near 5.0. This preempted the production of fatty acids in this reactor and so is most likely due to the dissolution of casein after incubation at 30°C.

This drop was not observed in the buffered control, and was less severe at 10 g L^{-1} casein without a buffer. This drop in pH could be responsible for the initial lag in ammonia and acetate production in the reactors with higher casein loads (Figure 3.2 B,D).

3.3.4 Volatile fatty acid profile

The VFA profile over the batch run was similar for both 10 g casein d^{-1} loaded digesters. Consumption of acetate after day 11 in these reactors led to the observed increase in pH in these reactors and methane production by the end of the incubation period (compare these parameters from Table 3.4 to 3.5). In the reactors experiencing higher casein loads, pH remained below 6.5 and acetate concentrations remained near 30 mM. This accumulation of fatty acids in the reactors with higher loadings from day 11 to 58 indicates methanogenesis was inhibited under these conditions. VFA values reported in these tables are in terms of per gram casein loaded, therefore the actual concentration observed in the reactors is 4- or 6-times higher in the 40 or 60 g casein L^{-1} loaded reactors, respectively.

3.3.5 Thermodynamics of amino acid fermentation

Four amino acid pathways were selected to investigate whether TAN, acetate, pH, and CO_2 levels could impose thermodynamic limitations on the fermentation of amino acids (Table 3.6). Included are glutamate fermentation to acetate, butyrate, and hydrogen (reaction 1), glutamate fermentation to acetate and propionate (reaction 2), alanine fermentation to acetate and propionate (reaction 3), and the

coupled fermentation of alanine (electron donor) and glycine (electron acceptor) to acetate (reaction 4). All reactions produce ammonium and carbon dioxide, while only reactions 1 and 4 consume protons. Reactions 1-3 were described by (Buckel, 2001), and reaction 4 was calculated from the half reactions described by (Nisman, 1954).

First, the effect of just one of these parameters was assessed for each fermentation reaction, over a range of concentration (or pH). Temperature was fixed at 30°C, and all reaction species were set at standard conditions (1 atm, 1M), except for the variable in question. Increasing either TAN, acetate, or pCO_2 decreased the magnitude of the free energy change for every amino acid fermentation reaction examined (Figure 3.4 A,C,D), but all reactions remained thermodynamically favorable (indicated by a negative ΔG). TAN had the greatest effect on glutamate fermentation (with hydrogen production, reaction 1) with free energy changing from -160 to -109 kJ mol^{-1} as TAN increased from 0.01M to 1M. The strongest effect was that of pH on coupled alanine-glycine fermentation. As the pH increased above 6 this reaction became thermodynamically unfavorable (Figure 3.4B). The pH had a strong effect on glutamate fermentation (with hydrogen production) as well, but free energy remained favorable up to pH 9 under the conditions examined. The pH had no effect on reactions 2 and 3, since no protons are consumed or produced in these reactions.

Next, free energies were calculated for each reaction under the conditions experienced in the non-buffered reactors treating 10, 40, and 60 g casein L^{-1} at day

0, day 1, day 11, and day 58. In calculating the free energies the proton, TAN, pCO_2, acetate, butyrate, and propionate concentrations were varied, based on what was measured experimentally. Temperature and hydrogen gas partial pressure were kept constant at 30°C and 1 atm, respectively. [Note that this hydrogen gas concentration may be conservatively high.] Glutamate, alanine, and glycine were estimated from casein composition (Table 3.2) for each reactor, and were not adjusted for consumption thus are likely overestimations. Free energies for all reactions under all casein loads experienced a sharp decrease in magnitude from day 0 to day 11 (Figure 3.5). Under the lowest casein load, free energies of all reactions dropped by day 58, corresponding to an increase in methane production and consumption of VFAs (Figure 3.2 B and D). This drop was greatest for glutamate fermentation by either pathway, with a drop in free energy from -146 to -203 (reaction 2) and from -84 to -158 (reaction 1) from day 11 to day 58. The drop in free energy under low casein loading conditions is probably a combined effect of VFA consumption and a decrease in pCO_2. Consumption of hydrogen by hydrogenotrophic methanogens is likely to contribute to a decrease in the free energy (i.e., more favorable) for reactions 1 and 4 at day 58. We did not measure hydrogen concentrations, and so corrections were not performed.

As with the SAOBs, bacteria that couple the fermentation of amino acids to hydrogen production can be thermodynamically limited if hydrogen concentrations are too high (Stams, 1994). As Oh and Martin demonstrated (2014), carbonate concentration can be a driver of syntrophic relationships in reactors as well. Here,

the thermodynamic estimations for each of the four reactions showed more favorable thermodynamic potential when methanogenesis (consuming acetate and hydrogen) became active, despite hydrogen consumption not being a factor for two of these reactions.

Overall, these findings suggest that pH and TAN likely had an inhibitory effect on protein fermentation in the mixed anaerobic community that was evaluated. It seems unlikely, however that increases in ammonium caused any absolute thermodynamic limitation for the proteolytic process. Hydrolysis and fermentation of protein was rapid, occurring in the first few days even as TAN concentrations reached 6 g N L^{-1}. This occurred without an acclimation period, and could likely be optimized under continuous conditions. Methanogenesis on the other hand was completely inhibited under the high casein loading, and methane production was still very low even at low casein loadings. Separation of the two stages (hydrolysis/fermentation, and methanogenesis) could be implemented to enable rapid ammonia release in the first stage, where recovery techniques (such as stripping, or electrochemical extraction) could be implemented, followed by a second stage where methane formation is optimized. Such two stage digesters have been investigated (Nakashimada *et al.*, 2008; Yabu *et al.*, 2011), but to our knowledge are not yet applied at full scale.

3.4 Chapter 3 tables

Table 3.1 Minimal Salts Medium composition

Component	**Amount per L**
KCl (g L^{-1})	1.3
KH_2PO4 (g L^{-1})	0.2
NaCl (g L^{-1})	1.17
NH4Cl (g L^{-1})	0.5
$CaCl2{\cdot}2H_2O$ (g L^{-1})	0.1
$MgCl2{\cdot}6H_2O$ (g L^{-1})	0.18
$NaHCO_3$ (g L^{-1})	2.5
Resazurin solution (mL L^{-1})[a, f]	1
Vitamin solution (mL L^{-1})[b, f]	5
Trace salts I solution (mL L^{-1})[c]	1
Trace salts II solution (mL L^{-1})[d]	0.1
Sodium sulfide solution (mL L^{-1})[e, f]	1

[a]resazurin stock solution was composed of 1 g L^{-1} resazurin in Milli-Q filtered water
[b]vitamin solution was composed of (mg L^{-1}): d-biotin (20), folic acid (20), pyridoxine hydrochloride (100), thiamin hydrochloride (50), riboflavin (50), nicotinic acid (50), DL-calcium pantothenate (50), vitamin B12 (10), p-aminobenzoic acid (50), lipoic acid (50), 1,4-naphthaquinone (40), nicotinamide (100), and hemin (10); dissolved in Milli-Q filtered water
[c]trace salts I solution contained (g L^{-1}): $MnCl_2{\cdot}6H_2O$ (5), H_3BO_4 (0.5), $ZnCl_2$ (0.5), $CoCl_2{\cdot}H_2O$ (0.5), $NiCl_2{\cdot}6H_2O$ (0.5), $CuCl{\cdot}2H_2O$ (0.3), $NaMoO_4{\cdot}2H_2O$ (0.1), and $FeCl_2{\cdot}4H_2O$ (0.1)
[d]trace salts II solution contained (mg L^{-1}): $NaSeO_3$ (30) and (80) Na_2WO_4; dissolved in Milli-Q filtered water
[e]sodium sulfide solution contained 500 g L^{-1} $Na_2S{\cdot}9H_2O$ in Milli-Q filtered water
[f]filter sterilized

Table 3.2 Typical amino acid composition of casein

Amino Acid Component	**g amino acid per 100 g Casein**
isoleucine	5.9
leucine	9
lysine	7.3
phenylalanine	5.2
threonine	4
tryptophan	1.3
valine	6.9
methionine	2.9
cystine	3.6
alanine	2.8
arginine	3.7
aspartic acid	5.8
glutamic acid	21.1
glycine	1.9
histidine	2.7
proline	11
serine	5.6
tyrosine	5.6

Table 3.3 Maximum ammonia production rate measured for each treatment

Treatment	**Ammonia production rate (mg TAN g^{-1} casein d^{-1})**	**Day of peak ammonia production**
Control (killed)	1.3 ± 2	6
Control (background)	0.08 ± .01	5
Control (buffer)	2.2 ± 0.2	1
10 g casein L^{-1}	2.1 ± 0.1	1
40 g casein L^{-1}	1.2 ± 0.2	3
60 g casein L^{-1}	1.15 ± 0.1	3

Table 3.4 Performance parameters from casein anaerobic digesters at Day 11

Parameter	**Controls**		**Experimental (g L^{-1})**			
	killed	**background**	**10 (buffer)**	**10**	**40**	**60**
Cumulative methane[a] (mL)	(<.1)	0.1, .05	0.7, 0.2	0.5, 0.1	0.3, 0.1	0.1, 0
pH	6.16 ± 0.07	7.1 ± .03	6.5 ± .1	6.1 ± .04	6.2 ± .05	6.4 ± .13
TAN (g L^{-1})	1.0 ±.07	0.1 ±0	1.4 ± .05	1.3 ±.03	3.5 ±.02	5.3 ± .03
N released from Casein (%)	56 ± 6	n/a	83 ± 4	81 ± 2	64 ± 0.5	66 ± 4
Acetate[a] (mM)	37.5± 5.1	0	47.2± 1.0	44.1± 0.5	29.5± 0.8	31.7±4.6
Butyrate[a] (mM)	16.9±0.4	0	8.8±0.3	11.5± 0.4	12.8± 0.6	11.2± 0.1
Propionate[a] (mM)	1.4± 0.8	0	3.3±.2	2.2± .6	2.7±.2	3.3±.5
Isovalerate[a] (mM)	9.5± 9	0	8.1± .1	8.3±.3	7.0± .2	6.2± .2
Isobutyrate[a] (mM)	5.3± .1	0	3.8± .6	3.8± .3	2.9± .0	2.9± 1.2

All values reported from final samples at day 11
n/a: not applicable
[a]values calculated as "per g casein substrate", except for background control where this does not apply

Table 3.5 Performance parameters from casein anaerobic digesters at Day 58

Parameter	**Controls**			**Experimental (g L^{-1})**		
	killed	**background**	**Buffer**	**10**	**40**	**60**
Cumulative CH_4 (mL)[a]	0	1.8 ± 1	170 ± 15	150 ± 3	1.0 ± 0.4	1.5 ± 0.3
pH	6.1 ±0	7.0 ± 0	7.0 ± 0	6.9 ± 0.2	6.4 ± 0.2	6.5 ± 0.1
TAN (g L-1)	1.2 ± .1	0	1.4 ± .1	1.5 ± .1	4.1 ± 0	6.2 ± .1
Nitrogen released from casein as TAN (%)	72 ± 4	n/a	88 ± 8	96 ± 6	74 ± 1	78 ± 6
Acetate (mM) [a]	39 ± 3	0	3.4 ± 1.2	0.6 ± 1.1	30 ± 0.5	33 ± 2.7
Butyrate (mM) [a]	43 ± 3	0	0	0	20, 1	19 ± 1
Propionate (mM) [a]	3 ± 0.4	0	14 ± 1	10 ± 1	4 ± 0.1	5 ± 0.5
Isovalerate (mM) [a]	0	0	5 ± 0.4	8 ± 0.5	8 ± 0.4	9 ± 1
Isobutyrate (mM) [a]	6 ± 0.2	0	1 ± 2	5 ± 1	5 ± 0.3	5 ± 0.1
TAN (mM)	85.3 ± 4.0	3.09 ±5.5	101.6± 5.3	106 ± 5.1	290 ± 4.5	444 ± 34
FAN (mM)	.08 ± .004	.02 ± .04	0.9 ± .04	0.7 ± .03	0.6 ± .01	1.1 ± .09

All values reported from final samples at day 58
n/a: not applicable
[a]values calculated as "per g casein substrate", except for background control where this does not apply

Table 3.6 Fermentation reactions considered for thermodynamic calculations[a]

Reaction	Fermentation Pathway	ΔG°' (kJ electron donor^{-1})
1	5 glutamate- + $6H_2O$ +$2H^+$→ $5NH_4^+$ + $5CO_2$ + 6 acetate$^-$ +2 butyrate$^-$ +H_2	-85
2	3 glutamate$^-$ +$3H_2O$ → $3NH_4^+$ + $2CO_2$ + 5 acetate$^-$ + propionate$^-$	-153
3	alanine + $2H_2O$ → 3 NH_4^+ + CO_2 + acetate + 2 propionate$^-$	-50
4	alanine + 2 glycine + $2H_2O$ + $3H^+$ → 3 acetate$^-$ + $3NH_4^+$ + CO_2	-93

[a] *values calculated at pH 7*

3.5 Chapter 3 figures

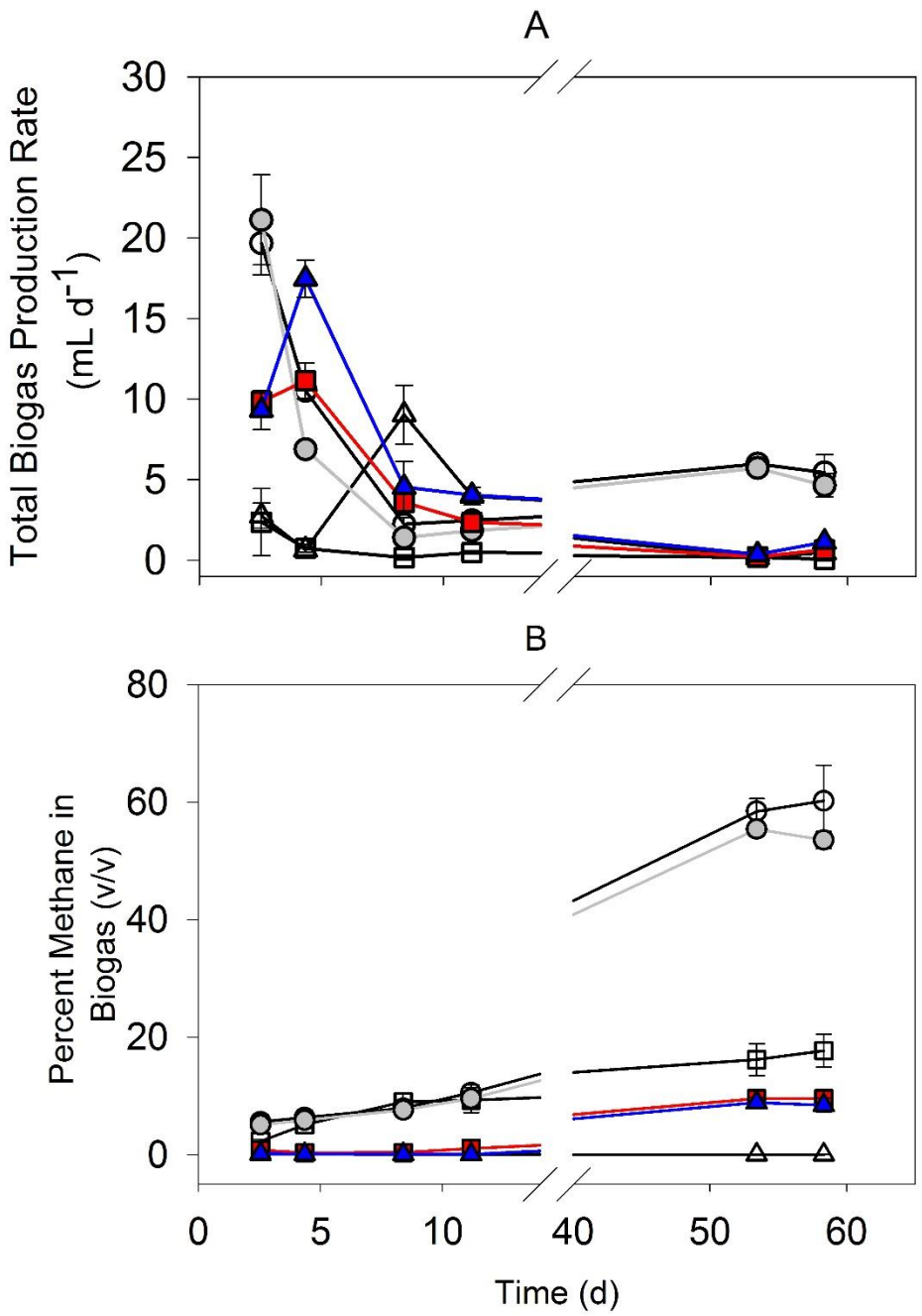

Figure 3.1 Total biogas production rates (A), and percent (v/v) methane (B) for each treatment. Controls: killed (open triangles), background (open squares), 10 g L^{-1} buffered (open circles). Experimental 10 (grey closed circles), 40 (red closed squares), and 60 (blue closed triangles) g casein L^{-1}. Total biogas production is reported on a per g casein basis for all reactors except the no substrate control.

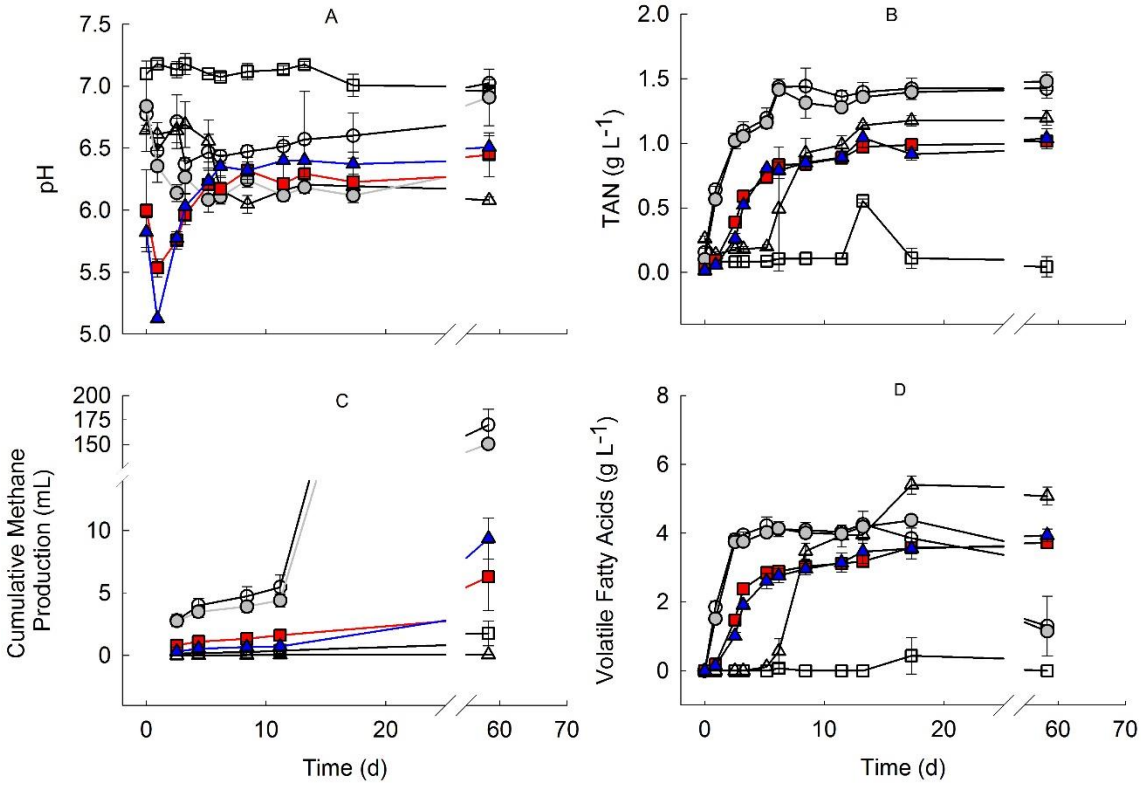

Figure 3.2 Average pH (A), TAN (B), methane accumulation (C), and volatile fatty acids (D) for triplicate reactors with standard deviations over time. Controls: killed (open triangles), background (open squares), 10 g L^{-1} buffered (open circles). Experimental 10 (closed grey circles), 40 (closed red squares), and 60 (closed blue triangles) g casein L^{-1}. TAN, volatile fatty acids, and cumulative methane production are calculated on a per gram casein added basis for all reactors except the no substrate control.

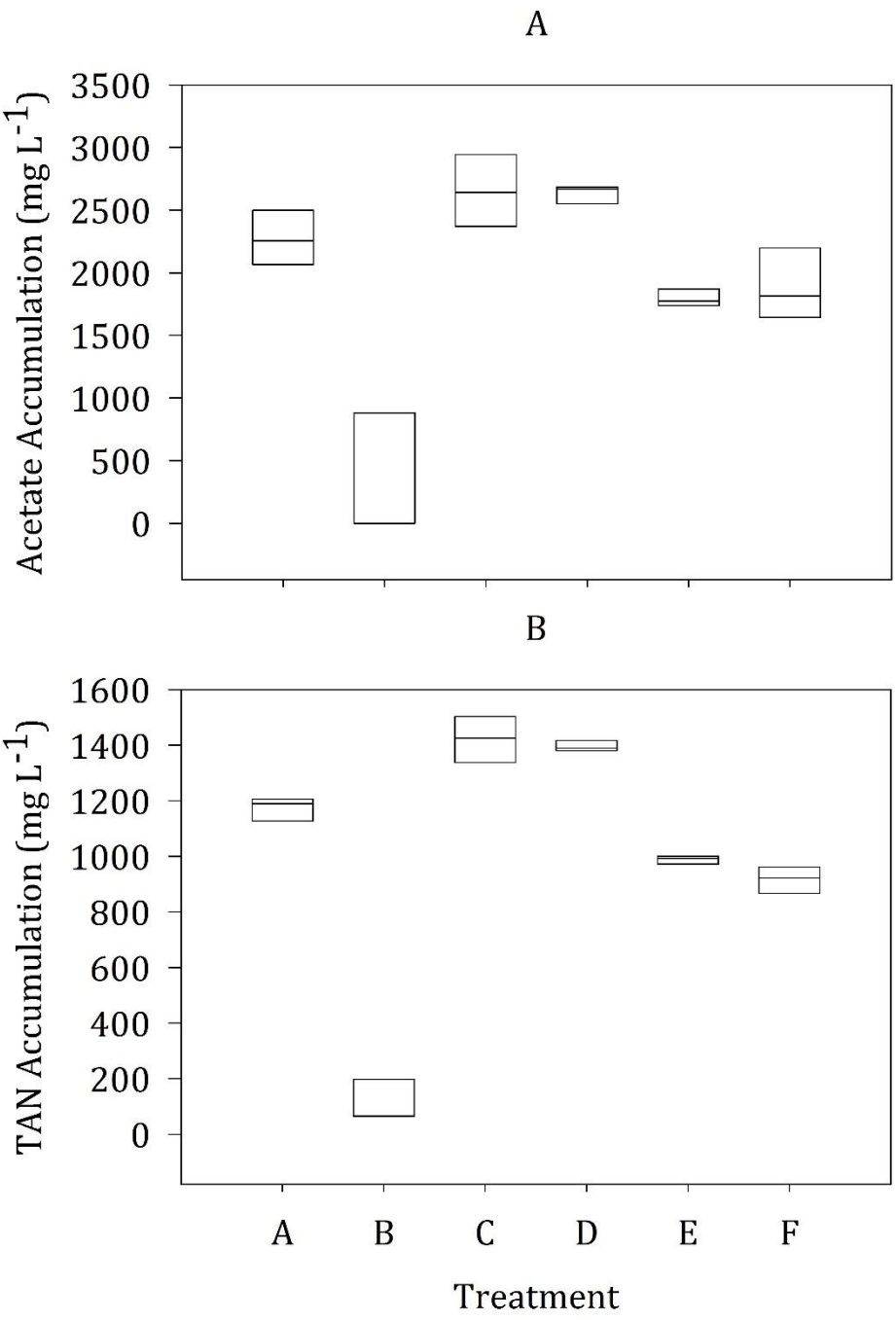

Figure 3.3 Variation in acetate accumulation (A) and TAN accumulation (B) at 17d for each treatment; A, killed control; B, no substrate control; C, 10 g L^{-1} casein buffered control; D, 10 g L^{-1} casein; E, 40 g L^{-1} casein; and F, 60 g L^{-1} casein. Lower box limit represents the 25th percentile, upper limit represents the 75th percentile, and the line within the box indicates the median value.

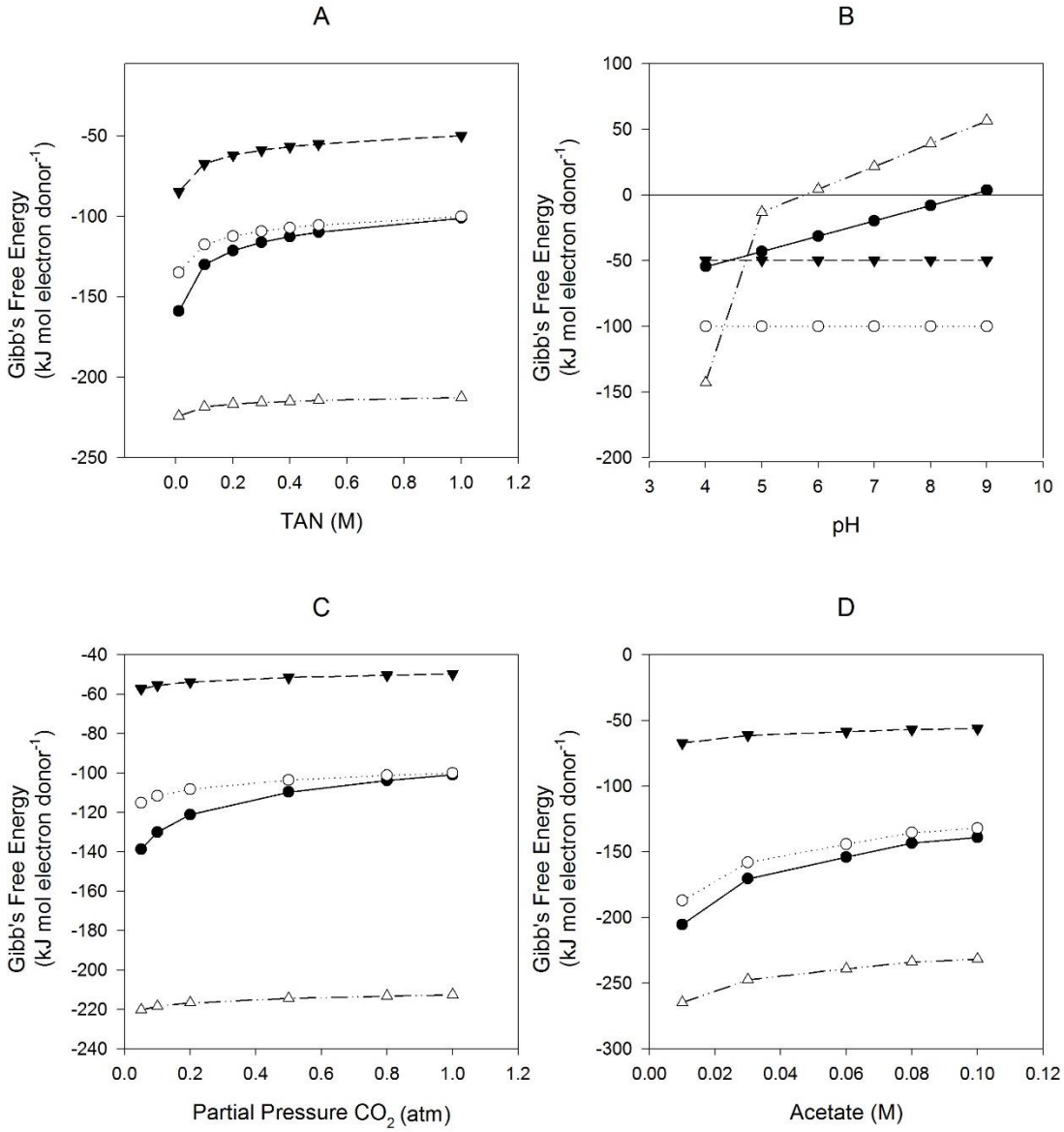

Figure 3.4 Change in Gibb's free energy with TAN concentration (A), pH (B), CO2 partial pressure (C), and acetate (D) for glutamate fermentation with hydrogen production (closed circles), glutamate fermentation without hydrogen production (open circles), alanine fermentation (closed triangles), and coupled fermentation of alanine and glycine (open triangles).

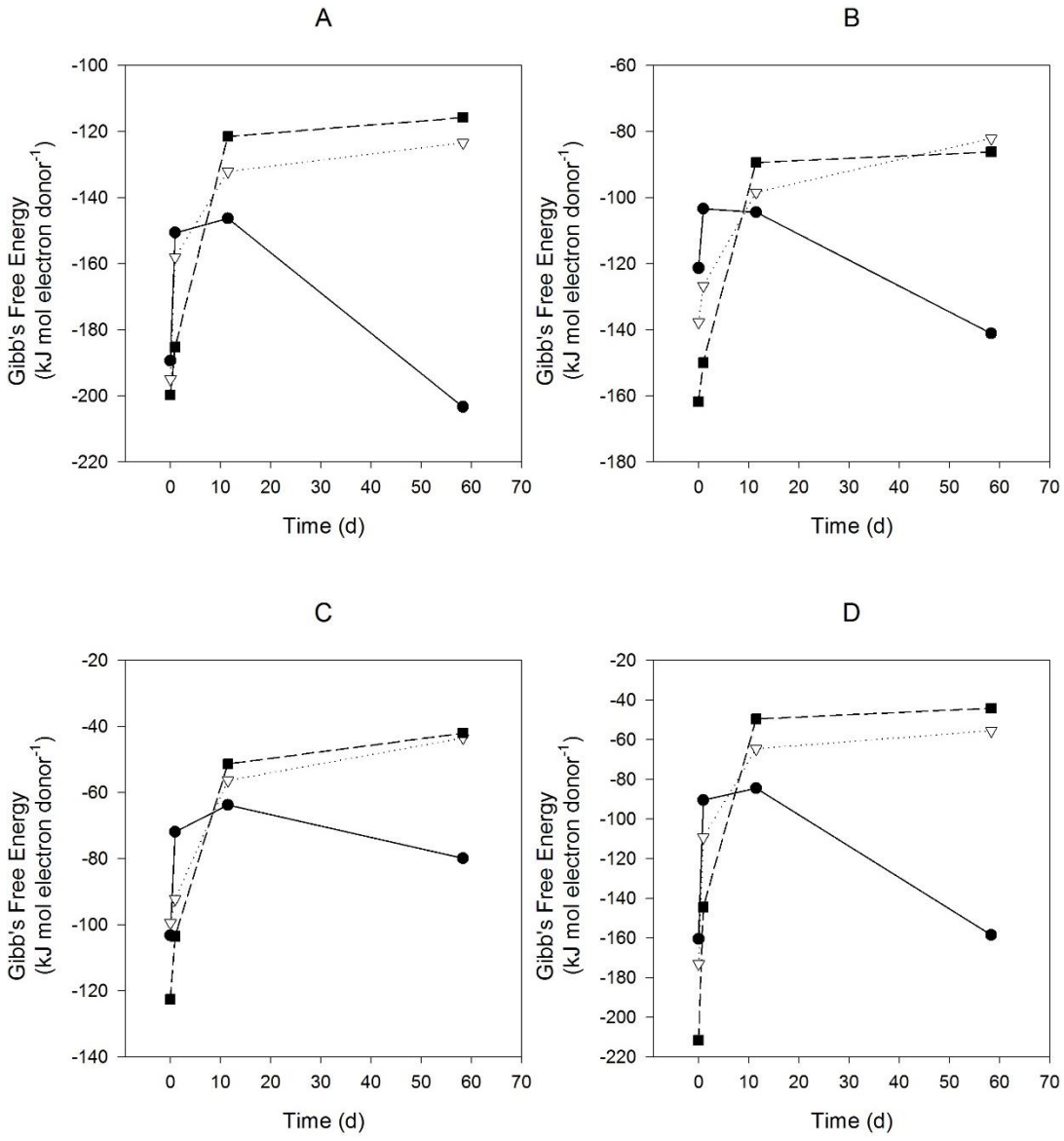

Figure 3.5 Change in Gibb's free energy for glutamate fermentation without hydrogen production (A), alanine coupled to glycine fermentation (B), alanine fermentation (C), and glutamate fermentation with hydrogen production (D), calculated for live reactor treatments of 10 (closed circles), 40 (closed squares), and 60 (open triangles) g casein L^{-1}. Free energies are corrected for reactor pH, TAN concentration, pCO2, and VFA end product concentration for each treatment at each time point. Amino acid substrate is assumed to be constant (Table 3.2), and hydrogen is assumed to be 1 atm.

Chapter 4: A metabolic model of amino acid fermentation in *Peptostreptococcus russellii*

4.1 Introduction

Amino acids can be utilized as a source of carbon by a number of chemotrophic bacteria with recycling of internal peptides and amino acids being a common trait of nearly all bacteria. The use of amino acids as sole carbon and energy source by anaerobic fermentative processes is less common, and so far limited to *Clostridia* spp. and *Fusobacteria* spp. (Buckel, 1980). One of the earliest descriptions of this process was of the Clostridia in the 1930s by Stickland (1934, 1935a, 1935b), who observed that these bacteria utilized amino acids in pairs; one amino acid serving as electron donor, and the other as acceptor (for review, see Nisman, 1954). Since then extensive studies in *Clostridium* spp. and some Fusobacteria bacteria (Jackins and Barker, 1951) have highlighted great diversity in the patterns of amino acid usage (Mead, 1971; Barker, 1981), and in the pathways of utilization (Andreesen, 1994; Buckel, 2001). End products of these fermentations can include short chain fatty acids, CO_2, H_2, ammonia, and δ-aminovaleric acid. Many of the bacteria described by Barker were isolated from soil enrichments (Barker, 1981), while others have since described these fermentations in the human colon (Smith and Macfarlane, 1997; Richardson *et al.*, 2013), the rumen (Russell *et al.*, 1988), and manure handling systems (Siebert and Toerien, 1969; Ramsay and Pullammanappallil, 2001; Whitehead and Cotta, 2004).

Fermentation of amino acids in anaerobic digesters contributes to the accumulation of ammonia that can become inhibitory to the process and lead to reactor instability. (for a review, see Rajagopal et al., 2013). This fact has been long noted for AD technology (Graef and Andrews, 1974) and constrains the use of high nitrogen wastes (HNOWs) as sole feedstocks to anaerobic digesters. Rather, blending of HNOWs with high carbon wastes is usually necessary to maintain reactor stability (see for example: Parameswaran and Rittmann, 2012; Drennan and DiStefano, 2014). This path has led to a need for blending strategies and models to optimize methane production (see, for example Kayhanian, 1999 and García-Gen et al., 2014). If HNOWs could be anaerobically digested under stable conditions, higher concentrations of biologically-released ammonia (bioammonia) could be produced. High concentration bioammonia could then be recovered more economically for fertilizer or energy use (Babson *et al.*, 2013).

In the interest of further understanding the specific toxicity of ammonia to the microorganisms in this environment, we chose to sequence the genome of a protein fermenting bacterium, *Peptostreptococcus russellii.* The governing hypothesis of this study is that organisms of this type are: (i) responsible for ammonia production in these systems, (ii) produce ammonia directly from their substrates and are likely exposed to transiently high ammonia concentrations, and (iii) are therefore likely to have a high ammonia tolerance. We therefore chose to study *P. russellii* as a model protein-fermenting, ammonia-producing, ammonia-tolerant bacterium for anaerobic digestion of proteinaceous HNOWs.

This bacterium was originally isolated from a swine manure holding pit (Whitehead *et al.*, 2011), and exhibits rapid growth on proteins, peptides, and amino acids. Members of *Peptostreptococcus* spp. are classified as follows: Firmicutes (Phylum), Clostridia (class), Clostridiales (order), *Peptostreptococcaceae* (family). It is most closely related to *Peptostreptococcus anaerobius* with 95.5% identity shared between the 16S rRNA sequences. Clostridia is a highly diverse class that contains members important in the hydrolytic and fermentative stages of the anaerobic digestion process. At the order level, members of Clostridiales have been identified as dominant populations in full-scale anaerobic digestion studies (Werner *et al.*, 2011). In a recent study of full-scale anaerobic digesters, members of the order Clostridiales were present at high relative abundances under conditions of higher TAN (De Vrieze *et al.*, 2015), although it was not reported which genera were mainly present. The authors suggested that this increased abundance could be associated with an increase in anaerobic acetate oxidation. Members of the genus *Peptostreptococcus* have been identified specifically in some digestion studies (Siebert and Toerien, 1969; Iannotti *et al.*, 1982). In a seeded plug flow reactor experiment treating swine manure, *Peptostreptococcus anaerobius* became the dominant species in the hydrolytic/acidogenic stage of the digestion (Talbot *et al.*, 2010).

Here we sequenced the genome of *Peptostreptococcus russellii* and used a transcriptome study of growth on casamino acids to develop a metabolic model for amino acid fermentation for this potentially ammonia tolerant bacterium. In follow-

up studies (Chapter 5) we examine the effect of ammonia stress and sodium stress on the organism.

4.2 Materials and Methods

4.2.1 Culture growth conditions

P. russellii RT-10B (type strain) (Whitehead *et al.*, 2011) was purchased from the Leibniz Institute DSMZ-German Collection of Microorganisms and Cell Cultures (DSMZ), Braunschweig, Germany.

For genomic DNA isolation, cells were grown in a modified chopped meat medium broth adapted from the recipe provided by DSMZ (medium 78). The medium was composed of the following (g L^{-1}): beef extract powder (10), bacto casitone (30), yeast extract (5), potassium phosphate dibasic (5), resazurin (1 mg L^{-1}), and sodium hydroxide (0.025 N). The medium was made anoxic by flushing 100% nitrogen gas (high purity grade) through the liquid for 30 minutes. Cultures were incubated anaerobically for 24 h at 35°C.

Cells for the transcript sequencing experiment were grown in a modified minimal salts medium (Zinder, 1998) (Table 4.1). Sodium carbonate was replaced by a mixed solution of sodium bicarbonate/sodium carbonate (molar ratio 1:3) at a final concentration of 0.5% (v/v) (5.6 mM carbonate). The headspace was replaced with 100% N_2, and the pH was adjusted to 8.5. Bacto® casitone (Difco Laboratories, now Becton, Dickinson and Company, Franklin Lakes, NJ, USA) was provided as the sole carbon and energy source at 1.5% (w/v). Cultures were incubated in triplicate,

statically at 35°C, and harvested at mid exponential phase for messenger RNA (mRNA) recovery.

4.2.2 Nucleic acids isolation

P. russellii proved to be highly resistant to standard lysis methods. The following lysis methods were tested and found to be ineffective for recovery of nucleic acids: enzymatic digestion by lysozyme or proteinase K, mechanical disruption by homogenization, or any combination of the previous three methods; freeze/thaw cycling in 16 mM EDTA buffer; or the RNAsnap® method (Stead *et al.*, 2012). Achromopeptidase was shown to be effective against a number of lysozyme resistant anaerobic cocci bacteria (Ezaki and Suzuki, 1982). Achromopeptidase (Sigma-Aldrich, St. Louis, MO) was found to be quite effective in lysing *P. russelli* cells.

For isolation of genomic DNA, cells were incubated at 37°C in tris-EDTA buffer with addition of lysozyme (15 mg mL^{-1}) and achromopeptidase (9mg mL^{-1}). Nucleic acid extraction was then carried out by the phenol chloroform method described by Kerkhof and Ward (Kerkhof and Ward, 1993), with the following modifications: following the phenol chloroform extraction step, 40 µL of 3.0 M sodium acetate and 2 µL of glycogen were added to the aqueous phase, and nucleic acids were precipitated by addition of 800 µL 100% ice cold ethanol. DNA was further purified by RNase I (Promega, Madison, WI, USA) treatment, followed by a second nucleic acid precipitation. DNA was resuspended in 25 mM tris-Cl, pH 8.0, and sent for sequencing.

For RNA isolation, cells were lysed by freeze/boil cycling in a 2% SDS solution (50 mM glucose, 10 mM EDTA, and 25 mM Tris-Cl pH 8, 2% SDS) to minimize RNA degradation. Addition of 2% SDS apparently increased the effectiveness of this method. The cycle consisted of a two minute incubation in boiling water bath followed immediately by a quick freeze in liquid nitrogen and this was repeated for 3 cycles. Nucleic acids were extracted by the same modified phenol-chloroform method described above, but with an acidic phenol-chloroform solution to limit DNA recovery. The precipitation was repeated a second time, and the pellet was air dried and resuspended in 1mM EDTA. This nucleic acid preparation was then treated with Invitrogen Turbo DNase (Life Technologies, Grand Island, NY, USA) to remove residual DNA, then further purified and concentrated using the Qiagen RNeasy RNA extraction kit (Qiagen, Inc., Venlo, Netherlands), but following the method for RNA cleanup protocol from the RNeasy® MiniElute® Cleanup Handbook (October, 2010 version). Messenger RNA (mRNA) was enriched using the Ambion MICROBExpress Kit (Life Technologies)), which selectively removes 16S and 23S ribosomal RNA (rRNA) through a capture hybridization approach. Final samples were resuspended in RNase free water (Qiagen, Inc.).

DNA or mRNA concentrations were measured using Qubit® Fluorometric Quantitation (Life Technologies). mRNA quality was assessed visually by electrophoresis using a 1.5% agarose gel prepared in 1x tris-EDTA buffer. For quality analysis, 5-10 µL of mRNA extract was subjected to electrophoresis at 120 V for 1 h. mRNA extracts were also analyzed using an ND-1000 spectrophotometer

(NanoDrop, Wilmington) to obtain A_{260}:A_{280} ratios. Ratios for all mRNA enriched samples were between 2.1 and 2.2, which is an indicator that the samples are free of impurities such as DNA or proteins. Extraction and enrichment of mRNA was carried out the same day for a given sample and mRNA was stored at -80°C until sequencing. All solutions used throughout the RNA processing work were prepared with water that was first treated with diethylpyrocarbonate (DEPC) to remove RNases, then subsequently autoclaved to inactivate the DEPC.

4.2.3 Genome sequencing and annotation

Genomic DNA from *P. russellii* RT-10B (type strain) was sequenced on the Illumina® Miseq (Illumina, San Diego) (600 cycle) using 2 x 300 paired-end sequencing. Genomic DNA libraries were generated using the Illumina® Nextera DNA Sample Preparation Kit (cat#FC-121-1030).

The genome assembly consisted of nine contigs totaling 2.02 Mbs with an average coverage of ~4500X. GeneMarkS (Georgia Institute of Technology, Atlanta, GA, USA) was used for gene calling, which predicted 1,808 coding sequences (CDSs). Predicted protein sequences were entered into the Basic Local Alignment Search Tool (BLAST) of the National Center for Biotechnology Information (NCBI) non-redundant (nr) protein database to annotate the CDSs. The genome assembly was also processed by the Rapid Annotation using Subsystem Technology (RAST) pipeline for annotation (Aziz *et al.*, 2008) and subjected to subsystem analysis through the SEED platform (Overbeek *et al.*, 2005) for comparison and to glean additional information for building the metabolic model. Predicted CDSs were also

analyzed against the Kyoto Encyclopedia of Genes and Genomes (KEGG) database to aid in analysis of central metabolic processes. The KEGG orthology (KO) BlastKOALA tool was provided by KEGG (http://www.kegg.jp/blastkoala/; accessed on the internet February 2015). Putative transporter genes were predicted against the transporter classification database (TCDB) using the TransportTP tool (http://bioinfo3.noble.org/transporter/; accessed on the internet February 2015) which compares sequences against the transporter classification database (TCDB) using the approach of Li et al. (2008). The open source software tool *P*o*R*table *F*ront *E*nd for the *C*ommand *T*erminal BLAST+ (prfectBLAST) (Santiago-Sotelo and Ramirez-Prado, 2012) was used to build a custom database for *P. russellii* from the predicted nucleotide sequences and/or amino acid sequences, for performing nucleotide or amino acid similarity searches against the sequences predicted in *P. russellii.*

4.2.4 Transcriptome sequencing and analysis

Libraries for each mRNA sample were generated using the Illumina® TruSeq RNA Sample Preparation Kit v2 (Illumina, San Diego, CA, USA). Briefly, 100 ng of enriched mRNA was brought to 18 µL with Elute/Prime/Fragment mix and heated to 94 °C for 8 min. Complementary DNA (cDNA) preparation and library generation were carried out according to the Illumina® protocol, using appropriate indices for multiplexing. Library quality was validated using Qubit® Fluorometric Quantitation (Broad Range DNA) (Life Technologies, Grand Island, NY, USA) and an Agilent 2100 Bioanalyzer (High Sensitivity DNA chip) (Agilent, Santa Clara, CA, USA). The

libraries were pooled in equimolar concentrations and analyzed using the Illumina® MiSeq at a final concentration of 20 pM using a MiSeq Reagent Kit v3 (Illumina, San Diego) (600-cycle) for a 2x300-cycle paired end run.

To determine relative gene expression under unstressed growth, MiSeq reads from triplicate samples were pooled and mapped to the annotated genome. An expression value was generated as reads per kilo base per million (RPKM), which is equal to the number of mapped reads per kilo base of transcript per million mapped reads. This calculation serves to normalize the data to gene length and library size. A threshold of RPKM > 1 is commonly used to determine whether a gene is expressed, any gene with RPKM < 1 can be considered not expressed.

4.3 Results and Discussion

4.3.1 Genome overview

The 2.02 Mb genome sequence is distributed onto 9 scaffolds. Of the 1808 predicted CDS, 1206 (67%) are contained on scaffold 1, 7.2% on scaffold 2, 12% on scaffold 3, 13% on scaffold 5. The remainder (0.8%) are distributed across scaffolds 4 and 6 through 9. Of the 1808 predicted CDS, 19% were annotated as hypothetical or conserved hypothetical proteins by protein BLAST analysis against the non-redundant protein database. Only 895 genes (49.5%) were assigned a KO. The KO system develops pathway maps and functional hierarchies based on experimental data, used to define ortholog groups that can be compared across different species. Thus, far fewer genes from the genome were functionally annotated via KO analysis than through the basic protein BLAST analysis. RAST

returned 1854 features (1770 CDSs + 84 RNAs), and predicted that only 16 genes were likely to be missing from the genome. Of the 1770 CDSs, 920 (52%) were assigned to a described subsystem. SEED annotation is performed by an expert annotator to assign genomic data to subsystems under which Fellowship for interpretation of Genomes (FIG) protein families are defined. All CDSs discussed in this manuscript will refer by number to CDS predicted by GeneMarkS. CDSs will be referred to by a genome identifying prefix ("PR" for *Peptostreptococcus russellii*) and gene number (i.e. one of the total 1808 predicted CDSs). Expression level data for any individual CDS will be referred to by the RPKM value.

4.3.2 Global metabolic features

Several of the known metabolic pathways for generation of key metabolic precursors were identified in the genome analysis. *P. russellii* appears to have a complete pathway for glucose metabolism through glycolysis and gluconeogenesis, but during growth on amino acids, the important intermediates of this pathway must be supplied by alternative means. Twelve metabolic precursors are considered key intermediates for essential metabolic pathways. These twelve precursors are listed in Table 4.2 along with the predicted available source(s) under these growth conditions in *P. russellii*.

To highlight a few of these pathways, L-serine ammonia-lyase (PR276) and pyruvate carboxylase (PR1337), can each supply pyruvate from serine and oxaloacetate, respectively; both were expressed near 150 RPKM. Since *P. russellii* lacks a complete citric acid cycle, alternative pathways must be present to supply α-ketoglutarate,

succinyl-CoA, and oxaloacetate. CDSs coding for glutamate dehydrogenase (PR35), 2-oxoglutarate ferredoxin oxidoreductase (PR6-9), and two for an aspartate aminotransferase (PR989) were all highly expressed (RPKM >1000), and these supply α-ketoglutarate, succinyl-CoA, and oxaloacetate, respectively. A partial (non-oxidative) pentose phosphate pathway is available to supply ribulose-5-phosphate and erythrose-4-phosphate via intermediates of glycolysis.

Peptidases and transporters are required for utilization of the mixed peptides provided as substrate via casitone. Peptides are likely imported into the cell and hydrolyzed further into individual amino acids within the cytoplasm, as is the case for lactic acid bacteria (Savijoki *et al.*, 2006). Annotation of the genome identified 32 proteases, and eight peptidases. Of these, three peptidases (PR1504, PR1505, PR1484) and one ATP dependent protease (PR1772-PR1774) were expressed (i.e.,RPKM >200). Transporter analysis identified putative transporter domains in 132 of the predicted protein sequences. These included six within the alanine or glycine: cation symporter family, five within the amino acid-polyamine-organocation family, five within the branched chain amino acid:cation symporter family, 2 in the dicarboxylate or amino acid:cation symporter family, and 7 in the major facilitator superfamily. Sixty-eight of the predicted transporter proteins were within the ATP binding cassette superfamily. Most putative amino acid transporters were expressed at relatively low levels, as examples: an alanine:sodium symporter (PR842, RPKM243), three branched chain amino acid transporters (PR498, RPKM183; PR539, RPKM149; PR1440, RPKM132) and an MFS transporter (PR1503,

RPKM262). A branched chain amino acid (isoleucine, leucine, valine) transporter (PR496, RPKM2068) was highly expressed, suggesting this transporter plays a major role in the preferred amino acid fermentation pathway under these growth conditions.

4.3.3 Amino acid fermentations

P. russellii expressed two putative 2-hydroxy acid dehydratases during fermentation on casitone. One is part of a cluster of CDSs (PR488-497) that were highly expressed (RPKMs between 1000-6400), henceforth referred to as "HAD 488". The other is part of a second gene cluster (PR1432-1442), expressed at about half that level (RPKMs between130-800), and henceforth referred to as "HAD 1432". These dehydratases are key enzymes in a set of recently described protein complexes that carry out a reversible stereospecific dehydration reaction on (R)-2-hydroxyacyl-CoA involving a highly oxygen sensitive activation step, followed by a dehydration, and have only been characterized in a few amino acid fermenting bacteria (Kim *et al.*, 2004). The 2-hydroxy acid dehydratases characterized thus far act on substrates including 2-hydroxyglutarate (Buckel, 1980), (R)-3-phenyllactate (Dickert *et al.*, 2002), 2-hydroxyisocaproate (Kim *et al.*, 2005), and (R)-lactyl-CoA (Hofmeister and Buckel, 1992), as key enzymes in the fermentation pathways of glutamate, phenylalanine, leucine, and alanine, respectively.

BLAST searches were performed for amino acid sequences for each 2-hydroxy acid dehydratase and Co-A transferase against the *P. russellii* protein database to determine sequence similarity. Results of these comparisons are summarized in

Table 4.2. HAD 448 and HAD 1432 share less than 50% similarity with each other, indicating they likely act on different substrates. When comparing HAD 443 against the known dehydratases, it shared the highest similarity to phenyllactate dehydratase from *Clostridium sporogenes*, and 2-hydroxyglutaryl-CoA from *Acidaminococcus fermentans*. HAD 1432 proteins showed the greatest similarity to the 2-hydroxyisocaproyl-CoA dehydratase subunit of both *Peptoclostridium difficile* and *Clostridium botulinum.* Due to the high level of similarity to the proteins in all complexes, sequence identity alone is not sufficient to predict the likely functional assignment for these complexes in *P. russellii.* Furthermore, these 2-hydroxyacid dehydratases have been shown to display some activity on alternate substrates (Buckel, 1980; Dickert *et al.*, 2002).

Whitehead *et al*. (2011) reported the following fermentation products by growth on 1% tryptone/1% casamino acids, in mM: acetate (8.5), propionate (2.2), isobutyrate (2.7), methyl-butyrate (2.6), and trace amounts of butyrate after 24 hours of growth. In this study isobutyrate (3.9) was measured as the major fatty acid followed by isovaleric (3.0) and valeric (3.0) acids, then formate (2.6) and acetate (2.6). We also observed several additional chromatographic peaks in samples, but the corresponding organic acids were not identified. Casitone and tryptone are both pancreatic digests of casein; however, the use of casamino acids by Whitehead *et al.* could have an effect on the final end products when comparing results. Considering the proposed end products from these pathways that utilize 2-hydroxy acid dehydratases (Figure 4.1), glutamate or alanine produced during peptide hydrolysis

might be the likely amino acids utilized as primary substrates for fermentation. Serine and glutamine may also be used, since these can be easily transformed to the precursors to the lactyl-CoA dehydratase and 2-hydroxyglutaryl-CoA dehydratase (Kim *et al.*, 2005), respectively.

Looking to the model alanine fermentation pathway in *Clostridium propionicum* (Figure 4.2), seven of the ten enzymes required were tentatively expressed (>30% amino acid sequence similarity) from CDSs in *P. russellii*. These include a lactate dehydrogenase (PR1439) and the putative lactyl-CoA dehydratase (PR1433, 1434, 1439). Enzymes corresponding tosteps 6, 8, 10 (Figure4.2) may be missing due to poorly conserved amino acid sequences lack of a complete genome sequence, or it may be that an alternative reaction or pathway takes place in *P. russellii.*

The glutamate fermentation pathway via 2-hydroxyglutarate has been described in *A. fermentans* (Buckel, 2001), and is shown in Figure 4.3. Putative CDSs from *P. russellii* corresponding to reactions in the pathway are given in the legend. Although not all enzymes could be accounted for (enzymes for step 5 and most of 6 not found, Figure 4.3), CDSs putatively encoding the enzymes for steps 1-4 were highly expressed (>2000 RPKM). These include glutamate dehydrogenase (PR35) and phosphoglycerate dehydrogenase (PR495), the latter having been shown to also reduce α-ketoglutarate to 2-hydroxyglutarate (Zhao and Winkler, 1996). Putative hydrogenase coding genes were identified, but not highly expressed. *P. russellii* may utilize an alternate pathway to acetate via glutaconate, or alternately, the amino acid sequence of these enzymes may be poorly conserved.

Additional support for the assignment of the 2-hydroxyacid dehydratase pathways is found in the arrangement of the CDSs within each putative HAD operon. Figure 4.4 shows CDS clusters for HAD 488 (A), and HAD 1432 (B). CDSs were expressed at similar levels from each operon. Two key enzymes from each of the above pathways are found on these operons: lactate dehydrogenase (alanine fermentation pathway), and 2-hydroxyglutarate dehydrogenase. The co-expression of these genes with the respective dehydratases provides further evidence that HAD 488 codes for 2-hydroxyglutaryl CoA dehydratase, and HAD 1432 for lactyl-CoA dehydratase.

4.3.4 Energy conservation in P. russellii

P. russellii appears to utilize glycine and proline as electron acceptors to dispose of excess reducing equivalents (e.g., NADH), and to produce ATP through substrate level phosphorylation. Genes coding for glycine and proline reductase were identified in *Clostridium sticklandii* (Fonknechten *et al.*, 2010). Proteins for the glycine reductase complex in *C. sticklandii* (GrdA-D) shared 50-70% amino acid sequence identity with CDSs (PR1049-PR1053) expressed (RPKM 500-700) in *P. russellii.* Proteins for the proline reductase complex (PrdA-C) in *C. sticklandii* shared 50-65 % identity with two sets of CDSs in *P. russellii,* one (PR1124, 1126, 1128, 1130) expressed between 200 and400 RPKM, and a second (PR458, 459, 461) that was not highly expressed (RPKM <4). Reduction of glycine produces acetate and ammonia, while reduction of proline produces α-aminovalerate.

Putative pyruvate ferridoxin and 2-oxoglutarate oxidoreductases (PR672, PR6-9) were highly expressed (1800 and 1300 RPKM), and may be the major source of cellular reduced ferredoxin (required for the 2-hydroxy acid dehydratase reaction). This oxidation of pyruvate to acetyl-CoA could drive additional ATP production via phosphate acetyl transferase and acetate kinase.

Two putative operons coding ATP synthases (ATPases) components were identified in the genome of *P. russellii*: an F-type ATPase (PR1616-1622), and a V-type ATPase. Only the F-type was expressed under these growth conditions. ATPases couple ATP hydrolysis to proton translocation, producing a membrane potential that can be used to do work (e.g., drive transport) by the cell. These can also function in the

reverse to produce ATP at the expense of the membrane potential. V-type ATPases are often coupled to solute transport driven by this proton potential (Beyenbach and Wieczorek, 2006).

P. russellii expressed (RPKM ~300) a putative ion (H+ or Na+) translocating NADH:ferredoxin oxidoreductase complex (PR1172-1176). This complex is similar to the *rnf* complex used to drive electron transfer from NADH to ferredoxin via proton/sodium translocation across the membrane (into the cell), to generate the reducing power for nitrogen fixation. Similar complexes have been recently described in various bacteria and archaea, to act in the reverse, transferring electrons from reduced ferredoxin to NAD^+, and generating a membrane potential through electrogenic sodium/proton translocation out of the cell (Biegel and Müller, 2010). Proton pumping Rnf clusters have been found in a number of amino acid fermenting bacteria including *Clostridium tetani*, *Clostridium kluyveri*, *Acetobacterium woodii* and *C. sticklandii* (Fonknechten *et al.*, 2010).

In summary, *P. russellii* appears to utilize a number of different amino acids, including glutamate, serine, aspartate, alanine, proline, and glycine. ATP is produced through substrate phosphorylation from reduction of glycine and proline, as well as through the 2-hydroxy acid pathways for glutamate and alanine/serine. Membrane potential may be generated via the F-type ATPase, as well as by the Rnf-like complex. This versatility in carbon and energy source may give *P.russellii* an advantage in highly competitive environments such as anaerobic digestion.

This Whole Genome Shotgun project has been deposited at DDBJ/EMBL/GenBank under the accession JYGE00000000. The version described in this paper is version JYGE000000000

4.4 Chapter 4 tables

Table 4.1 Modified minimal salts medium

Component	Amount per L
Bacto casitone (g L^{-1})	1.5
Yeast extract (g L^{-1})	0.3
KCl (g L^{-1})	1.3
KH_2PO4 (g L^{-1})	0.2
NaCl (g L^{-1})	1.17
NH4Cl (g L^{-1})	0.5
$CaCl2{\cdot}2H_2O$ (g L^{-1})	0.1
$MgCl2{\cdot}6H_2O$ (g L^{-1})	0.18
10% $NaHCO_3$ solution (mL L^{-1})	3.75
10% Na_2CO3 solution (mL L^{-1})	1.25
Resazurin solution (mL L^{-1}) [a, f]	1
Vitamin solution (mL L^{-1}) [b, f]	5
Trace salts I solution (mL L^{-1})[c]	1
Trace salts II solution (mL L^{-1})[d]	0.1
Sodium sulfide solution (mL L^{-1}) [e, f]	1

[a]resazurin stock solution was composed of 1 g L^{-1} resazurin in Milli-Q filtered water
[b]vitamin solution was composed of (mg L^{-1}): d-biotin (20), folic acid (20), pyridoxine hydrochloride (100), thiamin hydrochloride (50), riboflavin (50), nicotinic acid (50), DL-calcium pantothenate (50), vitamin B12 (10), p-aminobenzoic acid (50), lipoic acid (50), 1,4-naphthaquinone (40), nicotinamide (100), and hemin (10); dissolved in Milli-Q filtered water
[c]trace salts I solution contained (g L^{-1}): $MnCl_2{\cdot}6H_2O$ (5), H_3BO_4 (0.5), $ZnCl_2$ (0.5), $CoCl_2{\cdot}H_2O$ (0.5), $NiCl_2{\cdot}6H_2O$ (0.5), $CuCl{\cdot}2H_2O$ (0.3), $NaMoO_4{\cdot}2H_2O$ (0.1), and $FeCl_2{\cdot}4H_2O$ (0.1)
[d]trace salts II solution contained (mg L^{-1}): $NaSeO_3$ (30) and (80) Na_2WO_4; dissolved in Milli-Q filtered water
[e]sodium sulfide solution contained 500 g L^{-1} $Na_2S{\cdot}9H_2O$ in Milli-Q filtered water
[f]filter sterilized

Table 4.2 Pathways to key metabolic precursors in *P. russellii*

Metabolic Intermediate	**Source**	***P. russellii* CDS ID**
pyruvate	Serine, via serine ammonia-lyase or oxaloacetate via pyruvate carboxylase	PR276, or PR1337
glucose-6-phosphate	pyruvate, via reverse glycolysis	PR1785
fructose-6-phosphate	pyruvate, via reverse glycolysis	PR514/PR1082
ribose-5-phosphate	fructose-6-phosphate, via the pentose phosphate pathway	PR1612
erythrose-4-phosphate	fructose-6-phosphate via the pentose phosphate pathway	PR1209
triose phosphate	glycolysis	PR241
3-phosphoglycerate	via reverse glycolysis	PR242
phosphoenolpyruvate	glutamate, via α-ketoglutarate	PR515
acetyl-CoA	pyruvate, via pyruvate ferredoxin oxidoreductase	PR672
α-ketoglutarate	glutamate, via glutamate dehydrogenase	PR35
succinyl Co-A	glutamate via 2-oxoglutarate ferredoxin oxidoreductase	PR6-9
oxaloacetate	aspartate, via aspartate aminotransferase	PR989, PR499, PR1559, PR497

Table 4.3 Sequence similarity (%) between characterized 2-hydroxy acid dehydratases and putative 2-hydroxy acid dehydratase complex proteins in *Peptostreptococcus russellii*.

Query[a]	**Putative 2-hydroxyacid dehydratase complex proteins in *P. russellii* showing similarity (% identity) to sequences of known complexes**							
	PR488 (A)[b]	**PR489 (B)**	**PR490 (C)**	**PR491 (D)**	**PR1432 (A)**	**PR1439 (B)**	**PR1433 (C)**	**PR1434 (D)**
P. russellii putative 2-hydroxy acid dehydratase	PR1432 (40)	PR1439 (51)	PR1433 (46)	PR1434 (43)	PR488 (40)	PR489 (51)	PR490 (46)	PR491 (43)
C. sporogenes phenyllactate dehydratase	FldA	FldI	FldB	FldC	FldA	FldI	FldB	FldC
	(55)	(59)	(63)	(44)	(43)	(54)	(49)	948)
C. propionicum lactyl-CoA dehydratase	Not present	activator	dehydratase	dehydratase	Not present	activator	dehydratase	dehydratase
		(57)	(41)	(36)		(55)	(39)	(44)
A. fermentans 2-hydroxyglutaryl-CoA dehydratase	GctABC	HgdC	HdgA	HdgB	GctABC	HgdC	HdgA	HdgB
	no match	(55)	(57)	(39)	no match	(53)	(56)	(39)
C. botulinum/C. difficile 2-hydroxyisocaproate dehydratase	HadA	HadI	HadB	HadC	HadA	HadI	HadB	HadC
	(44)/(42)	(40)/(56)	(50)/(50)	(40)/(45)	(57)/(53)	(42)/(63)	(78)/(80)	(57)/(59)

[a]*indicates the representative bacterium and corresponding 2-hydroxyacid dehydratase complex against which P. russellii sequences were compared, where the first query is the corresponding HAD complex protein in P. russellii itself.*
Each cell contains the protein abbreviation followed by the (%) similarity to the putative protein in P. russellii
[b]*(A)= putative coA transferase, (B)= putative dehydratase activator protein, (C) and (D) = putative dehydratase*

4.5 Chapter 4 Figures

		$\Delta G^{\circ\prime}$= kJ mol^{-1} electron donor
1)	3(S)-phenylalanine + 2H2O → 3NH4+ + CO2 + phenyllacetate- + 2Phenylpropionate -	-118
2)	5Glutamate- + 6H2) + 2H+ → 5NH4+ + 5CO2 + 6Acetate- + 2Butyrate- + H2	-62.6
3)	3L-leucine + 2H2O → 3NH4+ + CO2 + isovalerate- + 2 isocaproate-	-49
4)	3alanine +2H2O → 3NH4+ + CO2 + acetate + propionate	-118

Figure 4.1 Complete fermentation reactions from potential pathways mediated by 2-hydroxy acid dehydratase (Buckel, 2001; Kim *et al.*, 2004).

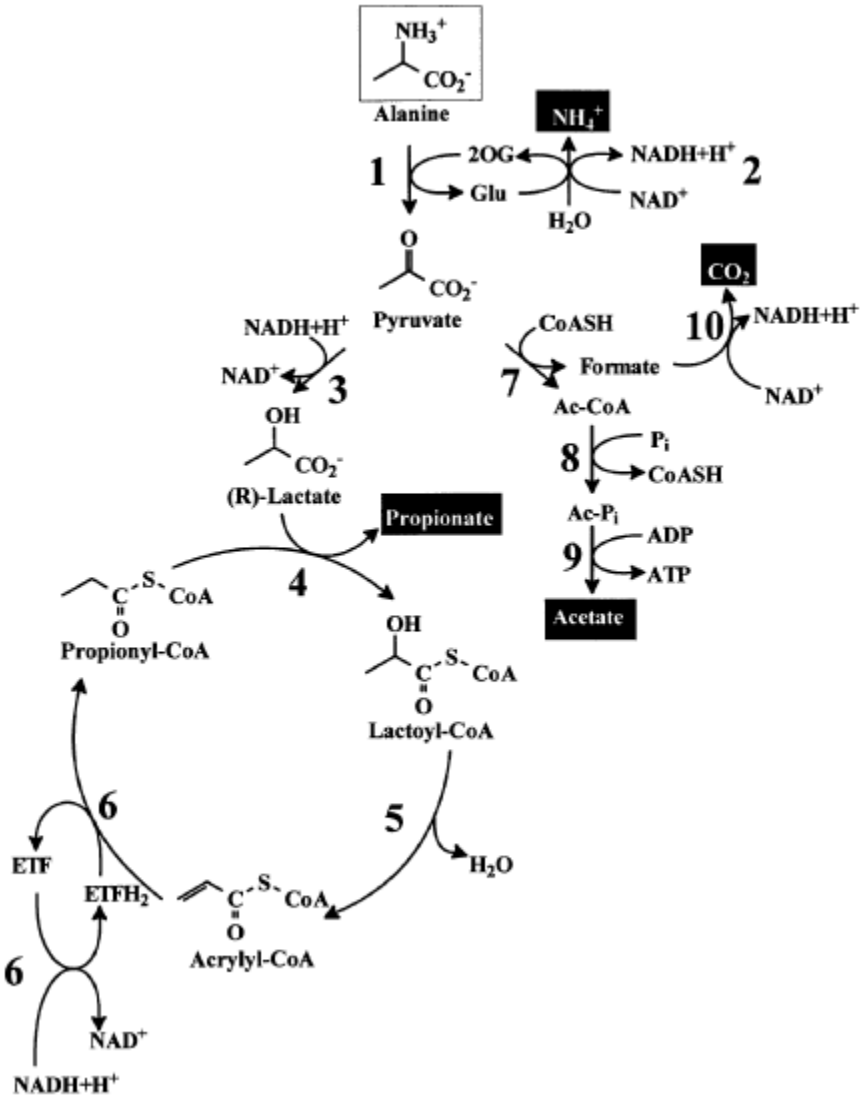

Figure 4.2 Alanine fermentation reaction in *Clostridium propionicum.* Reactions and putative corresponding (CDS) in *Peptostreptococcus russellii*: **1,** pyruvate glutamate transaminase (PR1441); **2,** glutamate dehydrogenase (PR35); **3,** lactate dehydrogenase (PR1438); **4**, propionate CoA transferase (PR1432?); **5**, lactyl-CoA dehydratase (PR1433-1434); **6,** acrylyl-CoA reductase; **7**, pyruvate formate lyase (PR116); **8**, phophotransacetylas; **9**, acetate kinase (PR1085); **10**, formate dehydrogenase. Figure from (Selmer *et al.*, 2002).

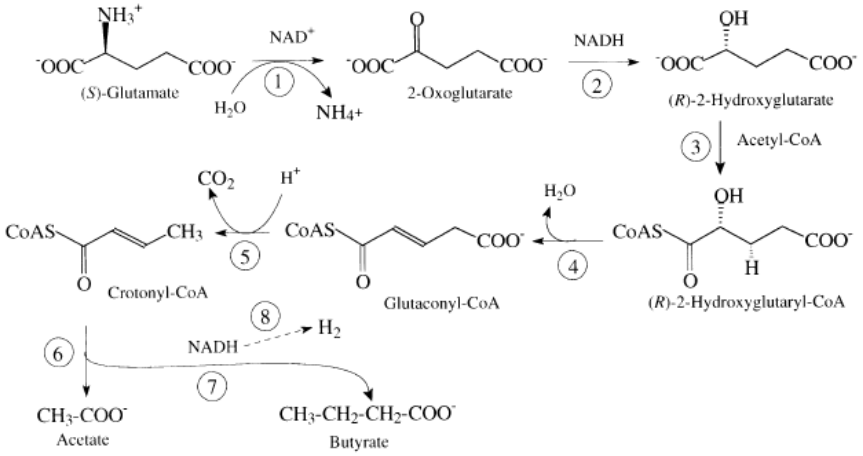

Figure 4.3 Proposed pathway of glutamate fermentation via 2-hydroxyglutarate pathway in *A. fermentans*. Reactions: **1**, glutamate dehydrogenase (PR35);**2**, 2-hydroxyglutarate dehydrogenase (PR495); **3**, 2-hydroxyglutarate-CoA-transferase (PR488); **4**, 2-hydroxyglutaryl-CoA dehydratase (PR489-491); **5**, glutaconyl-CoA decarboxylase; **6**, acetate production via crotonase , 3-hydroxybutaryl-CoA dehydrogenase, and phosphateacetyltransferase (PR630, 1085); **7**, butyrate production via butyryl-Coa dehydrogenase (PR492), phosphate butyryl-transferase (PR27), and butyrate kinase (PR4); **8**, NADH ferredoxin (flavodoxin)oxidoreductase driven by proton gradient/NA+(PR1173-1176) and hydrogenase (PR1159, 1739). Figure by (Buckel, 2001).

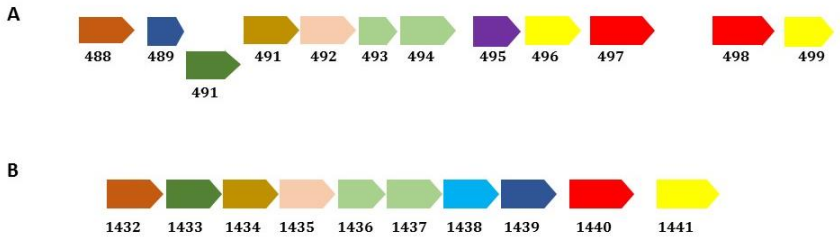

Figure 4.4 Organization of coding sequence (CDS) clusters containing HAD 488 (A) and HAD 1432 (B) in *Peptostreptococcus russellii.* Genes that code for functionally similar proteins have the same color: burnt orange, CoA transferase; dark blue, activator protein of dehydratase; dark green and mustard, 2-hydroxyacyl-CoA dehydratase; pink, acyl-CoA dehydrogenase; mint, electron transport flavoproteins; yellow, aspartate aminotransferase; red, branched chain amino acid transporter; purple, phosphoglycerate dehydrogenase; turquoise, lactate dehydrogenase. CDS 492 codes for a putative acyl-CoA dehydrogenase that shares 51% identity to 1435. CDSs 1435 and 1438 both code for putative acyl-CoA dehydrogenases but share less than 30% identity

Chapter 5: Transcriptional response to growth in high ammonia/ammonium environment in *Peptostreptococcus russellii*

5.1 Introduction

Anaerobic digestion (AD) is an attractive technology for recovering energy (as biogas) and nutrients (N, P, K) from organic waste streams such as animal manures and food waste. During AD complex organic materials are mineralized stepwise through hydrolysis, fermentation and methanogenesis, mediated by distinct microbial community members (Stams, 1994; Worm *et al.*, 2011). During hydrolysis and fermentation of nitrogen-containing organic compounds such as urea and protein, ammonia is released and its accumulation can result in inhibition of AD (Rajagopal *et al.*, 2013; Yenigün and Demirel, 2013), measured by a decrease in biogas (methane) production.

There are a limited number of physiological models describing the mechanism of ammonia stress on bacteria and archaea. The basis for the toxicity of ammonia is twofold, due to the chemical speciation of this molecule. Total ammonia nitrogen (TAN) exists as both free ammonia nitrogen (FAN, NH_3-N), and ionized ammonium (NH_4^+-N). The equilibrium between the two forms is pH and temperature dependent. In neutral to acidic solutions NH_4^+ is predominant and NH_3 will remain very low, while at alkaline pH (>9.3) NH_3 is predominant. Digesters are commonly operated at neutral or slightly alkaline pH, thus it is widely assumed that NH_3 is the more toxic form of TAN in AD systems (see for example, Yenigün and Demirel,

2013). The toxicity of NH_4^+ to bacteria at low to neutral pH may result from an increase in external osmotic potential, (Müller *et al.*, 2006).

There are two proposed models describing the mechanism of ammonia toxicity (Sprott and Patel, 1986) from experiments with methanogens. One proposes a specific toxicity of NH_4^+ (Sprott *et al.*, 1985) by direct interference with peripheral methanogenic proteins found externally on the cell membrane. This interference was alleviated in some methanogens by the addition of magnesium or calcium to the growth media. A separate mechanism (Sprott *et al.*, 1984) was proposed for free ammonia toxicity whereby the cellular pH homeostasis is disrupted by diffusion of free ammonia across the cell membrane, which results in an increase in the intracellular pH. The authors observed potassium depletion from the cells (up to 98% of cellular supply) in immediate response to exposure to increasing free ammonia concentration.

Only two studies have examined the genetic response of microbes to ammonia stress, and both studies looked at methanogens. In both these studies, methanogens (*Methanosarcina thermophile* TM-1 and *Methanosarcina mazei* S-6) were shown to exhibit a dose dependent response in induction of *trkA* expression under ammonia stress (Hofman-Bang *et al.*, 1999; de Macario and Macario, 2003). Trk transporter systems regulate pH and osmotic homeostasis through the action of a potassium-proton antiporter. TrkA is a regulatory protein that acts on this transporter, and its upregulation would appear to support the supposition that ammonia disrupts the pH homeostasis of cells. To our knowledge, there are no studies besides these two

that report the genetic response to ammonia stress in either bacteria or methanogens.

Peptostreptococcus russellii is an obligate protein fermenting bacterium originally isolated from a swine manure holding pit (Whitehead *et al.*, 2011). *Peptostreptococcus* species have been detected in anaerobic digesters, and are particularly relevant to digestion of swine manure (Talbot *et al.*, 2010). Talbot et al. (2010) examined the spatial distribution of the microbial community during AD of swine manure in a plug flow reactor, and found that *Peptostreptococcus sp.* and aceticlastic methanogens dominated during the early stage of digestion, while syntrophic hydrogenotrophic methanogenesis dominated in the later stages.

P. russellii was selected as a model to study ammonia stress because it is an important member of fermentative bacterial communities in swine manure and in AD (Siebert and Toerien, 1969; Russell *et al.*, 1988; Whitehead and Cotta, 2004). Further, since *P. russellii* mediates the release of ammonia during its activities (Whitehead and Cotta, 2004), we hypothesized that it could tolerate high ammonia concentrations, and as such could be an ammonia-tolerant bacterial species. The overall goal of this work was to gain an understanding of the specific genetic response of *P. russellii* that allows its growth at high concentrations of free and ionized ammonia. Analysis of differentially regulated genes under ammonia inhibited versus non-ammonia inhibited growth was performed in order to develop a model of its molecular response to ammonia. Such a model could provide potential genetic targets for monitoring ammonia stress in AD communities, *in vivo* or *in vitro.*

5.2 Materials and Methods

5.2.1 Experimental set-up for comparative transcriptomic study

To identify genes involved in the transcriptional response to ammonia stress, triplicate *P. russellii* cultures were grown under three growth conditions: ammonia stressed, sodium stressed, and unstressed. Stressed growth was defined by inhibition of growth rate, and for ammonia stress could include inhibition caused by both NH_3 and/or NH_4^+. *Ammonia stress* will be used as a general term to refer to the effect of either or both species. Sodium stress was selected to induce a hyperosmotic or salt stress response that would hypothetically have an overlapping response mechanism with the response to NH_4^+, allowing identification of the genes induced specifically by free ammonia toxicity under ammonia stressed growth. Additionally, a general stress response may be shared between the two stress conditions (NH_4^+ and sodium), and this too might help elucidate genes specific to ammonia stress. All cultures were grown at an elevated pH of 8.5 so that the ammonia-stressed condition could have inhibitory NH_3 concentrations. Differential analysis was performed in order to analyze differential expression of transcripts between each pair of conditions: ammonia vs. unstressed and sodium stressed vs. unstressed.

5.2.2 Bacterium and culture conditions

P. russellii was purchased from the Leibniz Institute DSMZ-German Collection of Microorganisms and Cell Cultures, Braunschweig, Germany. A minimal anaerobic growth medium (Zinder, 1998) was prepared according to Table 5.1, except that the buffer (and atmosphere) was modified to meet the buffering needs of the different

growth experiments. Modification for alkaline media was based on a recipe for alkaline yeast extract malt medium. Bacto® casitone, (Difco Laboratories, now Becton, Dickinson and Company, Franklin Lakes, NJ) a pancreatic digest of the milk protein casein, was added at 1.5% (w/v) as the sole carbon and energy source, and 0.3% yeast extract was added to the medium as a trace nutrient source. Cells were grown anaerobically at 35°C without shaking.

In the growth studies designed to test both TAN and FAN tolerance range, 1% sodium bicarbonate was added as buffer with either a 100% nitrogen (for pH 8.5) or 30% CO_2/70% nitrogen (for pH 7.0) atmosphere. Further pH adjustments were made by addition of hydrochloric acid or sodium hydroxide. Ammonium chloride was added to induce ammonia stress in the range of 0.07 to 1 M (1 to 14 g TAN L^{-1}). To evaluate sodium tolerance, sodium chloride was added in the range of 0.07 to 1.0 M. In separate experiments to test the effect of pH alone, media were prepared at pH 7, 8, and 9 by substituting the carbonate/bicarbonate buffer with sodium phosphate (60 mM).

The medium was prepared according to Table 5.1 for the RNA sequencing experiment except that the sodium bicarbonate to sodium carbonate ratio was adjusted to account for high TAN concentration (bicarbonate solution/carbonate solution ratio (v/v) was 1:3 for unstressed and sodium stressed, 4:1 for TAN stressed). To induce sodium or ammonia stress 0.5 M sodium or 0.29 M TAN (74 mM FAN) was added, respectively. Unstressed cultures were grown under 9 mM TAN (2.5 mM FAN).

Samples (3 mL) for RNA extraction were recovered during mid-exponential growth phase, cells were pelleted by centrifugation for 10 min at 14,000 *g* in a 5424 series microcentrifuge (Eppendorf™, Hamburg, Germany) and cell pellets were immediately stored at -80°C. Cell growth was monitored by absorbance at 660 nm on a Genesys 20 spectrophotometer (Cole Parmer, Vernon Hills, Illinois) and the specific growth rate (μ) was calculated by plotting absorbance against time and determining the slope from early exponential growth, according to equation 5.1

$$\ln(x) = \mu * t + \ln(b) \qquad \text{Equation 5.1}$$

where x is the absorbance, μ the specific growth rate, t is time, and b is the Y-intercept.

5.2.3 Cell Lysis, DNA extraction, and mRNA extraction

Cell lysis and nucleic acid extraction were carried out by the method of Kerkhof and Ward (Kerkhof and Ward, 1993), with the following modifications. For isolation of genomic DNA, cells were incubated at 37°C in tris-EDTA buffer with addition of lysozyme (15 mg mL^{-1}) and achromopeptidase (9 mg mL^{-1}). To avoid RNA degradation likely to occur during incubation at 37°C, and alternative method was developed for cell lysis for RNA isolation. For isolation of RNA cells were resuspended in a 100 μL solution of 2% SDS, 50 mM glucose, 10 mM EDTA, 25 mM Tris-Cl pH 8, and lysed by multiple cycles of rapid freezing and boiling. The cycle consisted of a two minute incubation in boiling water bath followed immediately by freezing in liquid nitrogen, and was repeated for 3 cycles. Following the phenol

chloroform extraction, 40 µL of 3.0 M sodium acetate and 2 µL of glycogen were added to the aqueous phase, and nucleic acids were precipitated by addition of 800 µL 100% ice cold ethanol. The precipitation was repeated a second time, and the pellet was air dried and resuspended in 1 mM EDTA. This nucleic acid preparation was then treated with Invitrogen Turbo DNase (Life Technologies, Grand Island, NY, USA) to remove residual DNA, then further purified and concentrated using the Qiagen RNeasy RNA extraction kit (Qiagen, Inc., Valencia, CA, USA), but following the method for RNA cleanup protocol from in RNeasy® MiniElute® Cleanup Handbook (October, 2010 version). Messenger RNA (mRNA) was enriched using the Ambion MICROBExpress Kit (Life Technologies), which selectively removes ribosomal RNA (rRNA). The rRNA removal was confirmed visually by agarose gel electrophoresis, to confirm the disappearance of the 16s and 23s bands after mRNA removal treatment. An example gel is provided in Figure 5.1.

DNA or mRNA concentrations were measured using a Qubit® Fluorometric Quantitation (Life Technologies). mRNA quality was assessed visually by electrophoresis using a 1.5% agarose gel prepared in 1x tris-EDTA buffer. A 5 to 10 µL volume of mRNA extract was subjected to electrophoresis at 120 V for 1 h. mRNA extracts were also analyzed using a NanoDrop™-1000 spectrophotometer (NanoDrop, Wilmington, DE) to obtain A_{260}:A_{280} ratios for assessing purity. Ratios for all mRNA enriched samples were between 2.1 to 2.2, which is an indicator that the samples were free of impurities such as DNA or proteins. Extraction and enrichment of mRNA was carried out the same day for a given sample and mRNA

was stored at -80°C until sequencing. All solutions used throughout the RNA processing work were prepared with water that was first treated with diethylpyrocarbonate (DEPC) to remove RNases, then subsequently autoclaved to inactivate the DEPC.

5.2.4 Chemical analyses and calculations

Liquid samples (1.5 mL) for both total ammonia nitrogen (TAN) and volatile fatty acids (VFAs) determination were removed from the reactors using a sterile plastic 3 mL syringe with an 18 gauge sterile needle that had been flushed with sterile N_2. The slurry sample was adjusted to pH < 3 by addition of 10 N sulfuric acid, then centrifuged for 5 minutes at 13000 rotations per minute (rpm) (14000 x g) by a 5424 series desktop centrifuge (Eppendorf, Hamburg, Germany). The supernatant was transferred to a clean 1.5 mL microcentrifuge tube and stored for up to 30 d at 4 °C , according to standard method 4500-NH3 (Clesceri *et al.*, 1998) for ammonium samples.

TAN concentrations were determined using a Dionex ICS 1000 ion chromatograph equipped with a Dionex IonPac™ CS12A column and CSRS™300 4 mm suppressor (all Thermo Scientific, Waltham, MA). A solution of 20 mN methanosulfonic acid was used as the mobile phase, and samples were quantified against standard concentrations (0.325 to 100 mg TAN L^{-1}) of NH_4Cl. TAN accumulation and production rates are reported on a per gram casein basis for all treatments where casein is added.

Free ammonia (NH_3-N) concentrations were calculated from TAN and pH measurements for each time point using Eq. 3.1.

$$NH_3\text{-}N = TAN \times \frac{10^{pH}}{\left(\frac{Kb}{Kw}\right)\times 10^{pH}} \quad \text{Eq. 5.1}$$

where K_b is the base dissociation constant for ammonia (1.82×10^{-5} at 30°C (Bates and Pinching, 1950) and K_w is the water dissociation constant (1.46×10^{-14} [5] at 30°C (Marshall and Franck, 1981).

The pH was determined directly from 1.5 mL samples using a SymPHony calomel glass micro combination pH electrode (VWR International, Radnor PA) that was calibrated against standard solutions of pH 4.0 and 7.0 (Oaklon, Vernon Hills, IL) at 25°C.

5.2.5 DNA and mRNA library preparation, sequencing, and data processing

Library preparation, sequencing, and bioinformatics were completed by the Genome Cooperative at the Rutgers University School of Environmental and Biological Sciences (http://dblab.rutgers.edu/genome_cooperative/). Genomic DNA libraries were generated using the Illumina® Nextera DNA Sample Preparation Kit (Illumina Inc., San Diego, CA; #FC-121-1030). Libraries for each mRNA sample were generated using the Illumina® TruSeq RNA Sample Preparation Kit v2 (Illumina Inc.). Briefly, 100 ng of enriched mRNA was brought to 18 µL with Elute/Prime/Fragment mix and heated to 94°C for 8 min. Complementary DNA (cDNA) preparation and library generation were carried out according to the

Illumina® protocol, using appropriate indexes for multiplexing. Library quality was validated using Qubit® Fluorometric Quantitation (Broad Range DNA) (Life Technologies, Grand Island, NY) and an Agilent 2100 Bioanalyzer (High Sensitivity DNA chip) (Agilent, Santa Clara, CA). The libraries were pooled in equimolar concentrations and analyzed using the Illumina® MiSeq at a final concentration of 20 pM using a MiSeq Reagent Kit v3 (Illumina) (600-cycle) for a 2x300-cycle paired end run.

GeneMarkS (Georgia Institute of Technology, Atlanta, GA, USA) was used for gene calling, and predicted 1808 coding sequences (CDSs). Protein sequences for these CDSs were blasted against the National Center for Biotechnology Information (NCBI) non-redundant protein database to annotate the CDSs. The predicted CDSs were further analyzed against the Kyoto Encyclopedia of Genes and Genomes (KEGG) database (http://www.genome.jp/kegg/; accessed on the internet February 2015) to predict putative gene functions. Kegg orthology (KO) assignments were made using the BlastKOALA (http://www.kegg.jp/blastkoala/; accessed on the internet February 2015) to predict putative gene functions genes were predicted against the transporter classification database (TCDB) using the TransportTP tool (http://bioinfo3.noble.org/transporter/), which is based on the approach of Li et al. (Li *et al.*, 2008).

Statistical analysis of the sequencing data was also completed by the Genome Cooperative at Rutgers University. Differential gene expression analysis was performed using the DESeq2 package in the statistical software, R (http://www.r-

project.org), which is based on the negative binomial distribution. This method normalizes data between samples based on the assumption that most genes are not differentially expressed. The program generates a p-value for each gene comparison and then uses a false discovery rate (FDR) (a modified p-value) to correct for multiple comparisons (type I errors, e.g., false positives). A cutoff of FDR <0.05 was used to indicate statistical significance, corresponding to a 5% chance or less that the differential genes might be false positives.

To determine relative gene expression under unstressed growth, MiSeq reads from triplicate samples were pooled and mapped to the annotated genome. An expression value was generated as reads per kilo base per million (RPKM), which is equal to the number of mapped reads per kilo base of transcript per million mapped reads. This calculation serves to normalize the data to gene length and library size. A threshold of RPKM > 1 is commonly used to determine whether a gene is expressed, any gene with RPKM < 1 can be considered not expressed.

Differential expression discussed in the Results section 5.3 refers to the differential expression of putative genes (CDS) in either ammonia stressed growth, or sodium stressed growth, *as compared to unstressed growth*. References to expression levels (RPKM) in unstressed growth refer to the separate analysis of the transcript data by itself for estimating background expression levels in “normal” conditions

5.2.6 Modeling chemical speciation in the media using MINEQL

Chemical speciation modeling was performed using the equilibrium modeling program MINEQL+ (v 4.6), to estimate the precipitation potential of phosphate in the media under the stressed and unstressed ammonia concentrations. In our calculations the following species were considered at concentrations provided by the media: carbonate, phosphate, calcium, magnesium, ammonium, potassium, and chloride. Struvite ($MgNH_4PO_4 \cdot 6H_2O$), hydroxyapatite ($Ca_{10}(PO_4)_6(OH)_2$), and calcite ($CaCO_3$) were selected as potential precipitates. The model was run at 35°C.

5.3 Results and Discussion

5.3.1 Defining ammonia stress conditions

TAN was found to inhibit growth of *P. russellii* with increasing concentration in the range of 0.1 to 1.0 M TAN. At neutral pH, growth was observed up to 0.9 M TAN (Figure 5.1A). In this concentration range and pH, FAN concentrations can only reach 10 mM, which is near the inhibitory concentrations reported in AD, but below those reported in pure cultures (Chapter 2, Table 2.1 and Table 2.2). To test a higher range of FAN, the buffering system of the growth medium was adjusted to buffer near pH 8.5. The anaerobic atmosphere was replaced with 100% N_2, the concentration of sodium bicarbonate was increased, and pH was adjusted by addition of sodium hydroxide. With these modifications the medium remained buffered adequately through growth on 15 g L^{-1} casitone. At pH 8.5, within the same range of TAN tested at pH 7, FAN could now reach 260 mM. Growth at this elevated pH was observed only up to 0.6 M TAN, or 150 mM FAN (Figure 5.2B).

By close examination of growth rates during the batch tests at the lower range of TAN (<0.4 M), growth appears to be inhibited more strongly at pH 8.5 (Figure 5.3). Since FAN, TAN, and pH were all likely to have an effect on growth, these were each plotted against growth rate from 8 separate growth experiments to examine the effect of these variables on growth at each pH. Linearity was measured by linear regression (R^2 coefficient), and correlation was measured by the Pearson's correlation coefficient (R). TAN had a weaker linear negative correlation with growth at pH 7 (R^2=0.3, R = -0.5) compared to that at pH 8.5 (R^2= 0.6, R= -0.8) (Figure 5.3A). This effect could have been related to increasing levels of FAN at pH 8.5 (Figure 5.3B), which is linearly correlated with growth at both pH 7 and 8.5, though it is a direct function of TAN. There was no clear correlation between pH and growth rate from this data set (Figure 5.3C).

With increasing TAN, inhibition at pH 7.0 is therefore likely due to an effect of NH_4^+, while inhibition at pH 8.5 is likely a result of a combined effect of NH_4^+, NH_3, and pH. Growth experiments carried out at non-inhibitory levels of TAN demonstrated that growth rate decreased with increasing pH (Figure 5.4).

A concentration of 0.3 M TAN (75 mM FAN) at pH 8.5 was selected to impose ammonia stress in the hope that NH_3 levels would be high enough to show a specific response to this N species in the transcriptome. Ammonia stressed growth was compared with unstressed growth at 0.009 M TAN (2.4 mM FAN) at pH 8.5, and sodium stressed growth (0.5 M sodium) also at pH 8.5. Growth conditions were selected that would induce an approximately 50% decrease in the growth rate

under stressed, versus unstressed conditions. Growth curves from triplicate cultures harvested for transcriptomic analysis under each condition are shown in Figure 5.5. The average growth rates under ammonia stress, sodium stress, and unstressed growth were 0.35 ±0.03, 0.43 ±0.02, and 0.54 ±08 hr^{-1}, respectively. The sodium stressed growth caused a prolonged lag phase when compared to unstressed and ammonia stressed growth.

5.3.2 Sequencing quality

The genome assembly consisted of 12 contigs totaling 2.02 Mb with an average coverage of 4500x. Contigs 1-4 were assembled onto a single scaffold from paired-end reads. Of the total reads, only 30% mapped to the predicted ORFs, while 60-65% mapped to intergenic regions. This could have resulted from several potential problems including DNA contamination, inaccuracy in the ORF predictions, rRNA contamination, or an abundance of polycistronic transcripts. Visual inspection of sequenced reads mapped to the genome showed many reads mapping to sequence regions between highly expressed gene clusters, suggesting polycistronic transcription is at least one likely cause.

5.3.3 Global interpretations of differential transcriptomics

Between the two different stressed conditions, 1113 unique genes were differentially expressed compared to unstressed growth. Figure 5.6 illustrates the range of differential expression (x-axis) and the range of confidence in these values (y-axis).

Under ammonia stress, 680 genes were differentially expressed, with 344 over- and 335 under-expressed compared to the levels expressed during unstressed growth. Under sodium stressed growth, 708 genes were differentially expressed, with 328 over- and 380 under-expressed compared to the unstressed expression levels. Only 274 of the total differentially expressed genes (25%) were shared between the two stress conditions in either direction. Of these shared genes, 66 were over and 68 were underexpressed in both conditions. Lastly, 81 shared genes were overexpressed under TAN stress but underexpressed under sodium stress, and 59 were the reverse: overexpressed under sodium stress but underexpressed under TAN stress.

5.3.4 Functional clusters of highly differentially expressed genes

Amino acid metabolism

Close examination of the most highly differentially expressed genes (|log2 (fold change)|> 2) reveals several sets of contiguous genes either over- or under-expressed, which appear to be functionally related. Two of these highly differential clusters included the CDSs for the two putative 2-hydroxyacid dehydratase complexes (HAD 488 and HAD 1432) and neighboring genes (discussed in detail in Chapter 4). Briefly, these dehydratases are key enzymes in a set of recently described protein complexes that carry out a reversible stereospecific dehydration reaction on the (R)-2-hydroxyacyl-CoA, which have only been characterized in a few amino acid fermenting bacteria (Buckel, 2001; Kim *et al.*, 2004). The 2-hydroxy acid dehydratases characterized thus far act on substrates 2-hydroxyglutarate (Buckel,

1980), (R)-3-phenyllactate (Dickert *et al.*, 2002), 2-hydroxyisocaproate (Kim *et al.*, 2005), and (R)-lactyl-CoA (Hofmeister and Buckel, 1992), as key enzymes in the fermentation pathways of glutamate, phenylalanine, leucine, and alanine, respectively.

CDS PR488-PR499 was the highest differentially expressed gene cluster under either stress condition, at between -4 and -49 fold difference compared to unstressed growth (Figure 5.7A). These CDSs were highly expressed when compared within unstressed growth alone (RPKM > 1000). CDS PR488-PR491 encode for the components of the HAD 488 (35-49 fold underexpressed compared to the unstressed condition), presumed to encode for a 2-hydroxyglutaryl-CoA dehydratase. Also underexpressed in this cluster were an acyl-CoA dehydrogenase complex (PR492), an electron transport flavoprotein (PR493-PR494), D-3P-phosphoglycerate dehydrogenase (PR495), and an aspartate aminotransferase (PR497), by between 16 and 27 fold. A second aspartate aminotransferase (PR499) and a branched chain amino acid transporter (PR498) were underexpressed by only three to four fold. These were not differentially expressed under sodium stress. Aspartate aminotransferase oxidizes aspartate to oxaloacetate, which is likely used as a primary source of pyruvate in *P. russellii*. It appears that the major amino acid utilization pathway (likely glutamate fermentation, see Chapter 4) is turned down, or nearly off, under ammonia stress.

In the second highly differentially expressed cluster, CDS PR1432-1442 were overexpressed between four and seven fold under ammonia stress, but partially

underexpressed (PR1437-PR1442) by nine to 12 fold under sodium stress (Figure 5.7B). This cluster includes HAD 1432, as well as an acyl-dehydratase (PR1435), an electron transfer flavoprotein (PR1436-1437), a (putative) D-lactate dehydrogenase (PR1438), a branched-chain amino acid/cation symporter (PR1440), an aminotransferase (PR1441) and a nUDIX hydrolase (30% BLAST identity, PR1442). The nUDIX hydrolases are described as having a "housecleaning" function that may contribute to environmental adaptability in bacteria (McLennan, 2005). These latter three (PR1440-1442) were the most highly overexpressed at seven-fold over unstressed growth. The putative proteins encoded by these genes are key enzymes in a secondary amino acid pathway, predicted to be alanine or serine fermentation, that is turned *up* under ammonia stress, but *down* under sodium stress. CDS PR1443-PR1447 were underexpressed (four to tenfold) under sodium stress and code for a cysteine desulfurase (PR1443), three hypothetical proteins (PR1444, PR1446, PR1447), and a selenium metabolism protein (PR1445) (Figure 5.7B).

Glycogen metabolism

Proteins involved in glycogen metabolism were upregulated under ammonia stress. CDS PR871-PR877 code for proteins responsible for glycogen metabolism via ADP-glucose, with glycogen synthase (PR876) and glycogen phosphorylase (PR877) being overexpressed by nine and 14 fold, respectively. These genes are overexpressed under ammonia stress, but not under sodium stress (Figure 5.8), suggesting that upregulation of glycogen synthesis is a response to either high NH_4^+ or NH_3, or a combined effect of both. Glycogen is a polysaccharide of glucose used as

a carbon and energy storage macromolecule in both prokaryotes and eukaryotes. Glycogen is typically accumulated when there is excess carbon available, and when growth is limited either by lack of nutrients (e.g., nitrogen, phosphate), entry into stationary phase, or unfavorable pH (Preiss, 1984). Glycogen accumulation (up to 60% cell dry weight) from maltose in the ruminal bacterium *Prevotella ruminicola* (Lou *et al.*, 1997) was stimulated under low growth where it and accumulates glycogen at 60% of the dry cell weight. Accumulation of intermediates of glycolysis, fructose-1,6 phosphate and pyruvate, have also been shown to stimulate glycogen synthesis.

Glycogen accumulating organisms (GAO) have been reported and studied in anaerobic/aerobic bioreactors that are operated for enhanced biological phosphate removal (EBPR). GAOs are proposed to maintain intracellular pools of glycogen in the cell, then under anaerobic conditions with excess carbon (e.g., acetate), glycogen is degraded to fuel production of polyhydroxyalcanoate (another molecule used for storing carbon and energy) (Liu *et al.*, 1996). In this case, glycogen is used as a fuel during anaerobic substrate uptake when oxygen is not available, but not for growth. Since *P. russellii* was growing exponentially under stress for several hours prior to mRNA recovery, it seems unlikely that there would be a substantial pool of existing glycogen in the cells to serve as a fuel source. Perhaps it is more likely that the cells are producing glycogen during ammonia stressed growth. The ability to store carbon and energy in glycogen by GAOs gives these organisms a competitive advantage in the EBPR systems—i.e., GAOs can outcompete phosphate accumulating

organisms (PAOs) during enhanced biological phosphate removal, leading to process upset (Tu and Schuler, 2013).

A large number of CDSs encoding ribosomal proteins were underexpressed during ammonia stress, but were not differentially expressed under sodium stress. A decrease in ribosome synthesis indicates that these cells have decreased cell growth (White, 1995), which is apparent from the difference in growth rates observed between the three growth conditions (average growth rates under ammonia stress, sodium stress, and unstressed growth were 0.35 ±0.03, 0.43 ±0.02, and 0.54 ±08 hr^{-1}, respectively) (Figure 5.4). This genetic response was not apparent in sodium stressed cultures, indicating that sodium stress at the concentration imposed here does not inhibit growth of *P. russellii* to the same extent as ammonia.

Energy conservation

Expression of the putative rnf like NADH:ferredoxin oxidoreductase complex (PR1171-PR1176) was decreased eight to ten fold under ammonia stress. Expression of this complex under unstressed growth was between ~300-500 RPKM, suggesting it has a major role in energy conservation in this bacterium during normal growth on casein peptides. The function of this electron transport complex as described recently in a number of fermenting bacteria (Biegel *et al.*, 2010) may couple disposal of excess reducing equivalents from fermentation reactions to sodium (or proton) translocation, to generate a membrane potential. This complex was recently identified in the genome of *Clostridium sticklandii* (Fonknechten *et al.*,

2010). Reduced expression of this complex would suggest a reduced ability both in disposal of electrons, and in generation of a proton potential. Considering that the major amino acid fermentation pathways are also underexpressed, underexpression of this complex may be a necessary response to maintain a balance of cellular $NADH/NAD^+$.

CDSs PR1485-PR1493 code for the protein subunits for a functional V-type ATP synthase. All but one (PR1485, subunit G) were upregulated under TAN stress (2 to 4 fold over unstressed growth) but not differentially expressed under sodium stress. This complex was expressed at very low levels under unstressed growth (RPKM < 60). A second F-type ATP synthase (PR1616-PR1622) was expressed at higher levels under unstressed growth (RPKM 500-800), and was not differentially expressed under either stress condition. Thus under ammonia stress, two ATP synthases are simultaneously operational. Proton and sodium translocating ATPases in the lactic acid bacteria may be involved in regulating pH homeostasis (van de Guchte *et al.*, 2002). Overexpression of this second V-type ATP synthase complex under ammonia stress could be in response to disruption of pH homeostasis caused by high free ammonia concentration, while the F-type ATPase is used during unstressed growth for generation of the pmf from ATP hydrolysis.

5.3.5 Transcriptional regulators

A number of transcriptional regulators from CDS that had been expressed at very low levels under unstressed growth were highly over expressed during ammonia or sodium stress conditions. One of these, PR1351 was the most highly overexpressed

(19 fold change) of any CDS under either stress condition, and it was differentially expressed only under ammonia stress. PR104 is a second transcriptional regulator also highly overexpressed (14 fold) under ammonia stress, but not differentially expressed under sodium stress. Both putative regulators were expressed at very low levels under unstressed growth (RPKM <18), which may indicates that these are involved in one or more of the responses unique to ammonia. PR1351 is a putative MarR family transcriptional regulator. While no contiguous CDSs were differentially expressed, a functional cluster of CDS encoding the enzymes for ribose utilization upstream (PR1339-PR1344) were overexpressed in the range of a two to four fold change. This highly overexpressed transcriptional regulator could potentially be a regulator for a global response to stress in *P.russellii.* PR1351 and PR104 could serve as genetic biomarkers for ammonia stress if they prove to be expressed in other bacteria or archaea under ammonia stress. Further studies could be conducted using mixed cultures or digester communities experiencing ammonia stress to search for these genes.

5.3.6 Transporters

Several transporters were differentially expressed, but at lower levels (within one to four fold over- or under- expressed) compared with unstressed growth. Of the 159 transporter proteins predicted by conserved domains, 39 were upregulated under ammonia stress, and 23 were upregulated under sodium stress. Only six of these were shared between the conditions. Transporters shared and upregulated under ammonia stress are summarized in Table 5.2. Three potassium transporters

were overexpressed under ammonia stress. One is a cation:proton antiporter (CPA) family antiporter (PR878) and was overexpressed in both ammonia and sodium stressed conditions. Interestingly, the potassium transporter expressed from CDS PR878 is just downstream of the putative glycogen operon (Figure 5.8). CDS PR878 was expressed at very low levels (<10 RPKM) during unstressed growth. Two pairs of Trk family transporters (TrkAH) were differentially expressed. TrkH is a potassium/proton (or sodium) antiporter, and TrkA is proposed to regulate the transport activity (Schlösser *et al.*, 1995). The Trk transporter system coded by PR572 (TrkH) and PR573 (TrkA) was fully upregulated under ammonia stress, but partially expressed (only the regulatory component was down regulated) under sodium stress (Table 5.2). The second putative trk transport system (PR1695/1696) was partially upregulated under both stress conditions, whereas only the regulatory component (*trkA*) was overexpressed under ammonia stress.

CDSs (PR1228, PR1229) encoding a glycine/betaine/L-proline transport protein complex were overexpressed in both stress conditions by approximately three fold. Proline and betaine have been reported to function as osmolytes in response to osmotic stress (Csonka, 1989). Glycine and proline are also utilized by *P. russellii* as electron acceptors in fermentation reactions, though likely provided through proteolysis of peptides *within* the cytoplasm (discussed in Chapter 4). These CDSs were expressed at very low levels (RPKM 30) in unstressed growth. The functional role of this transporter may be linked to osmotic stress, or amino acid fermentation, but cannot be distinguished from these experiments.

5.3.7 Evidence for an osmotic stress response or mechanism of NH_4^+ toxicity

Potassium-proton antiporters are understood to respond to both osmotic stress and disruption of pH homeostasis across the cell membrane. In the case of hyperosmotic stress (high ion concentration outside the cell), the response is to bring potassium into the cell, whereas the response to ammonia stress is to pump potassium out of the cell. In the model for NH_3 toxicity (Sprott *et al.*, 1984) free transport of NH_3 into the cytoplasm leads to an increase in the cytoplasmic pH, inducing potassium efflux that serves to bring protons into the cell to reduce the pH. Thus, in the case of ammonia stress, hyperosmotic pressure imposed by NH_4^+ would have to elicit the opposite response of that which is induced by NH_3 toxicity. Osmotic pressure imposed by increasing levels of NH_4^+ will be partially dissipated by the passage of NH_3 into the cell alone, thus at higher pH the osmotic effect may be less active than the effect of NH_3. The clear difference in the transcriptional response between ammonia stress and sodium stress demonstrated here suggests that something quite different than osmotic stress is taking place.

Under osmotic stress, potassium import is only the initial response, and is replaced by a longer term solution, i.e., the production or import of osmolytes (Csonka, 1989). The potassium/ammonium exchange observed by Sprott (Sprott *et al.*, 1984) was examined in short term exposure experiments, so it is not known whether this was only a transient response as well. Since the *P. russellii* transcripts represent the cellular response during exponential growth, the transient response of potassium

transport, induced by either species of ammonia, may no longer be operational, or operating at a lower level.

5.3.8 Analysis of phosphorus limitation

Phosphorus limitation is also known to stimulate glycogen production. Some mineral precipitation was observed in the growth medium, thus we also considered the possibility that phosphorus may have precipitated (as struvite or hydroxyapatite) under the elevated pH and ammonia concentration. Light precipitation was observed in media with high ammonia concentrations, but not in the unstressed media. The MINEQL model of the medium composition under unstressed growth versus ammonia stressed growth indicated some precipitation of these compounds is energetically favorable. It was estimated that 27% of phosphorus might precipitate under unstressed conditions, while 64% of phosphorus may precipitate under ammonia stressed conditions. Using data from cell counts to estimate cell density, and assuming a carbon to phosphorus requirement of 50:1, phosphorus is likely to be present at a concentration in excess of ten-fold the cellular need in the unstressed media, and at five fold the cellular need at 0.3 M TAN. In addition, the technical report for Bacto casitone shows that this peptide mixture can contain 2.8% (w/w) phosphate, which would increase the level of phosphate by about five fold over the original medium concentration. We therefore assume phosphate is not likely to be limiting in this growth medium, and thus the differential expression of genes encoding proteins for glycogen metabolism is likely induced by the high concentration of free and/or ionized ammonium.

5.3.9 Summary

The major aspects of the differential expression experiment, discussed above, are summarized in Table 5.3 From this data, it appears that ammonia stress, either through NH_4^+ or NH_3 toxicity, or both, elicits a number of distinct metabolic responses, the strongest being a decrease in the primary fermentation pathway (glutamate) likely responsible for the observed decrease in growth rates. Interestingly, a second fermentation pathway (alanine or serine) was upregulated. In analyzing the transcriptional response, the genes that appeared to have the strongest response under ammonia stressed growth have been discussed in the previous sections. Many more genes were differentially expressed at lower levels, including many genes that code for proteins of unknown function. Further analysis of these gene products could reveal additional responses to either stressor.

This experiment demonstrates the first comprehensive study describing the genetic response to ammonia stress in a bacterium. Extensive growth studies were carried out to ensure that free ammonia itself was at least partly responsible for the decreased growth observed. The results suggest that in this bacterium, TAN stress induces a much different genetic response than sodium stress, lending support to the idea that free ammonia imposes a unique challenge to the cell.

Growth studies also demonstrated that ionized ammonium also inhibited growth at higher concentrations. An alternate theory for inhibition in this ammonia producing bacterium could be that high concentrations of ammonium outside the cell inhibit ammonium transport out of the cell. In this case ammonia stress may have a unique

effect on *P. russellii* since ammonia is a predominant product of its metabolism. Hydrolysis of proteins occurs outside the cell whereby large proteins are broken down into smaller peptides that can be transported into the cell. As the peptides and amino acids are fermented within the cell, ammonia produced here must be transported out of the cell. No known ammonium specific transporters were identified in the genome or transcriptome, however certain potassium transporters have been shown to transport ammonium cations in animal cells (Martinelle et al., 1996). Ammonium may also be transported by non-specific mechanosensitive channels. This theory could be tested by physiological experiments whereby specific transporters are inhibited or knocked out genetically, but those approaches were beyond the scope of this study.

5.4 Chapter 5 tables

Table 5.1 Modified minimal salts medium

Component	**Amount per L**
Bacto® casitone (g L^{-1})	1.5
Yeast extract (g L^{-1})	0.3
KCl (g L^{-1})	1.3
KH_2PO_4 (g L^{-1})	0.2
NaCl (g L^{-1})	1.17
NH_4Cl (g L^{-1})	0.5
$CaCl_2 \cdot 2H_2O$ (g L^{-1})	0.1
$MgCl_2 \cdot 6H_2O$ (g L^{-1})	0.18
10% $NaHCO_3$ solution (mL L^{-1})	3.75
10% Na_2CO_3 solution (mL L^{-1})	1.25
Resazurin solution (mL L^{-1}) [a, f]	1
Vitamin solution (mL L^{-1}) [b, f]	5
Trace salts I solution (mL L^{-1}) [c]	1
Trace salts II solution (mL L^{-1})[d]	0.1
Sodium sulfide solution (mL L^{-1}) [e, f]	1

[a]resazurin stock solution was composed of 1 g L^{-1} resazurin in Milli-Q filtered water
[b]vitamin solution was composed of (mg L^{-1}): d-biotin (20), folic acid (20), pyridoxine hydrochloride (100), thiamin hydrochloride (50), riboflavin (50), nicotinic acid (50), DL-calcium pantothenate (50), vitamin B12 (10), p-aminobenzoic acid (50), lipoic acid (50), 1,4-naphthaquinone (40), nicotinamide (100), and hemin (10); dissolved in Milli-Q filtered water
[c]trace salts I solution contained (g L^{-1}): $MnCl_2 \cdot 6H_2O$ (5), H_3BO_4 (0.5), $ZnCl_2$ (0.5), $CoCl_2 \cdot H_2O$ (0.5), $NiCl_2 \cdot 6H_2O$ (0.5), $CuCl \cdot 2H_2O$ (0.3), $NaMoO_4 \cdot 2H_2O$ (0.1), and $FeCl_2 \cdot 4H_2O$ (0.1)
[d]trace salts II solution contained (mg L^{-1}): $NaSeO_3$ (30) and (80) Na_2WO_4; dissolved in Milli-Q filtered water
[e]sodium sulfide solution contained 500 g L^{-1} $Na_2S \cdot 9H_2O$ in Milli-Q filtered water
[f]filter sterilized

Table 5.2 Differentially expressed transporters

Transport Protein Family	**Predicted Function**	**Fold Change TAN**	**Fold change Na^+**	**Gene ID**
ABC Superfamily	glycine/betaine/choline transport	2.5/3	3/3	1228/ 1229
Drug/Metabolite Transporter (DMT) Superfamily	uncharacterized	3	2	1272
ABC Superfamily	Phosphate transport system permease protein (pstA)	2.5	2.5	1405
The Amino Acid-Polyamine-Organocation (APC) Family	Large neutral amino acids transporter small subunit	4	2	1476
ABC Superfamily	Arginine-binding extracellular protein artP	3	2	1717
ABC Superfamily	polyamine-transporting ATPase activity	3.5	3.5	1742
ABC Superfamily	Ribose transport	~3	~ -3	1341-1344
ABC Superfamily	phosphate transport	2.5	2.5/NDE	1404-1406
ABC Superfamily	spermidine/putrescine transport	3 to 5	-2.5/NDE	655-657
LIVCS Family	IVL transport	2/7	NDE	957/1440
CPA1 Family	sodium/potassium/proton antiporter	5	2	878

The K+ Transporter (Trk) Family	proton/potssium antiport, trkH/trkA	2.5/2	NDE/ -2	572/573
The PTS Glucose-Glucoside (Glc) Family	PTS system	3.4	NDE	674
The PTS Fructose-Mannitol (Fru) Family	PTS system	2.4	NDE	803
The K+ Transporter (Trk) Family	proton/potssium antiport, trkA/trkH	2/NDE	1.5/NDE	1695/1696

ABC = the ATP-binding cassette, LIVCS = The Branched Chain Amino Acid:Cation Symporter, PTS=phosphotransferase system, CPA= Cation:Proton Antiporter-1

Table 5.3 Summary of differentially expressed CDS groups

Predicted Function Subsystem	TAN stress	Sodium stress	Gene IDs
Alanine/serine fermentation pathway	up-regulated	down regulated	1436-1442
glycogen metabolism	up-regulated	NDE	871-877
V-type ATP synthase	up-regulated	NDE	1486-1492
Na^+/H^+ translocating NADH-quinone oxidoreductase	down-regulated	partially up-regulated	1171-1176
Glutmate fermentation	down-regulated	partially down-regulated	487-499
Osmolyte uptake (betain/glycine/proline)	up-regulated	Up	1228, 1229
Potassium transporter (CPA1) CPA	up-regulated	up	878
TrkAH potassium transport system	up-regulated	partially down-regulated	572,573
TrkAH potassium transport system	up-regulated	up	1695
LSU Ribosomal proteins	down-regulated	NDE	1506-1512
LSU and SSU ribosomal proteins	down-regulated	NDE	1283-1312

NDE = not differentially expressed, CPA = cation:proton antiporter, LSU = large subunit, SSU = small subunit

5.5 Chapter 5 figures

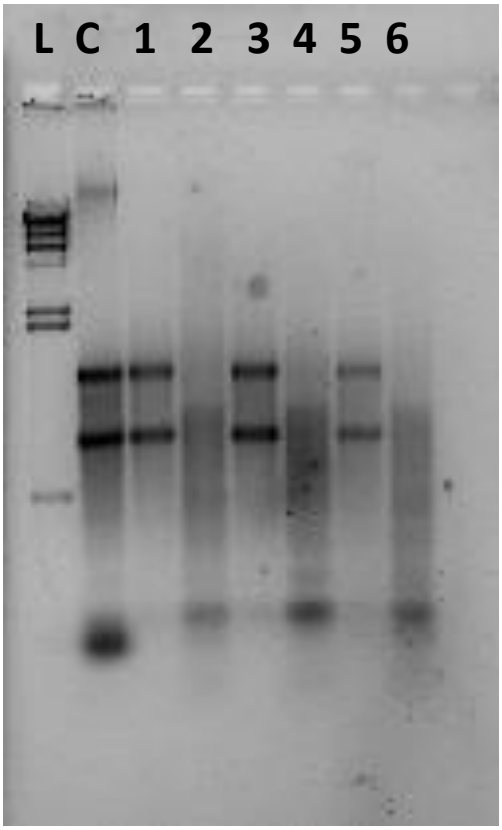

Figure 5.1. Example of RNA visual change in extracts from initial extraction to mRNA enrichment. Lanes: L, lambda HindIII (ladder); C, positive control (totRNA from another extraction); 1, sample A total RNA; 2, sample A after mRNA enrichment; 3, sample B total RNA; 4, sample B after mRNA enrichment; 5, sample C total RNA; 6, sample C after mRNA enrichment.

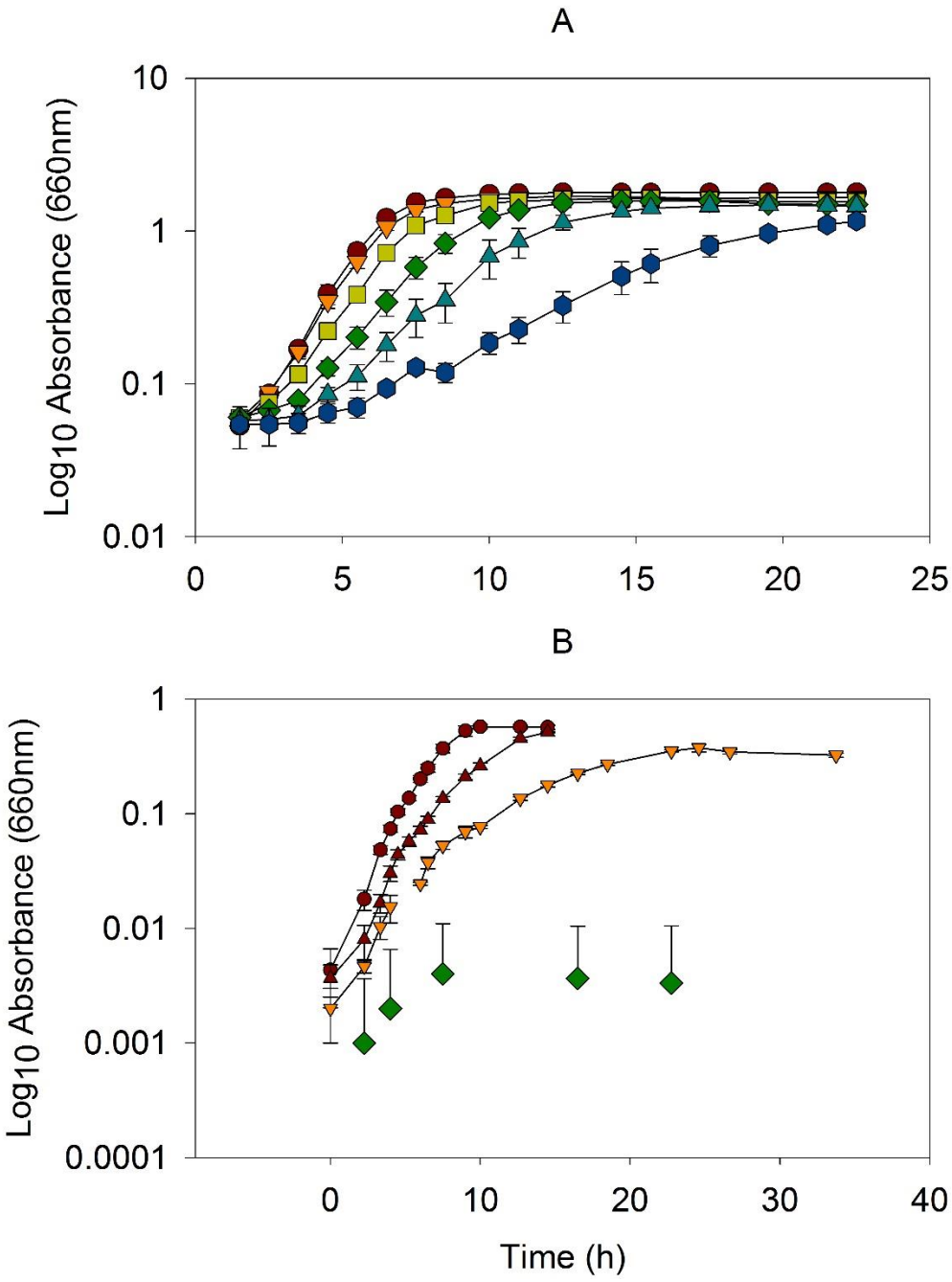

Figure 5.2 Growth curves from triplicate cultures of *Peptostreptococcus russellii* at pH 7 (A) with TAN (M): red circles (.07), orange inverted triangles (0.43), green squares (0.6), green diamonds (0.7), blue triangles (0.86), and blue circles (1); and pH 8.5 (B) in TAN range (M): red circles (.07), red triangles (0.2), orange inverted triangles (0.4), and green diamonds (0.7). Substrate was casitone; 3% for pH 7 and 1.5% for pH 8. Symbols are averages of triplicate culture and error bars are one standard deviation.

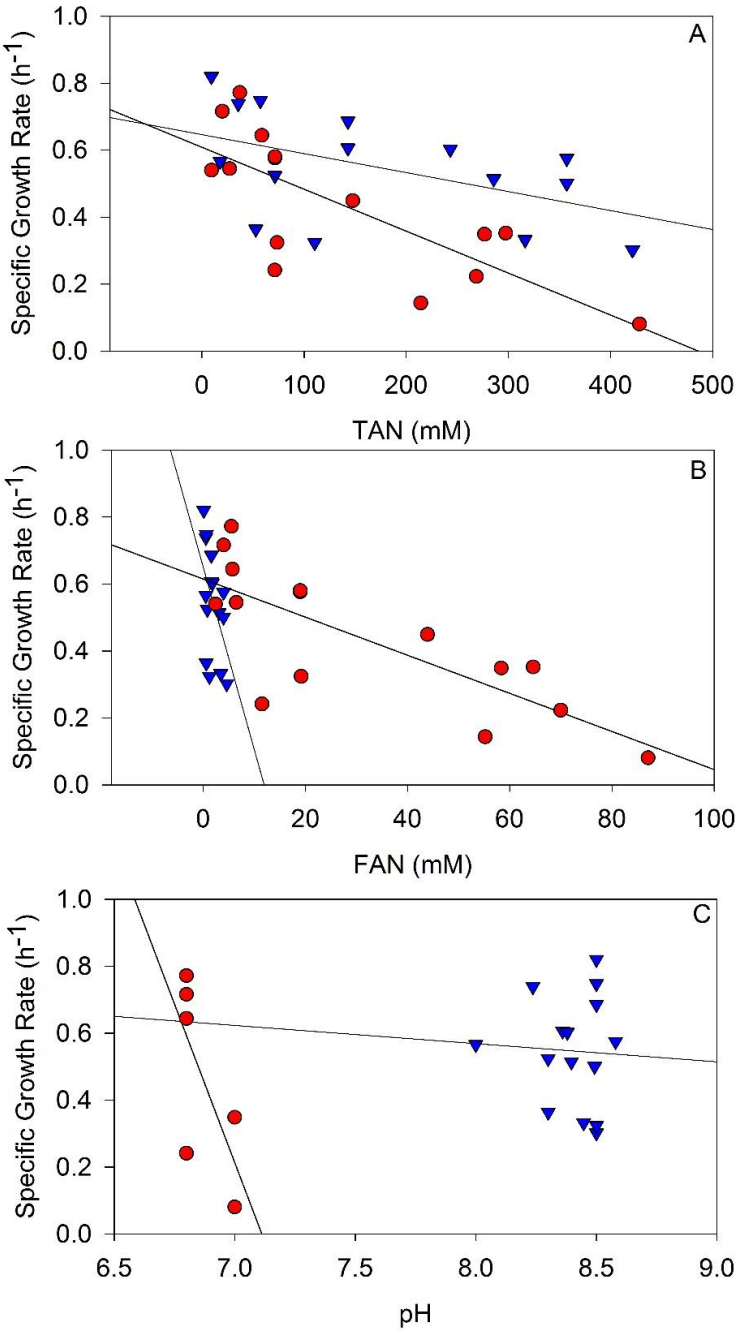

Figure 5.3. Average growth rates from 8 separate growth experiments with *Peptostreptococcus russellii* over a range of TAN and FAN at pH 7 (blue inverted triangles) or pH 8.5 (red circles). Growth rates are plotted against TAN (A), FAN (B), and pH (C). Regression coefficients (R^2) for pH 7/8.5 for each graph are as follows: A (0.2/0.6), B (0.3/0.6), C (0.5/0.0). Symbols are averages of triplicate cultures.

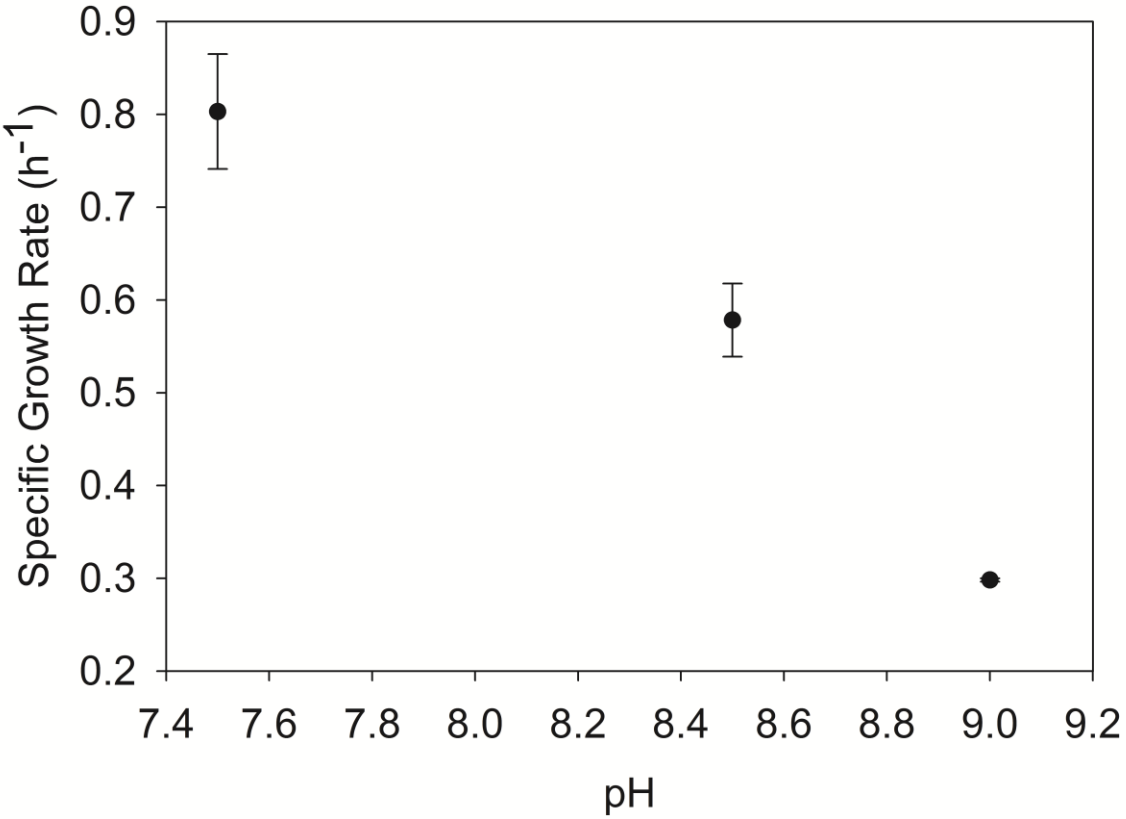

Figure 5.4 Effect of pH on growth of duplicate cultures of *Peptostreptococus russellii* under conditions of low (9 mM) TAN. Symbols are averages of triplicate culture and error bars are one standard deviation.

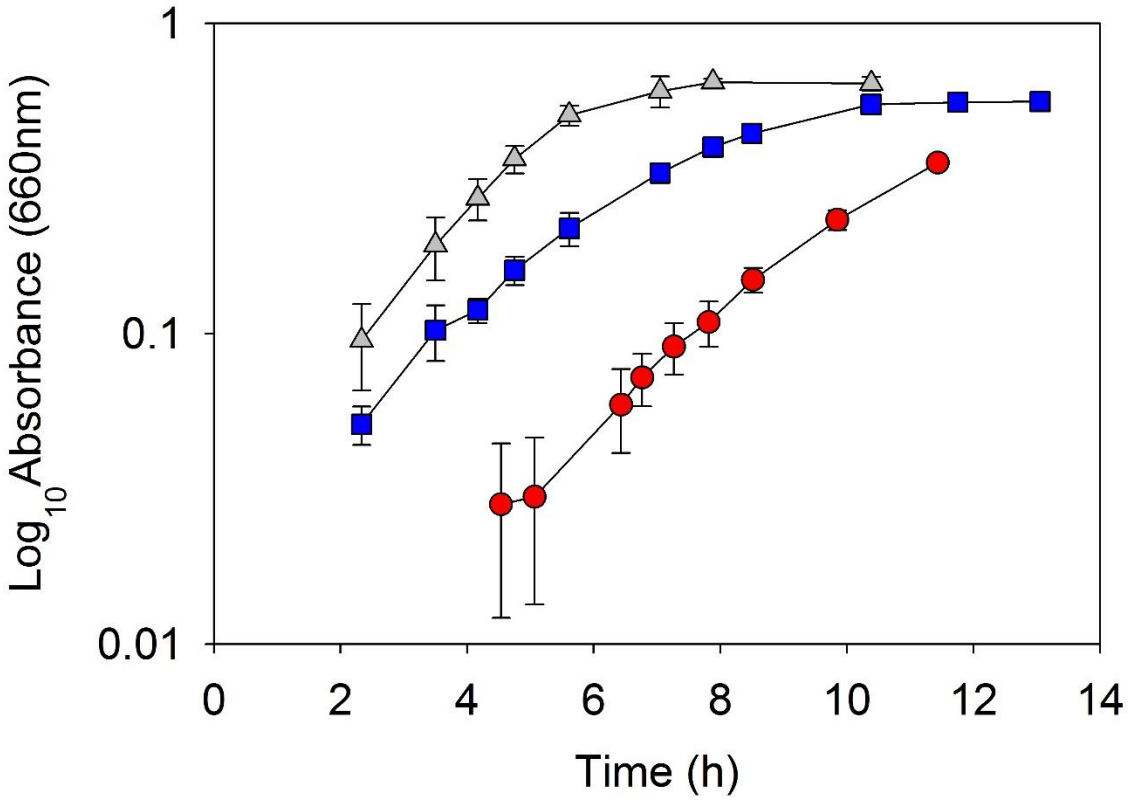

Figure 5.5 Growth curves for *Peptostreptococcus russellii* grown under no stress (grey triangles), ammonia stress (blue squares), or sodium stress (red circles). Symbols are average values for triplicate cultures used for mRNA recovery for metatranscriptomic analysis. Error bars represent one standard deviation. Corresponding growth rates for unstressed, ammonia stressed, and sodium stressed curves are 0.54 ±08, 0.35 ±0.03, and 0.43 ±0.02 h^{-1}, respectively

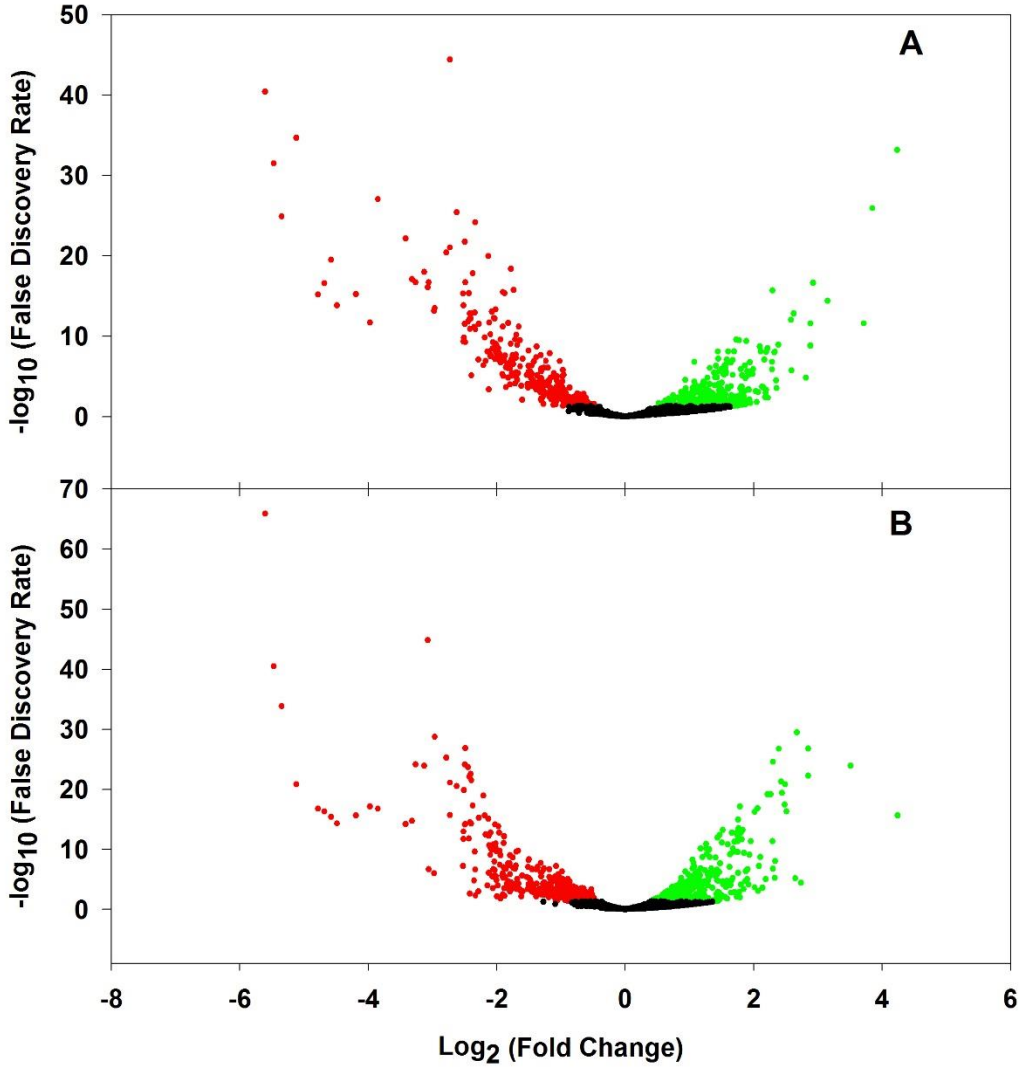

Figure 5.6 Results of differential expression analysis for *Peptostreptococcus russellii* showing mapped transcripts which were over- (green) or under- (red) expressed compared to unstressed growth, under ammonia stressed (A) and sodium stressed (B) conditions. Log_2 of the fold change is plotted to show the range more clearly. Black dots indicate transcripts that were not significantly differentially expressed.

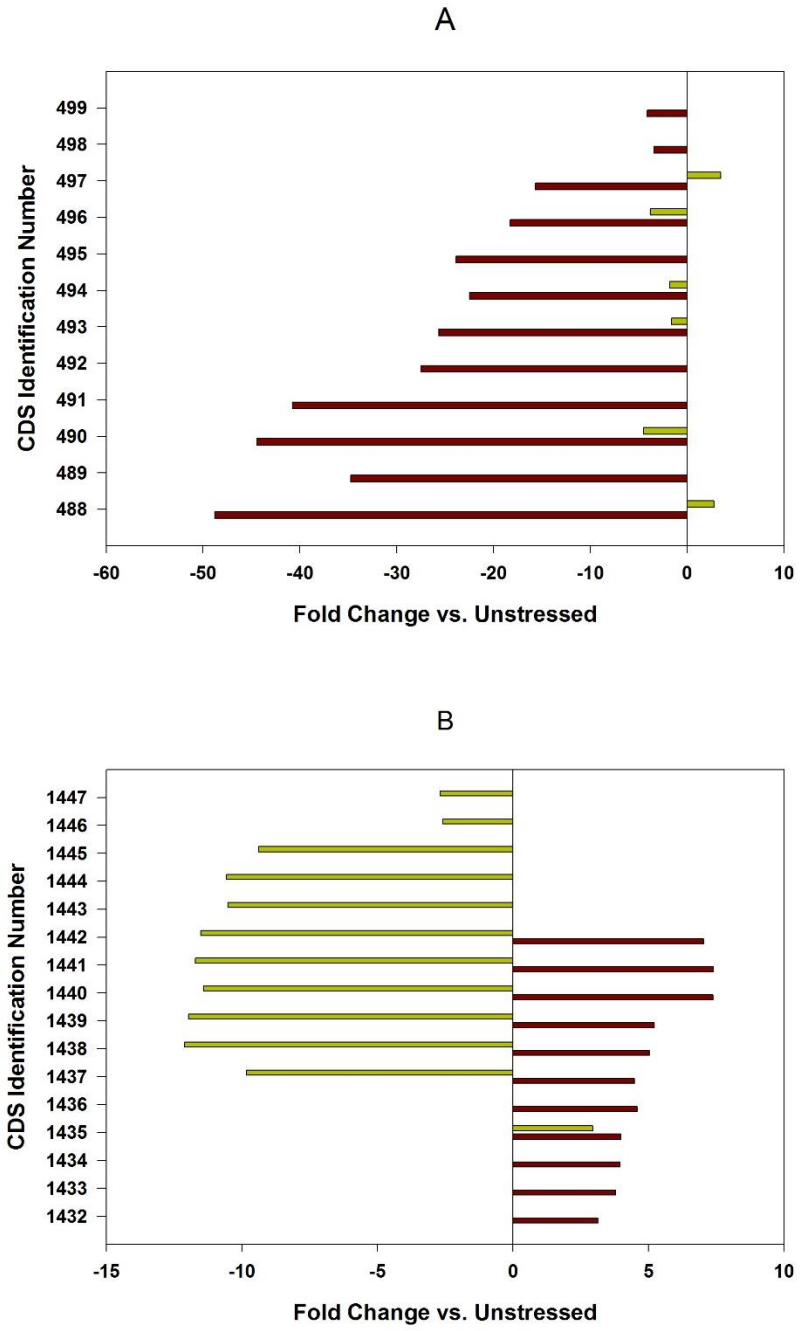

Figure 5.7 Fold change under ammonia stress (red) and sodium stress (gold) compared to unstressed growth in functional clusters PR488-499 (A) and PR1432-1447 (B) associated with amino acid fermentation pathways in *Peptostreptococcus russellii*.

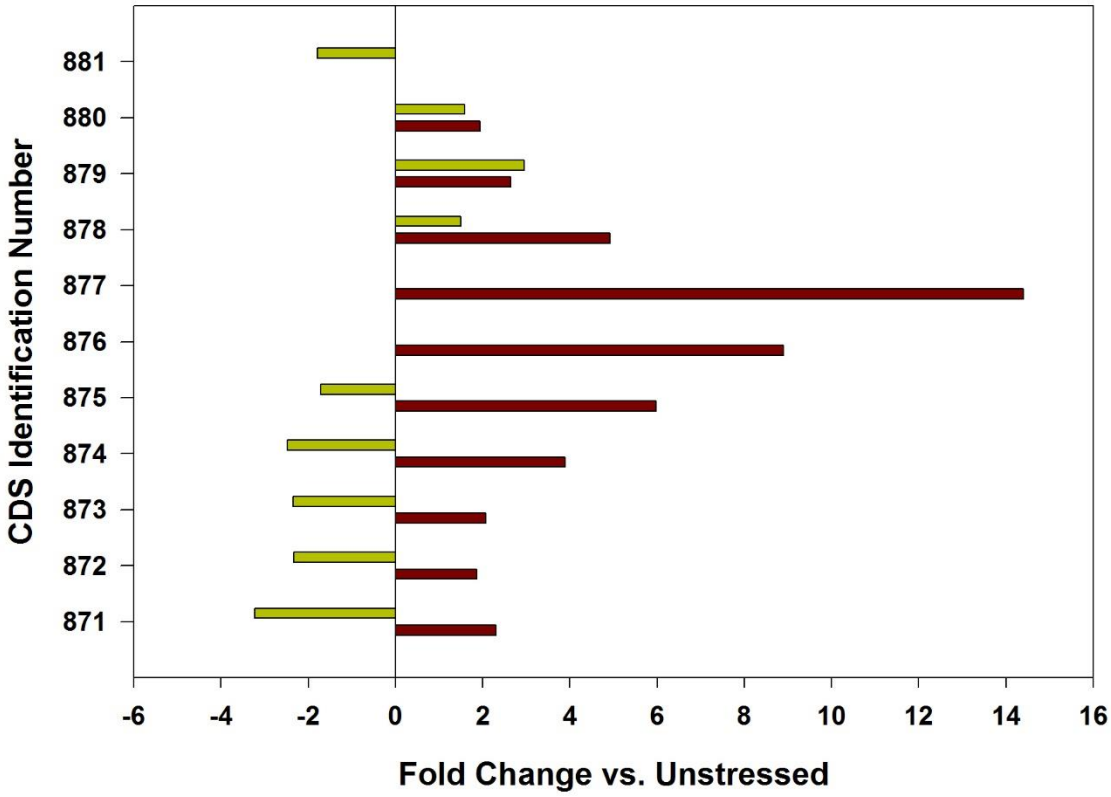

Figure 5.8 Fold change under ammonia stress (red) and sodium stress (gold) compared to unstressed growth in functional cluster expressing putative genes for glycogen metabolism, PR877-881 in *Peptostreptococcus russellii*.

Chapter 6: Electrochemically driven extraction and recovery of ammonia from human urine[a]

Luther, A., Desloover, J., Fennell, D.E., and Rabaey, K. (2015). Electrochemically driven extraction and recovery of ammonia from human urine. Accepted for publication in *Water Research*, September 2014.

[a]Research performed at the Laboratory of Microbial Ecology and Technology, Faculty of Bioscience Engineering, Ghent University, Ghent, Belgium

6.1 Introduction

Strict regulations exist for nitrogen discharge from some municipal wastewater treatment plants (WWTP). This results in considerable costs at the WWTP level in terms of energy expenditure for nitrogen removal. The major source of nitrogen in municipal wastewater is urine, accounting for 75% of the total nitrogen load (Larsen and Gujer, 1996) but less than 1% of the sewage volume. Separating urine from wastewater creates the opportunity for recovery of the ammonia at high concentration, thereby avoiding its energy intensive removal as nitrogen gas. Current established technologies for nitrogen removal from nitrogen rich wastewaters include nitrification/denitrification, direct stripping, and precipitation as struvite (for quantitative N recovery). Each of these technologies has an energetic cost that must be considered against the cost of production. The major process for ammonia production is the Haber-Bosch process, which uses natural gas or oil directly as an energy source at an electrical cost of approximately 10 kWh kg^{-1} N

(Maurer *et al.*, 2003). The Haber-Bosch process utilizes natural gas or oil directly, but the cost is represented based on electricity here for sake of comparing these technologies with the electrochemical system we evaluated. Energy expenditure for nitrification/denitrification, direct stripping, and struvite precipitation have been estimated at 4, 9, and 22 kWh kg^{-1} N, respectively (Maurer *et al.*, 2003). Considering an energy cost of approximately 10 kWh per kg of ammonia produced via Haber-Bosch, it follows that recovery of ammonia from wastewater could provide an attractive alternative source (Maurer *et al.*, 2003).

The current approaches for ammonia recovery typically produce chemically combined forms, either struvite ($MgNH_4PO_4 \cdot 6H_2O$) or ammonium sulfate through chemical precipitation (Doyle and Parsons, 2002) or stripping (Siegrist, 1996), respectively. These forms deliver limited return on investment due to their low market value. Moreover, substantial chemical addition is often needed e.g., for pH control in stripping, for quantitative nitrogen removal through struvite precipitation, or for carbon supplementation during denitrification. Here we investigate an alternative strategy, an electrochemical cell (EC) coupled to a stripping/absorption unit, for selective ammonium removal and recovery from urine. Ammonia is recovered as ammonium sulfate, but hydrogen production offers an additional high value resource if recovered. This approach was evaluated earlier for ammonia recovery from synthetic and real anaerobic digester effluents (Desloover et al., 2012, 2015). Two recent reports have demonstrated ammonia recovery from urine using a bioelectrochemical system (BES) approach via either a

microbial fuel cell (MFC) system (P. Kuntke *et al.*, 2012), or a microbial electrochemical cell (MEC) system (Kuntke *et al.*, 2014). In contrast to an EC, the BES are driven by current produced through microbial oxidation of organics in the anode.

The applied current in an EC system provides a potential difference between the electrodes great enough to drive water oxidation at the anode (oxygen and protons produced), and water reduction at the cathode (hydrogen gas and hydroxyl ions produced) leading to an acidic anode and basic cathode in the absence of buffer. The current drives electromigration of cations from anode to cathode across a cation exchange membrane (CEM). Thus NH_4^+ can be transferred from the anode to cathode where it is converted to NH_3 in the high pH environment, and then stripped (along with H_2) using an air flow. Continual removal of total ammonia nitrogen (TAN) allows constant flux of ammonium ions from the anode as the TAN concentration gradient remains constant across the membrane. The stripping gas is then passed through an acid trap or other means (such as condensation) where only NH_3 is captured and concentrated as a high purity ammonium product. Here, we used H_2SO_4 as the sorbent delivering $(NH_4)_2SO_4$. The H_2 produced at the cathode could serve as a second, high value product of this system. The excess alkaline solution from the cathode can be used for pH control during hydrolysis or for final pH equilibration of the urine.

Approximately 85% of the nitrogen in fresh urine is fixed as urea (Udert *et al.*, 2006) which is hydrolyzed by ubiquitous urease producing bacteria throughout collection

systems (Udert *et al.*, 2003) Equation 6.1 shows that hydrolysis of one mole of urea releases two moles of ammonia and one mole of carbonic acid (Mobley and Hausinger, 1989).

$$NH_2(CO)NH_2 + 2H_2O \rightarrow 2NH_3 + H_2CO_3 \qquad \text{Eq. 6.1}$$

The result of urea hydrolysis is a net increase in pH and an increase in conductivity, which enables the precipitation of calcium and magnesium ions present in the urine. Optimized precipitation via hydrolysis, upstream of EC, may provide a more suitable solution for electrochemical extraction of ammonia, which was examined in this study. Two recent reports have demonstrated treatment of real urine with ammonia recovery using a microbial fuel cell (MFC) system (Kuntke et al., 2012) and a microbial electrochemical cell (MEC) system (Kuntke et al., 2014). In these studies the MEC performed better in terms of nitrogen removal efficiency and flux; the MFC was able to produced current densities as high as 23 A m^{-2}.

The goal of this study was to evaluate the performance of an EC system for ammonia recovery from undiluted human urine under different operational parameters. To our knowledge, the application of electrochemical cell (EC) treatment for ammonia recovery from human urine has not previously been reported. Initial tests were performed with synthetic urine (ammonium carbonate solution with the pH and concentrations of hydrolyzed urine), without additional pH adjustment. After key parameters such as HRT and current density impact were established, EC treatment of real, undiluted human urine was evaluated.

6.2 Materials and Methods

6.2.1 Medium composition

A synthetic urine solution was developed from the model of fresh urine presented by Kuntke (2013). It was modified to reflect the change in composition that would result from biologically induced hydrolysis of urea and precipitation (e.g., hydroxyapatite, struvite, and calcite) in a urine collection system (Udert *et al.*, 2003). Synthetic urine contained (g L^{-1}): $(NH_4)_2CO_3$ (27.5), NaCl (4.72), KCl (3.6), Na_2SO_4-$10H_2O$ (3.9), KH_2PO_4 (70 mg L^{-1}), and K_2HPO_4 (90 mg L^{-1}). This assumes nearly 100% removal of magnesium and calcium. The pH of this solution was 9.1 without adjustment.

Approximately 14 L of fresh human urine was collected throughout one day from 23 females and 20 males. Urine was pooled, mixed and divided into two batches, designated A and B, and subsequently stored at 4°C prior to use (not exceeding 40 days). Batch A was used for System I experiments and batch B was used for Systems II and III experiments.

After storage at 4°C and prior to use as a feedstock, urine batches were pretreated with jackbean urease (Sigma, cat# U1875, St. Louis, MO, USA) at 1 mL (500-800U) per liter urine to hydrolyze urea and initiate salt precipitation. The urine was incubated for 4-5 days at room temperature without mixing. The extent of the hydrolysis was determined using samples taken before and after urease pretreatment for each run and analyzed for the following: TAN, total Kjeldahl nitrogen (TKN), pH, conductivity, chemical oxygen demand (COD), chloride, nitrite,

nitrate, phosphate, sulfate, potassium, calcium, magnesium, and sodium. After hydrolysis, precipitates (presumably struvite, $MgNH_4PO_4 \cdot 6H_2O$; hydroxyapatite ($Ca_5(PO_4)_3(OH)$); and calcite, $CaCO_3$ (Udert *et al.*, 2003) settled and the supernatant was carefully decanted to serve as reactor feed.

6.2.2 Experimental Setup

Three reactor configurations (systems) were used to assess electrochemical ammonia extraction and recovery on real urine (Figure 6.1). Tests were first performed on synthetic urine in a continuously electrochemical cell to establish operational parameters for subsequent testing with human urine. System I incorporated a stripping/absorption unit in which the catholyte was recirculated over the stripping column. System II utilized a vacuum pump (VWR International, Radnor, PA, USA) to strip ammonia from the headspace of the anode influent reservoir; this gas stream was then merged with the gas stream from the stripping column to feed directly into the absorption column. System III directed the anode directly over the stripping column without EC extraction. The EC and stripping/absorption unit materials and construction were identical to those used in a previous study (Desloover *et al.*, 2012) and a detailed schematic is given there. An important difference is that the air flow through the stripping/absorption units was run in an open circuit rather than in a closed circuit (Figure 1). Further modifications to air flow are described below. Additional details are provided in the materials section below.

6.2.3 Electrochemical Cell

The electrochemical cell (EC) consisted of two compartments (internal dimensions: 8 × 8 × 1.9 cm, 2 cm wall thickness) made from two square Perspex® frames separated by a cation exchange membrane (CEM) (Ultrex CMI-700, Membranes International Inc., USA). A titanium (Ti) electrode coated with iridium mixed metal oxide (Ir MMO) was used as the anode (dimensions: 7.8 × 7.8 cm; 1 mm thickness; specific surface area 1.0 m^2 m^{-2}, Magneto Special Anodes, The Netherlands) and a 316L stainless steel mesh was used as the cathode (mesh width 564 μm, wire thickness 140 μm, Solana, Belgium). These layers were sandwiched between rubber sheet seals, cut to the frame dimensions to create a liquid tight seal, and bolted between two Perspex® frames. The anode was placed 1 cm from the CEM, the cathode was placed approximately 4 mm from the CEM, and both had a projected surface area of 64 cm^2. The cathode was treated as the working electrode and the anode as the counter electrode. A VSP Multi Potentiostat (Bio-Logic Science Instruments SAS, Claix, France) was used for electrochemical control. The cathodic half-cell potential was measured by a Ag/AgCl reference electrode (assumed +0.197 V vs standard hydrogen electrode (SHE), Bio-Logic Science Instruments SAS, Claix, France) immersed in the cathode compartment.

6.2.4 Stripping/absorption unit

The stripping and absorption unit consisted of two tubular columns (height 0.7 m, width 0.07 m). The stripping column contained a liquid recirculation reservoir of 80 mL with a 6 cm (approximate) layer of large diameter (approximately 1 cm) plastic

filter bed rings immediately above the liquid to improve gas distribution through the column. The balance of the stripping column depth (0.5 m) was packed with AR-GLAS® Raschig rings (4 x 4 mm; Glasatelier Saillart, Meerhout, Belgium). Catholyte (or urine in system III) was distributed over the stripping column through a multi-spout nozzle (built in house) installed at the top of the column. The absorption column depth (0.5 m) was packed with AR-GLAS® Raschig rings (4 x 4 mm; Glasatelier Saillart, Meerhout, Belgium) and filled with 500 mL of 3 M H_2SO_4 in all experiments.

6.2.5 Systems operations

Table 6.1 shows the operation protocol for the EC and three system configurations examined. For the EC tests, a range of anode influent synthetic urine flow rates and applied currents were applied to assess EC performance at different anodic hydraulic retention times (HRTs) and applied currents. A solution of 0.1 M NaCl was fed through the cathode at a flow rate of 5 L d^{-1} (HRT 0.6 h). Anode and cathode were fed continuously and each compartment was internally recirculated at a rate of 6 L h^{-1} to provide mixing. EC runs were performed under open circuit (OC), and at 10, 30, or 50 A m^{-2} for each of the four HRTs tested, in duplicate, for a total of 32 runs. Anode and cathode effluents were sampled four times over a 4 to 6 hour period after steady state (three HRTs) was reached.

In Systems I and II, hydrolyzed urine was fed continuously at 0.5 L d^{-1} (6 h HRT), and the catholyte was internally circulated over the stripping unit (thereby increasing the total effective cathode volume to 202 mL). The cathode feed rate was

decreased to 0.5 L d^{-1} (11 h HRT, including the stripping column volume), and again internal recirculation rates for both anode and cathode were 6 L h^{-1}. The stripped gas was circulated via a vacuum pump from the top of the stripping column to the bottom of the absorption column in an open circuit (air flow rate: 2.5–4.5 L min^{-1}). In System I, the anode feed bottle was covered but not gastight. In configuration II the gas from the feed bottle headspace was evacuated via a second vacuum pump (gas flow rate: 2.5–4.5 L min^{-1}, open circuit) and combined with the stripping gas flow just prior to the absorption column. Anode influent, anode effluent, cathode effluent and the absorption column were sampled once daily after steady state conditions (3 HRTs) were reached.

In System III, the EC cell was omitted to determine nitrogen recovery from stripping alone. A 900 mL batch of hydrolyzed urine (reserved from batch B) was internally circulated from a 1L bottle at approximately 6 L h^{-1} directly over the stripping column. Stripping gas flow was the same as in System I setup. Samples were taken frequently over 3 days from the influent bottle and the absorption column. Samples from all experiments were stored at 4°C.

6.2.6 Chemical Analysis

Total Kjeldahl nitrogen (TKN) and ammonium (NH_4^+) were measured by steam distillation according to Standard Methods (Clesceri *et al.*, 1998). Sodium, potassium, calcium, and magnesium were measured by flame-atomic adsorption spectrometry (AAS) (Shimadzu AA-6300, Shimadzu Scientific Instruments, Somerset, NJ, USA). Prior to analysis samples were acidified with hydrochloric acid

(K^+ and Na^+) or nitric acid (Mg^{2+} and Ca^{2+}). Additionally 2% of a 1 g L^{-1} lanthanum standard solution (Chem-Lab, Zedelgem, Belgium) was added to Mg^{2+} and Ca^{2+} samples before measurement. Nitrate, phosphate, chloride, and sulfate were measured by a Metrohm 761 compact ion chromatography system (Metrohm AG, Herisau, Switzerland). COD was measured directly using a Nanocolor® COD kit (Machery-Naegel GmbH & Co., Düren, Germany).

6.2.7 Calculations

Ammonium flux, current efficiency (CE), nitrogen (TAN) removal efficiency, and power input per kg TAN extracted were calculated for all EC systems to assess performance. Current efficiency refers to the molar fraction of an ion transferred across the membrane per mole of electrons transferred, and refers to ammonium nitrogen (NH_4^+-N) unless otherwise specified. Nitrogen removal efficiencies reflect the efficiency of NH_4^+-N transfer through the EC while nitrogen recovery efficiencies reflect efficiency of NH_3-N stripping from the catholyte, thus these are useful in comparing EC performance in different systems. Power input is reported as kWh and reflects only the electrical input to the EC. TAN recovery through the entire system (EC + stripping/absorption) was calculated to compare the performance of different systems in terms of nitrogen recovery by performing a mass balance of each system. The maximal theoretical migrational flux was computed for each system using Equation 6.4 and compared to actual performance.

The nitrogen flux (J_N, g N m^{-2} d^{-1}) from anode to cathode was calculated as:

$$J_N = \frac{(C_{An,in} - C_{An,out}) \times Q_{an}}{A} \quad \text{Eq. 6.1}$$

where $C_{An,in}$ (g N L^{-1}) and $C_{An,out}$ (g N L^{-1}) are the measured ammonium concentrations of the anode influent and effluent, respectively. Q_{an} (L d^{-1}) is the anode flow rate and A (m^2) is the membrane surface area (equal to projected anode and cathode surface area).

The nitrogen flux can be presented as a current density (I_N, A m^{-2}) by:

$$I_N = \frac{J_N \times z_{NH_4^+} \times F}{M \times 86400\ s\ d^{-1}} \quad \text{Eq. 6.2}$$

where z_{NH4+} (-) is the charge of NH_4^+, F is the Faraday constant (96485 C mol^{-1}) and M is the molecular weight of nitrogen (14 g mol^{-1}).

The current efficiency (CE, %) was calculated as:

$$CE = \frac{I_N}{I_{Applied}} \times 100 \quad \text{Eq. 6.3}$$

Where $I_{Applied}$ (A m^{-2}) is the applied current density.

The theoretical maximum nitrogen flux ($J_{N,max}$, g N m^{-2} d^{-1}) was calculated as:

$$J_{N,max} = \frac{I_{Applied} \times z_{NH_4^+} \times M \times 86400\ s\ d^{-1}}{F \times A} \quad \text{Eq. 6.4}$$

The theoretical maximum nitrogen removal efficiency (RE_{max}, %) was calculated as

$$\text{Removal efficiency}_{max} = \frac{J_{N,applied} \times A}{C_{An,in} \times Q} \times 100$$

Eq. 6.5

where $J_{N,applied}$ (g N m^{-2} d^{-1}) is the applied current density expressed as a nitrogen flux.

Actual removal efficiency (RE, %) was calculated as

$$\text{Removal efficiency} = \frac{(C_{An,in} - C_{An,out})}{C_{An,in}} \times 100$$

Eq. 6.6

The power input per kg of nitrogen transferred to the cathode (P_N, kWh kg^{-1} N) was calculated as:

$$P_N = \frac{CellV \times I_{Applied} \times 1000 \times 86400 \text{ s d}^{-1}}{J_N \times 3600000 \text{ J kWh}^{-1}} \quad \text{Eq. 6.7}$$

where CellV is the cell voltage.

Nitrogen recovery efficiency (%) was calculated as:

$$Recovery\ Efficiency = \frac{\left((C_{an,in} - C_{an,out}) \times Q_{an}\right) - C_{cat,out} \times Q_{cat}}{\left((C_{an,in} - C_{an,out}) \times Q_{an}\right)} \times 100 \quad \text{Eq. 6.8}$$

where $C_{cat,out}$ (g N L^{-1}) is the measured TAN concentration in the cathode effluent and Q_{cat} is the cathode flow rate

Nitrogen removal rate (g N d^{-1}) for EC systems was calculated as:

$$Nitrogen\ removal\ rate = J_N \times A \quad \text{Eq. 6.9}$$

Nitrogen removal rate for the direct stripping (system III) was calculated as:

$$Nitrogen\ removal\ rate = \frac{V_{t_2} \times C_{t_2} - V_{t_1} \times C_{t_1}}{\Delta t} \quad \text{Eq. 6.10}$$

where C is the TAN concentration (g N L^{-1}) measured in the reactor at the time of sampling, V is the volume (L) in the reactor at time of sampling, and Δt is the time between sampling points (d).

Removal capacity was calculated for system I from the average nitrogen removal rate, divided by the volume of the anode compartment. Elimination capacity for system III was calculated from the nitrogen removal rate for a given time for comparison, divided by the influent vessel volume.

Current efficiency for NH_4^+ was calculated using Equation 6.3 where $I_{applied}$ = reported average current density produced during stable operation, and J_N = NH_4^+ flux at the middle of the run. Because diffusional transport was not measured, this value may actually be lower. Electrical power input per kg nitrogen recovered was calculated by Equation 6.7, where CellV= 1V, $I_{applied}$ = average current density produced during stable operation, and J_N = given flux for the middle of the run.

6.3 Results and Discussion

6.3.1 EC performance for ammonium (NH_4^+-N) extraction: Synthetic Urine

Decreasing the hydraulic residence time for a set current increases the nitrogen flux, but decreases the nitrogen removal efficiency. Nitrogen removal efficiency had a strong positive correlation with HRT (correlation coefficient (r) > 0.8) for all applied currents (Figure 6.2B), reaching a maximum of 86.7 ± 0.2 % at 50 A m^{-2}, 8.2 h HRT. As the HRT is increased more time is available for nitrogen transfer across the membrane. Nitrogen flux had a weak negative correlation with HRT (r < -0.5) under open current and an applied current of 10 A m^{-2} (Figure 6.2A). Increasing the HRT at high applied current eventually led to exhaustion of the buffer capacity of the anolyte, leading to a substantial drop in pH at 8.3 h or 6.3 h under applied current densities of 30 A m^{-2} and 50 A m^{-2}, respectively (Figure 6.3A). The drop in pH corresponded to a plateau in nitrogen RE, and a pronounced drop in nitrogen flux at 12h HRT. At 30 A m^{-2}, there was no linear correlation between HRT and flux.

Increasing the applied current density at any anode HRT increased both nitrogen flux and nitrogen removal efficiency. This is apparent from examination of results from each run (each represented by a single point) in Figure 6.2 A-B. When plotted against current density (not shown), both nitrogen flux and removal efficiency had a strong positive linear correlation (r > 0.9) with current density. Migrational flux is limited by the applied current density, so as the current is increased, maximal theoretical migrational flux (reference lines Figure 6.2A) is increased (see Eq. 6.4). When no current is applied both flux and RE are below 100 g N m^{-2} d^{-1} and 25%,

respectively when nitrogen transfer is driven by diffusion alone. Open current runs (zero applied current) indicate diffusional transport accounting for 4-11% of nitrogen flux at HRTs between 2.8 and 8.3 h, and 22% at the 12.4 h HRT. Cathode pH increased from 8.5 ± 0.2 at open current to 11.9 ± 0.1 at 50 A m^{-2} (Figure 6.3B). Cell potential was stable over each run, with an average of 2.6 ± 0.0 V and 3.8 ± 0.1 V at applied currents of 10 and 50 A m^{-2}, respectively.

Current efficiency (CE) decreased as both HRT and applied current increased (Figure 6.2C). CE had a stronger negative correlation with applied current than with HRT. A maximum CE of 108 ± 21 was observed at 10 A m^{-2}, 2.8 h HRT (Figure 6.2C). Increasing the applied current, or increasing the HRT both increased the proton concentration in the anode either by increasing proton production or accumulation, respectively. The synthetic urine solution is strongly buffered by the ammonium carbonate, which acts to limit proton accumulation. The buffer is consumed by protons, but also decreases as ammonium is removed. The substantial pH decrease observed here results in an approximately 10^5 increase in the concentration of protons that then compete with ammonium transfer, thus reducing the CE of ammonia.

Optimizing the EC system requires a compromise between nitrogen removal efficiency (treatment) and power input for this recovery (cost). Higher removal efficiency indicates lower residual nitrogen in the effluent i.e. a more complete treatment. However, achieving low residuals in this system requires a proportionally higher applied current and a longer HRT, both of which lead to a

lower CE, which in turn leads to an increase in the cost of nitrogen removal (kWh kg^{-1} N) from the system (Figure 6.4B). Figure 6.5 highlights the relationship between nitrogen flux and anode effluent as a function of current and HRT. High effluent levels (low nitrogen removal efficiency) cluster at low applied current densities for all HRTs, while the lowest effluent residuals are achieved at high flux matched with a long HRT. To balance cost and removal efficiency, current should be applied above 10 A m^{-2} with an HRT in the middle of the range tested (i.e, 4 to 6 h). HRT and current density can be adjusted to control the anode pH in order to optimize the reactor performance. The highest nitrogen flux (500 ± 22 g N m^{-2} d^{-1}) was achieved at the highest applied current matched with a 2.8 h HRT, while the maximum RE (86.7 ± 0.2%) required an HRT of 8.3 h (Figure 2D) at this same applied current.

6.3.2 Urine Pretreatment: Urea hydrolysis and salts precipitation

Total Kjeldahl nitrogen was lower in our sampled urine composite than expected from previous reports (Kuntke et al., 2013; Udert et al., 2006). This could be due to differences in the individual urine donors. Urea hydrolysis in real urine occurred rapidly upon urease addition, and initiated precipitation of phosphate, magnesium and calcium. Major components of each batch before and after hydrolysis are listed in Table 6.2 along with the synthetic urine recipe. Upon urease addition pH increased from 6.6 to 9.3, conductivity increased from 14 to 36 μS cm^{-1}, and approximately 91% of TKN was released (via hydrolysis) as TAN. Precipitates began to form immediately upon hydrolysis and settled to the bottom of the reaction

vessel. Phosphate, magnesium, and calcium precipitated and were removed from solution at 46-54%, 97-98%, and 48-56%, respectively.

The extent and distribution of these precipitates will vary depending on the concentration of these ions in the urine, which can vary from person to person, and in the water, which can vary in hardness by location. The degree of dilution by flushing will also determine precipitation dynamics. Formation of these precipitates throughout the collection system is problematic, and will require modifications in systems intended for low or no flush toilets. Precipitates, particularly those of calcium and magnesium, can also cause problems in EC systems through scaling of the CEM. Removal and optimization of precipitation dynamics upstream of the anode compartment will be an important step towards implementing this EC system.

Analysis of the molar ratios of ions before and after hydrolysis suggests the following precipitates formed. Assuming all Mg^{2+} removal is due to precipitation of struvite and/or potassium struvite, phosphate removal cannot be fully accounted for only by struvite precipitation. In both batch A and batch B hydrolysis experiments, phosphate was removed at a molar ratio of 1.2:1 (PO_4^{2-}:Mg_2^{+}). Enough calcium removal occurred to account for the formation of HAP from the remaining phosphate, leaving some additional calcium remaining. The last of this calcium could have precipitated as calcite.

6.3.3 Electrochemical extraction from real urine: EC performance

EC performance over the course of the experiment was stable for System I, but decreased steadily for System II where ammonia stripping was introduced to the influent headspace. Figure 6.6 shows key performance parameters under open circuit (day 1) and under an applied current density of 40 A m^{-2} (day 2-9 for System II; and day 3-10 for System I). 50 A m^{-2} was applied briefly on day 2 for System I. System I maintained an average nitrogen flux of 275 ± 5 g N m^{-2} d^{-1} (9% of this was from diffusion based on the OC run), while System II reached nearly the same level (235 g N m^{-2} d^{-1}) on day 2, but dropped steadily to 83 g N m^{-2} d^{-1} by day 9 (a nearly 3-fold decrease). Likewise, System I maintained stable power input, nitrogen RE, and CE while System II performed similarly at day 2, but thereafter deviated from the performance of System I (values provided in Table 6.3). Between days 2 and 4 the vacuum pump failed for System II which may account for the increase in flux and CE at day 4 (Figure 6.6 A,D). Without headspace stripping, System I experienced a 23% loss of TAN from the influent by day 3 but saw stable TAN for the remainder of the run (Figure 6.7A). This loss was likely due to initial volatilization then ultimate equilibration of NH_3 within the headspace of the influent vessel. On day 3 of the system II run, the anolyte flow rate was increased to reach 0.5 L d^{-1} (daily measurements indicated flow rate was low), which is the likely cause for the increased flux and CE values at day 4 (Figure 6.6 A,D).

The steady decrease in System II performance can be directly attributed to the loss of TAN in the anode influent feed due to ammonia stripping from the headspace

(Figure 6.7B). System II did not reach a true steady state (with respect to performance parameters) as a result of continuous headspace stripping of TAN from the anode influent; System II performance does serve to demonstrate the strong effect influent TAN concentration has on practically every measurement of EC performance. System II did succeed in maximizing total nitrogen recovery reaching a total of 79% compared with 57 ± 0.5% for System I (Table 6.3), but this was over the entire 10 d run. Thus recovery could be increased by the additional stripping, but overall HRT would be much higher. As influent TAN dropped from 4.1 to 1.6 g L^{-1} from day 6 to 9 (Figure 6.7B), power input rose sharply from 16 to 41 kWh kg^{-1} N (Figure 6.6D), a consequence of low anode effluent TAN.

Overall performance of System I was lower than expected based on that observed for synthetic urine (Table 6.3). For operation using real urine runs, a higher current was imposed in an attempt to maximize the current density, while minimizing the HRT to prevent a pH drop to below 6. Poorer performance is likely due to a lower buffer capacity of the real urine resulting from lower TAN and bicarbonate concentrations post-hydrolysis, than were present in the synthetic urine. This results in the drop in anode pH to 2.5, corresponding to a higher concentration of protons (competing with ammonium ions) and a lower maximum theoretical flux. Current efficiencies for other major ion species in the urine were calculated for runs with real urine. CEs were stable in System I, with ammonium transport dominant, followed by proton/hydroxyl ion, sodium, then potassium, respectively (Figure 6.8A). CEs in System II started out the same as in System I, but as anode influent

TAN decreased, the CE of ammonium decreased with a concomitant increase in the CE of protons/hydroxyl ion. This is likely the result of a drop in both the pH (Table 6.3) and TAN concentration (Figure 6.7B) in the anode effluent. Calcium CE was less than 0.1% in both systems, and no transport of magnesium was detected. Some hydroxyl leakage can occur even across a CEM, but could not be differentiated from proton flux here.

Although very little calcium was transferred, its accumulation in the cathode compartment could be the cause of scaling observed in cathode compartment at the end of experiments. Further experiments could be conducted to investigate the composition of the scale, since this will be an important issue for application of this technology. Further optimization of the stripping and absorption system is also necessary to improve this technology. In these experiments, absorption efficiency decreased over only ten days of operation. In part, this loss in efficiency may be due to the failure of the air pumps. In addition to reducing absorption efficiency losses, pump failures resulted in an increase in the catholyte ammonia concentrations. At higher catholyte TAN, efficiency of ammonium transfer across the membrane would also be reduced.

The current applied in the system is high enough to drive chloride oxidation in addition to water oxidation, which would produce chlorine gas in the anode compartment. Chlorine is highly reactive with ammonia and may produce ammonia chloride species which can be highly toxic. The use of the IrOx anode should discourage chlorine gas formation because it has a low activity towards chlorine

oxidation, however it does not eliminate this reaction totally. Further development of this technology should consider chlorine gas evolution to ensure safe operating conditions.

Finally, the cost of the electrochemical extraction is still higher than ammonia production from Haber-Bosch technology, and this does not consider the cost of air and liquid pumps. Since hydrogen gas is produced at the cathode, a modified reactor designed to strip the ammonia from the gas passively, may reduce the overall electrical cost.

6.3.4 Ammonia recovery by direct stripping from urine

Direct stripping of the hydrolyzed urine achieved high total nitrogen recovery at high HRT. Total nitrogen recovery by stripping increased from 3.3% at 1 hour to 83% after 77hours (Figure 6.9) with corresponding removal capacities from 7.6 to 0.9 g L^{-1} N d^{-1}, and a decrease in the absorption rate from 3.6 to 0.5 g N d^{-1}. The disparity between removal and absorption rates indicates nitrogen was lost from the system. The greatest disparity observed in the first hour corresponds to an absorption efficiency of only 49%, a loss of only 3.4% of the total nitrogen in the system. An average absorption efficiency of 95 ± 5% was observed for the remainder of the experiment, indicating these losses were limited to the first few hours. Equilibration of NH_3 within the headspace may account for this loss.

System III cannot be directly compared against system I since it was operated as a batch system. To roughly compare the performance of the EC to direct stripping in

terms of ammonia removal rates, removal capacities are used to compare the volumetric rate of ammonia removal in each system at similar HRT, since HRT has a substantial effect on removal rates in each system. The removal capacity for system III, calculated from the 6.2 h time point (reference line, Figure 6.9) was 1.6 g N L^{-1} d^{-1}, while that for system I was 14.5 ± 0.2 g N L^{-1} d^{-1}. Direct stripping displayed a lower removal capacity, by nearly 10 fold, e.g., a longer HRT or is required to reach the same level of ammonia removal as the EC. While direct stripping may be less costly, it would require more time to reach the same level of treatment.6.3.5 Stripping efficiency, absorption efficiency and nitrogen balance

Nitrogen recovery efficiencies, as calculated, reflect the stripping efficiency from the catholyte and were similar for both Systems I and II. Vacuum pump failure occurred in both System II and III runs, and pumps had to be removed and cleaned in each case, resulting in at least two days of pump downtime. This first failure resulted in an increase in the TAN concentration in the catholyte to 2.9 g L^{-1} on day 6 in System I (Figure 6.7A), however, the initial steady state TAN resumed after the pump was reinstalled. Excluding periods when stripping or headspace evacuation was off, System I had an average stripping efficiency of 75 ± 0.6%. System II had an initial stripping efficiency of 58%, which increased to an average of 76 ± 1.4% over the last three days (following a vacuum pump downtime) (Table 6.3).

Absorption efficiency in System I was initially 95% but decreased to 60% by the end of the run. System II exhibited an increase in the catholyte effluent concentration from day 2 through 4, at which point gas flow through the absorption unit had

noticeably slowed. The pump was replaced on day 6 and cathode effluent subsequently dropped sharply. Absorption efficiencies for System II thus reached 94% on day 2, and 96% on day 9, but dropped in between these two points. Absorption efficiencies remained > 90% after 5 hours for System III. The nitrogen balance at the beginning of the run for System I was 97%, but dropped to 79% by the end of the run. The overall, average, nitrogen balance was 80% for System II and 100% for System III.

6.3.6 Comparison of EC systems with BES for ammonia recovery from urine

Comparing ammonia recovery from urine via the EC systems described in this study versus recovery using bioelectrochemical systems (BESs) operated either as MFCs that produce electricity (85) or as MECs that require minimal electrical power input and produce hydrogen gas (9) is useful because of the increasing interest in these systems for wastewater treatment. Key operational parameters and performance measurements for EC systems investigated here versus BESs are shown in Table 6.3. The comparison is somewhat hindered because of differences in feed composition and reactor configurations. For the MFC (P. Kuntke *et al.*, 2012)and EC (this study) systems, undiluted urine with a TAN of (~ 4 to 5 g N L^{-1}) was used as a feedstock; however, the MEC system (Kuntke *et al.*, 2014) feedstock was 5-fold diluted urine (0.7 g TAN/L). Further, the MFC system utilized an air cathode in contrast to the liquid cathode utilized by the MEC and EC (this study) and so cell configuration was quite different. Additionally, both anode and cathode chambers in the MEC used a chambered flow through design, which is different than the design used here.

With respect to nitrogen flux and nitrogen removal efficiency, the EC system performed better than both the MEC (Kuntke *et al.*, 2014) and MFC (P. Kuntke *et al.*, 2012). Nitrogen flux in System I was 275 ± 4.57 g N m^{-2} d^{-1} compared with 175 in the MEC and 3.3 in the MFC (6.3). As the anode influent TAN dropped in the EC (System II) flux dropped to 82.7 g N m^{-2} d^{-1}, below that of the MEC. Nitrogen removal efficiencies in the EC were more than double that of the MEC, and 10-fold higher than in the MFC. The advantage of the EC is largely due to the higher currents that can be applied in these systems, since both flux and removal efficiency are limited by the current. In the BES current production is in turn limited by the microbial activity at the anode. In this type of system, pH, ammonia toxicity, and electron donor limitation are some of the most relative factors that will affect microbial activity. Electron donor limitation may be limited by the available reduced carbon, or by competition for carbon with non-electrogenic microbes in the anode.

Whereas the BES approach has the advantage of producing (MFC) or consuming (MEC) less power, the strictly electrochemical approach has the advantage of greater stability, predictability, and flexibility in terms of controlling the reactor, since biological systems are more sensitive to pH, temperature, and loading rates (e.g., ammonia concentration). This is an advantage when influent feed concentration and flow (urine collection throughout the day) can vary greatly. COD removal may be seen as a benefit to the BES system, however, this in fact limits the system with respect to obtainable current density (current production is dependent on microbial consumption of COD) and thus flux. Based on our data, it also appears

the electrochemical system is capable of a higher overall ammonia recovery, due mainly to the ability to produce higher current densities which deliver greater nitrogen flux.

We have demonstrated here that an electrochemical system can be used successfully to recover ammonia from concentrated urine with high efficiency. We envision application of this technology in a decentralized treatment scenario whereby highly pure ammonia and hydrogen gas are recovered as valuable products against the cost of treatment. Discharge of anode effluent to the sewer system would still substantially reduce the nutrient load to wastewater treatment plants and thus reduce costs at these facilities. The cost of the recovery through EC ($\sim$ 13 kWh kg^{-1} N) is higher the cost of ammonia production via Haber-Bosch ($\sim$10 kWh kg^{-1} N), but has the alternative benefits of decreased downstream wastewater treatment costs, lower emissions along the sewer line and in the case of the EC production of an alkaline solution that could aid in struvite precipitation. Furthermore, the Haber-Bosch process is lower cost because it utilizes fossil fuel as the hydrogen source and to fuel the reaction—a resource that would become more costly if climate change regulations are put into place.

6.3.7 Potential to reduce wastewater treatment costs

We have demonstrated here that an electrochemical system can be used successfully to recover ammonia from concentrated urine with high efficiency and moderate cost. We envision application of this technology in a decentralized treatment scenario whereby highly pure ammonia and hydrogen gas are recovered

as valuable products against the cost of treatment. The highest ammonia flux achieved here was with the synthetic urine, at 500 g N m^{-2} d^{-1}. By comparison the highest flux observed with real urine was only 276 g N m^{-2} d^{-1}. The higher flux observed with the synthetic urine is likely due to the higher TAN concentration of the synthetic feed (near 7 g TAN L-1), and the lower HRT (2.8 h in this particular run, vs 6 h HRT for real urine runs). Despite these differences, removal efficiencies were comparable for the synthetic and real urine, as we saw nearly 80 % ammonia removal efficiency across the EC for both feeds. Total nitrogen recovery from the real urine was 57%, reflecting losses due to the efficiency of the stripping/absorption unit. Discharge of anode and cathode effluent to the sewer system with these removal rates would still substantially reduce the nutrient load to wastewater treatment plants and thus reduce costs at these facilities. Considering that urine accounts for about 75% of the nitrogen input at a WWTP, this technology could reduce the nitrogen load to the plant by 43%. The cost of the recovery through the EC (~ 13 kWh kg N^{-1}) is higher than the cost of ammonia production via Haber-Bosch (~10 kWh kg N^{-1}), but has the additional benefits of decreasing downstream wastewater treatment costs lowering emissions along the sewer line, and production of hydrogen gas worth 3.8 kWh kg N^{-1}. Furthermore, the alkaline solution (cathode effluent) could aid in optimization of salt precipitation during the pretreatment, or holding stage. If additional benefits such as decreased treatment needs are considered, recovery of ammonia from wastewater could provide an attractive alternative source of ammonia nitrogen. The cost of EC recovery with and

without hydrogen recovery are presented with treatment costs of other leading technologies in Table 6.4.

One of the greatest advantages of electrochemical recovery over direct stripping or precipitation of ammonia from complex wastes, such as urine, is the high purity of the final product resulting from selective removal and absorption. While recovered ammonium sulfate could serve as a fertilizer, it could have higher value as a feedstock for production of edible microbial proteins (Matassa *et al.*, 2015) or other high-value products. The purity of the ammonium sulfate recovered in our systems was not determined, however urine contains a number of complex volatile compounds (Zlatkis and Liebich, 1971), which could be transferred to the acid trap in direct stripping. The added step of the EC extraction would reduce the chances of this contamination.

Further studies are necessary to assess the integrity of the electrodes and cation exchange membrane over long-term treatment. In this study, no corrosion was observed, but some precipitation was observed in the cathode compartment. Membrane integrity could be a primary limitation to this technology. It is also important to note that since this system relies on electricity, the primary energy source of the electricity used will greatly impact the true energy cost of the system (based on fuel conversion efficiencies). This may be seen as a disadvantage in a fossil fuel economy, but could be an advantage as alternative and sustainable electricity sources become available.

6.4 Chapter 6 tables

Table 6.1 EC and alternate system configurations overview

System	Description	Configuration	Parameters Tested
EC	synthetic urine, multiple runs, 3 HRT each	EC only	Open current and range of applied currents tested at different HRT
I	Pretreated urine, batch A, 10 d continuous run	EC + catholyte stripping/absorption	Measure performance stability
II	Pretreated urine, batch B, 10 d continuous run	EC + catholyte stripping/absorption + anode feed headspace absorption	Measure performance stability
III	Pretreated urine, batch B, 3 d batch run	No EC, stripping/absorption, recirculation of urine over stripping column	Measure N removal from influent

Table 6.2 Chemical composition of urine batches A and B before and after urease treatment

Component	**Synthetic Urine**	**Urine Batch A**		**Urine Batch B**	
		Before Hydrolysis	**After Hydrolysis**	**Before Hydrolysis**	**After Hydrolysis**
TKN (g L^{-1})	8	5.5	5.8	5.6	6.0
TAN (g L^{-1})	8	0.3	4.8	0.2	4.9
PO_4^{2-} (g L^{-1})	0.1	0.5	0.2	0.6	0.3
Mg^{2+} (mg L^{-1})	0	59.8	1.5	59.2	1.5
Ca^{2+} (mg L^{-1})	0	105.4	55.2	107.9	47.5
K^+ (g L^{-1})	1.9	1.9	1.9	1.9	1.9
Na^+ (g L^{-1})	2.4	2.4	2.4	2.1	2.0
Cl^- (g L^{-1})	4.5	3.2	2.9	3.2	2.9
SO_2^- (g L^{-1})	1.1	0.7	0.7	0.8	0.8
pH	9.1	6.6	9.4	6.6	9.2
Conductivity (mS cm^{-1})	54	15.5	35.7	12.7	37.8
COD (g L^{-1})	0	6.9	6.5	7.0	7.0

Table 6.3 Comparing performance and operational parameters for the EC, system I, and system II, with two different BESs treating urine

Parameters	**Synthetic Urine System (I)**	**EC System (II)**	**EC System (III)**	**MEC[b]**	**MFC[c]**
Applied Current Density (A/m2)	50	40	40	14.64 ± 1.65	0.5
Influent TAN (g N L^{-1})	6.5	4.8 ± 0.0	5.1, 1.7	0.7	4.1
Influent pH	9.1	9.2 ± 0.1	9.2, 8.5	9.1	8.9
Nitrogen Flux (g N m^{-2} d^{-1})	384 ±7.7	275 ± 4.57	235, 82.7	175	3.3
Anode Effluent TAN (g L^{-1})	1.3 ± 0.1	1.2 ± 0.03	1.1, 0.6		
Current Efficiency (%)	61.3 ± 1.2	55 ± 0.9	47, 16	95[d]	30[d]
Nitrogen Removal Efficiency (%)	80.7 ± 1.6	75 ± 0.5	76, 65	33.9 ± 0.6	0.7
N Recovery Efficiency (%)	n.a	76 ± 0.6	58, 76	n.r	n.r
Total Nitrogen Recovery (%)	n.a.	57 ± 0.5	79	n.r	n.r
Power Input (kWh kg^{-1} N)	12.4	12.7 ± 0.37	14.7, 41.0	2[d]	n.a
Anode pH	1.9 ± 0.1	2.5 ± 0.12	2.0, 1.5	7.5 ± 0.3	8.9
Cathode pH	11.8 ± 0.02	10.2 ± 0.2	10.6, 10.3	9.7 ± 0.1	n.r.
Anode HRT (hour)	6.2	6.0 ± 0.09	6.2 ± 0.5	1	0.015

Cathode HRT (hour)	0.66, 0.66	10.5 ± 0.49	10.7 ± 0.9	6	air cathode
Cell Potential (V)	4.0	3.7 ± 0.1	3.6 ± 0.1	1.0	0.5

n.a. indicates not applicable, n.r. not reported
[a]*values reported for days 2 and 9*
[b]*from* (Kuntke *et al.*, 2014) *an MEC treating diluted urine with catholyte NH_3 stripping*
[c]*from* (P. Kuntke *et al.*, 2012) *an MFC with air cathode and NH_3 stripping*
[d]*calculated values see section 6.2.7*

Table 6.4 Energy cost of different nitrogen removal, recovery, and production technologies

Treatment method	**MJ kg^{-1} N**	**kWh kg^{-1} N**
Nitrification/denitrification in WWTP[a]	14	4
Struvite precipitation for nitrogen removal[b]	81	23
Stripping[c]	32	8.9
Electrochemical extraction[d]	47	13
Electrochemical extraction with hydrogen recovery[e]	31	9
Ammonia production by Haber-Bosch[f]	37	10

[a]*includes electrical costs (aeration), WWTP = wastewater treatment plant, see* (Maurer *et al.*, 2003)
[b]*includes chemical costs (magnesium oxide and phosphoric acid), see* (Maurer *et al.*, 2003)
[c]*includes chemical costs (calcium oxide and sulfuric acid) and electrical costs (aeration), see* (Maurer *et al.*, 2003)
[d]*includes average electrical cost of ammonium transfer through system I of this study, (catholyte stripping only) andchemical cost of sulfuric acid included assuming 1.1 MJ kg^{-1}N*
[e]*savings from recovery of hydrogen deducted from cost of electrochemical extraction, assuming conversion factor of 33 kWh kg^{-1} H_2*
[f]*includes fuel costs (supplied by natural gas), see* (Maurer *et al.*, 2003)

6.5 Chapter 6 figures

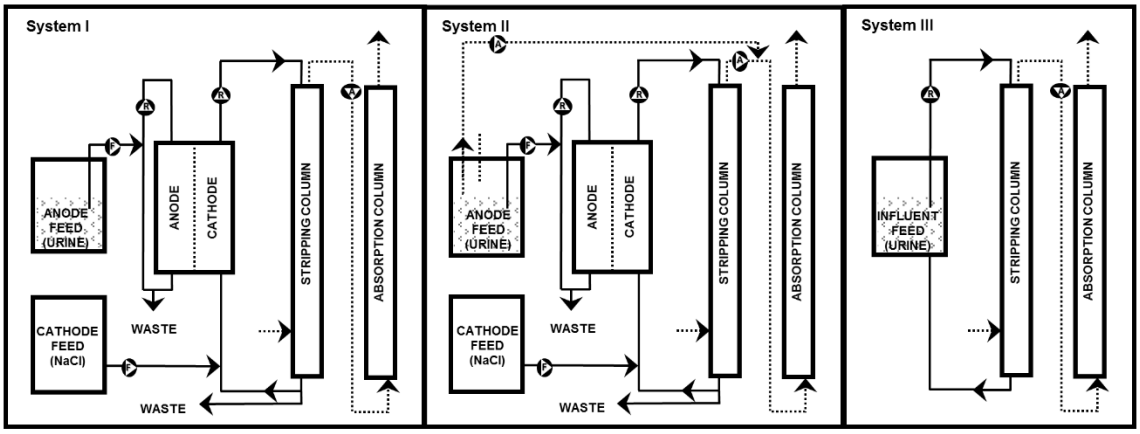

Figure 6.1. Overview of Systems I, II, and III showing system components, liquid flow (solid lines), and air flow (dotted lines).

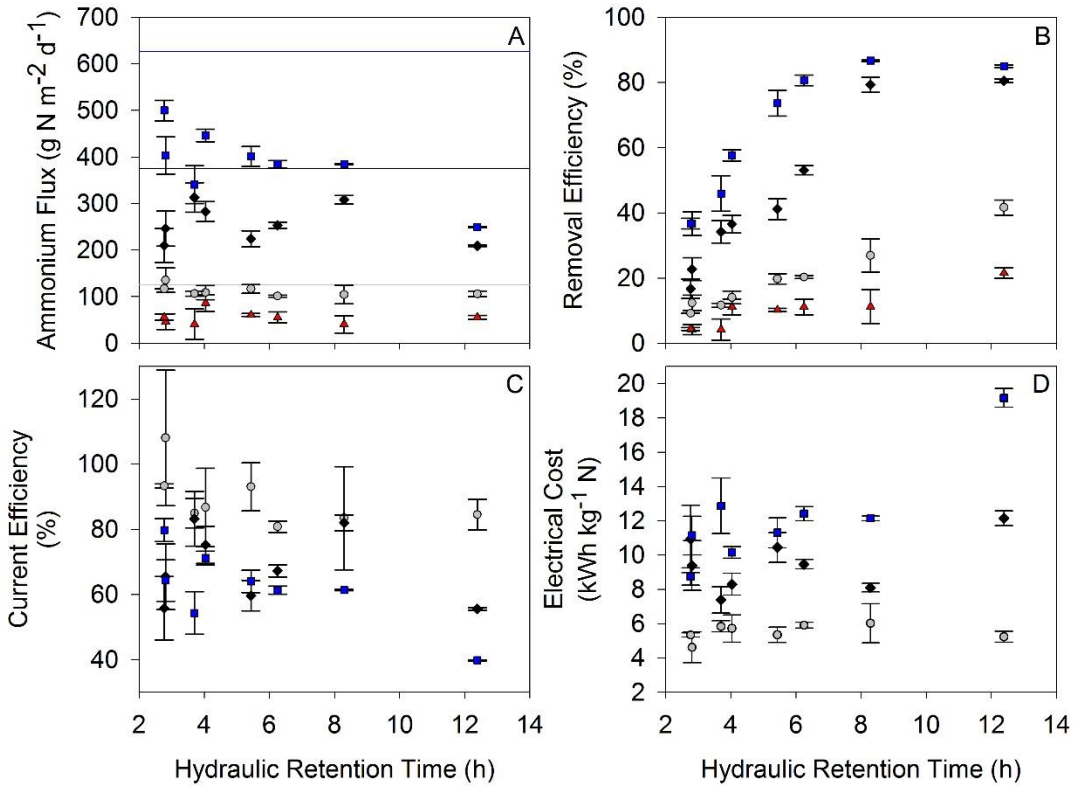

Figure 6.2 Effect of hydraulic retention time on ammonium ion flux (A), ammonia removal efficiency (B), current efficiency of ammonium ion (C), and electrical cost (D) for runs at open circuit (red triangles) and applied currents of 10 (grey circles), 30 (black diamonds), and 50 (blue squares) A m^{-2}. Averages of three samples over steady state are reported with standard deviation. Reference lines indicate maximum migrational flux, color coded for each applied current.

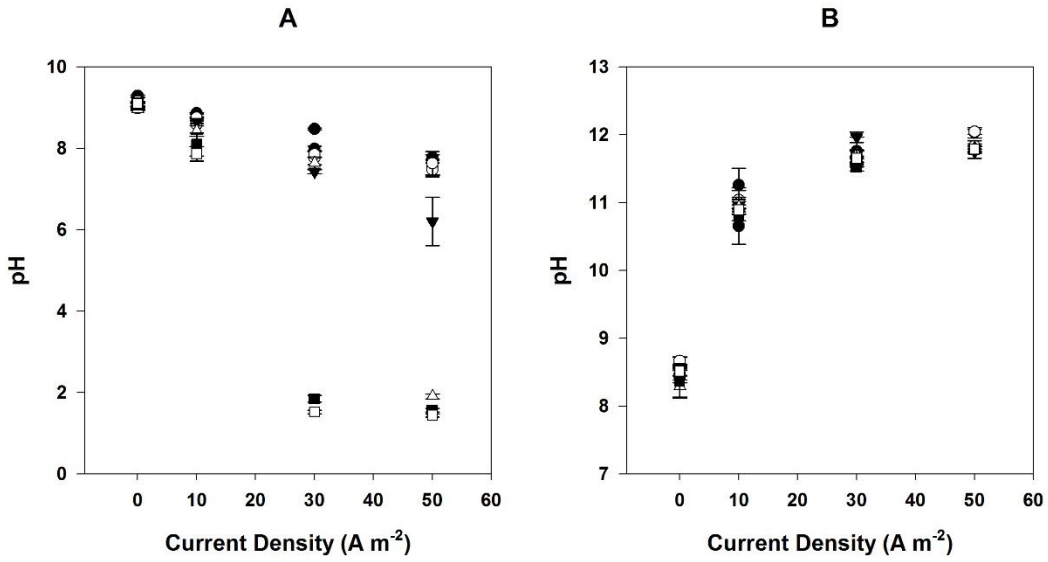

Figure 6.3 Anode (A) and cathode (B) pH for each EC run. HRTs (h): 2.8 (closed circles), 4 (open circles), 5.4 (closed triangles), 6.3 (open triangles), 8.3 (closed squares), 12.4 (open squares).

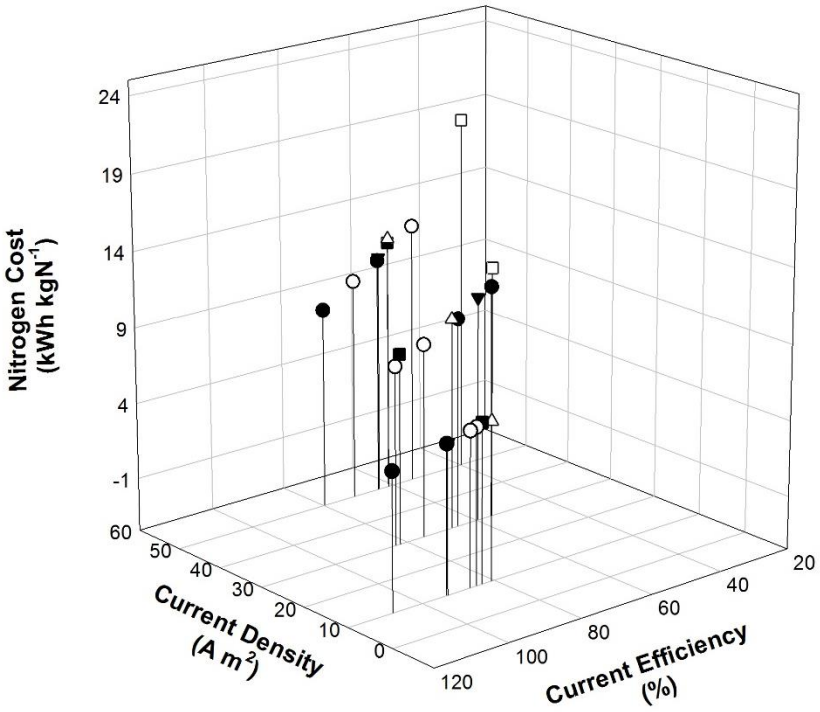

Figure 6.4 Nitrogen cost as a function of applied current density and current efficiency from all runs with synthetic urine. Series correspond with HRT (h): closed circles (2.8), open circles (4), closed triangles (5.4), open triangles (6.2), closed squares (8.3), open squares (12).

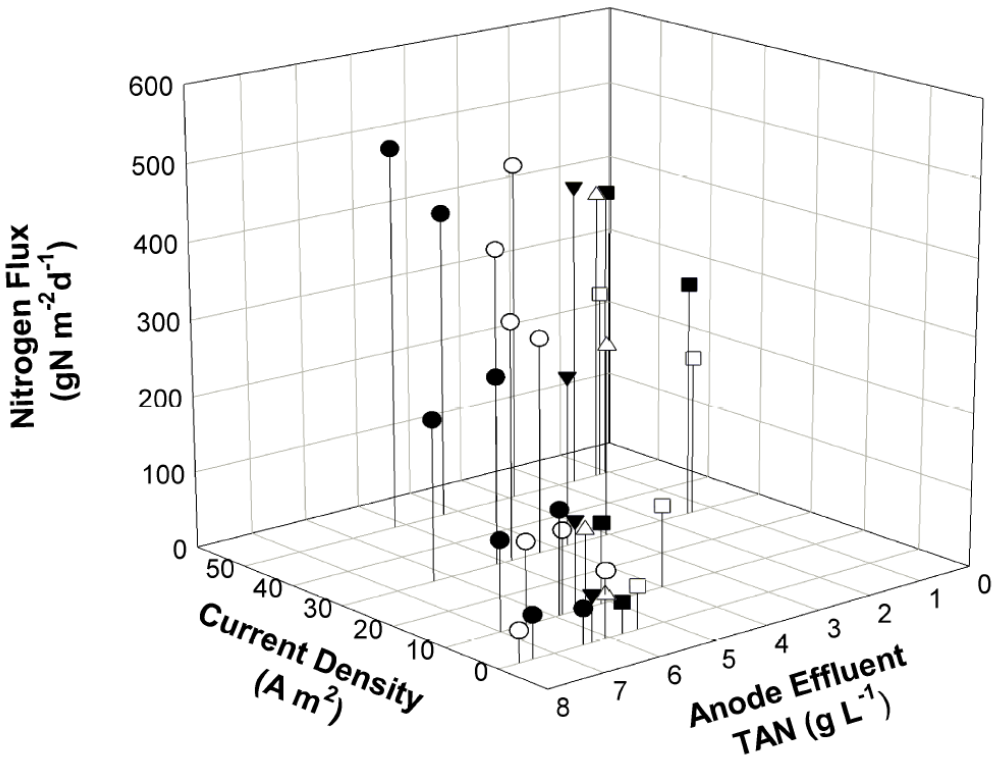

Figure 6.5 Summary of synthetic urine results. Series correspond with HRT (h): closed circles (2.8), open circles (4), closed triangles (5.4), open triangles (6.2), closed squares (8.3), open squares (12).

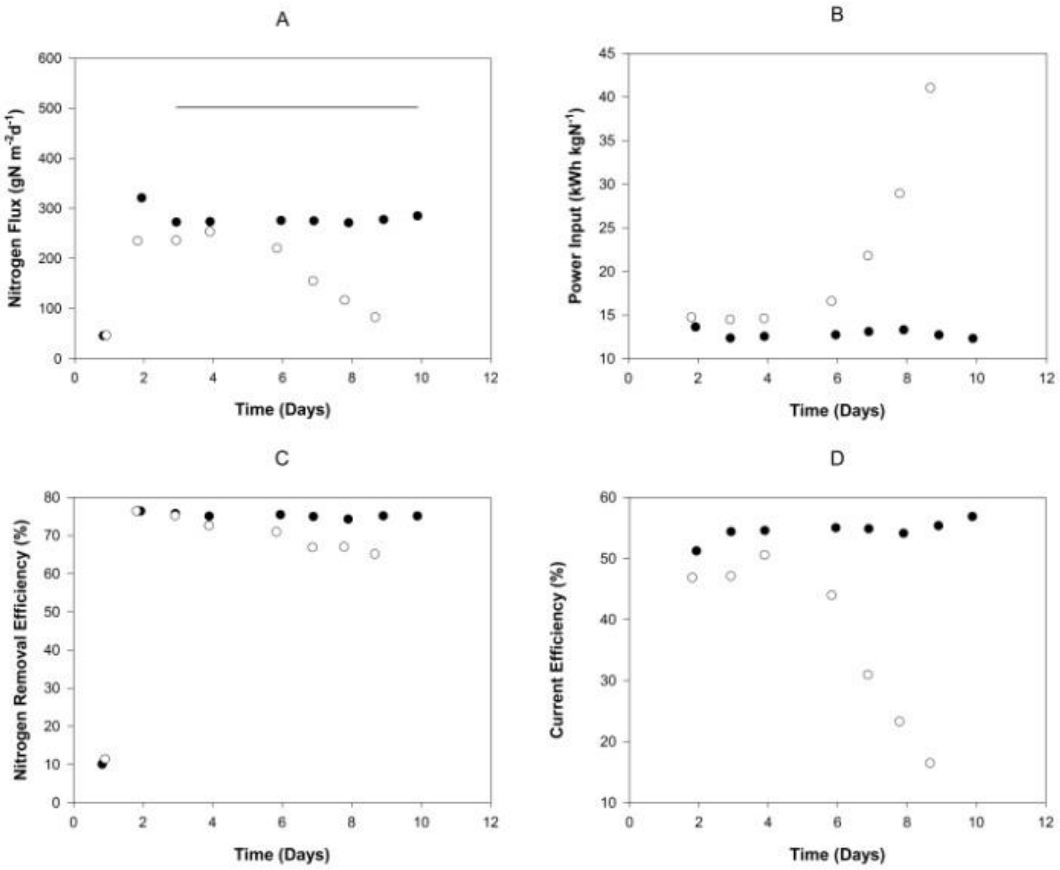

Figure 6.6 Performance of EC System I (closed circles) and System II (open circles) over the course of each run with real urine. Reactors were operated for one day under open circuit. Beginning on day 2 a current density of 40 A m^{-2} (System II) or 50 A m^{-2} (System I) was applied, and by day 3 both reactors were operating at 40 A m^{-2}. The solid line on graph C indicates maximum theoretical ammonium flux for both systems.

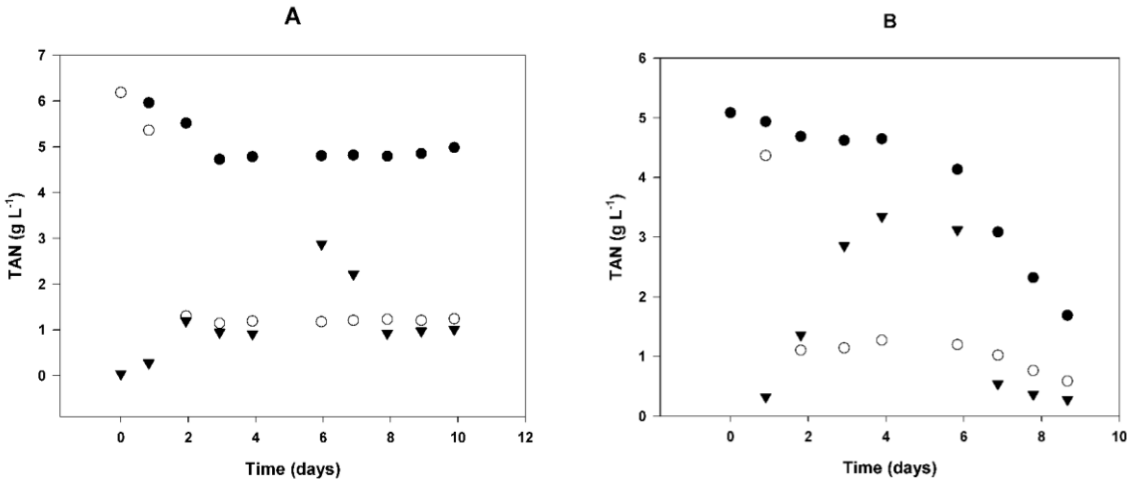

Figure 6.7 Ammonia concentrations in anode influent (closed circles), effluent (open circles), and cathode effluent (closed triangles) during Systems I and II operation.

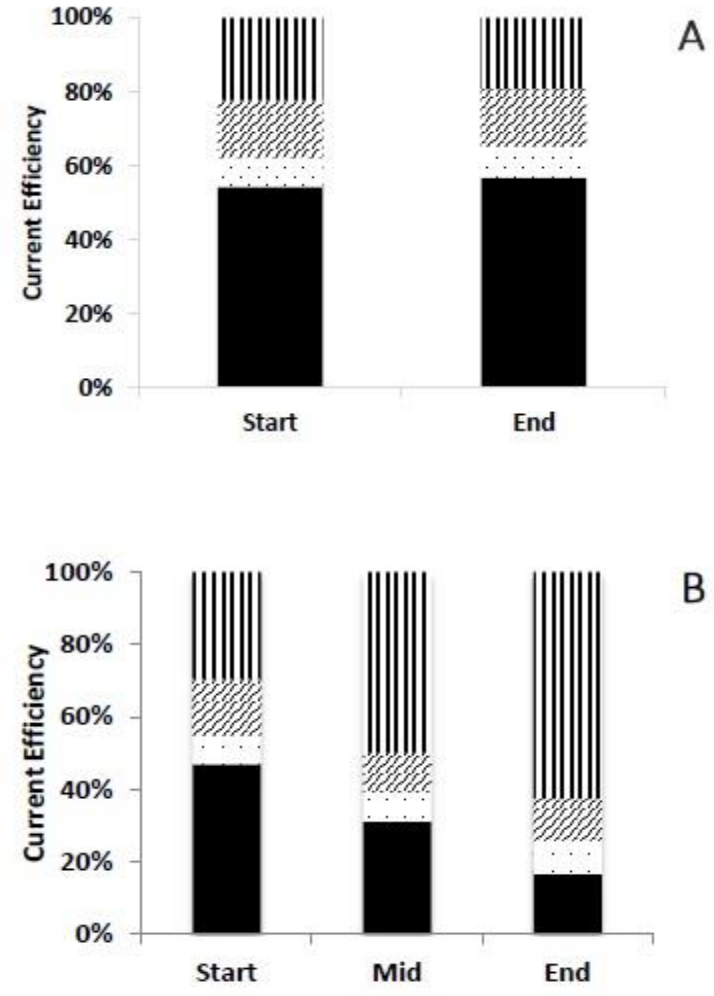

Figure 6.8 Relative proportion of major cations transported across the CEM in Systems I (A), and II (B). Ammonium (solid black), potassium (black dots), sodium (diagonal lines), and protons/hydroxyl ions (vertical lines).

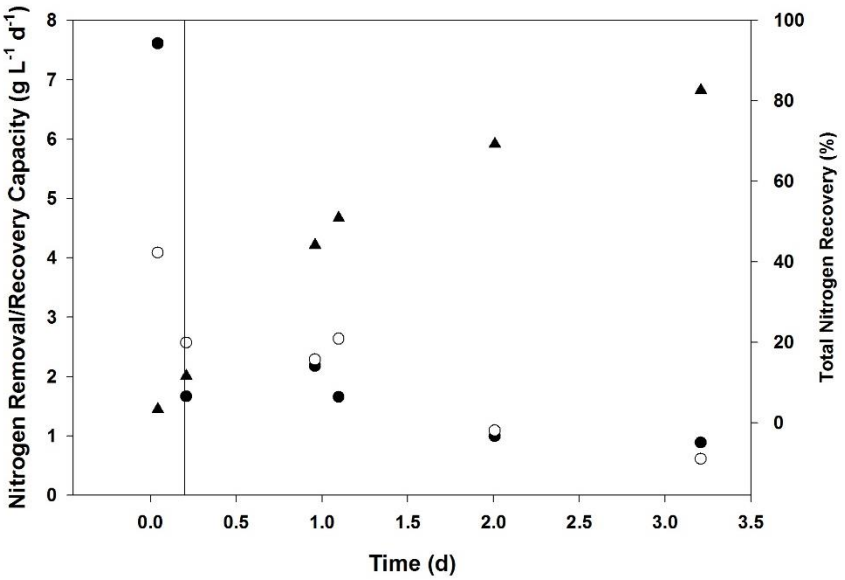

Figure 6.9 Nitrogen removal rate (closed circles), nitrogen absorption rate (open circles), and total nitrogen recovery (closed triangles) from direct stripping (System IV). Solid reference line marks a 6.2 hour hydraulic retention time for comparison with Systems II and III incorporating EC.

Chapter 7: Conclusions, Significance, and Recommendations

7.1 Conclusions

1. Amino acid fermentation by a mixed anaerobic microbial community was inhibited at casein loads of 40 and 60 g L^{-1} when compared to loads of 10 g L^{-1} during batch anaerobic digestion experiments, corresponding to TAN accumulation to 3.5 g L^{-1}, VFA accumulation to 30 mM, and high partial pressures of CO_2.
2. Increases in ammonium ion concentration were not thermodynamically limiting to the selected amino acid fermentation reactions examined here, rather pH and volatile fatty acids concentrations may have a stronger impact on thermodynamic favorability of amino acid fermentations.
3. Two putative 2-hydroxyacid dehydratase enzyme complexes are coded by two separate operons in *Peptostreptococcus russellii* and were highly expressed under fermentative growth on mixed peptides. These enzymes probably catalyze separate reactions, allowing *P. russellii* to utilize alternate fermentation pathways under different conditions of amino acids presence. Ammonia stress imposed differential regulation of these complexes, leading to increased expression of one complex, and decreased expression of the other.
4. *P. russellii* expressed the genes required for both glycine and proline reduction during growth on casein derived peptides, indicating that coupled

amino acid fermentations were utilized together with two single amino acid fermentation pathways.

5. *P. russellii* growth was inhibited by both ionized and unionized ammonia. Inhibition by NH_4^+-N was observed in the range of 6 to 9 g TAN L-1 (0.4-0.9 M), at pH 7, while inhibition by NH_3 was observed in the range of 3 to 6 g TAN L-1 (0.2-0.4 M) at pH 8.5.
6. Ammonia stressed growth induced overexpression of genes in *P. russelli* that code for enzymes used for glycogen synthesis. When grown under conditions of sodium stress, this response was not observed, which suggests that glycogen storage was specifically related to high ammonia/ammonium.
7. Down-regulation of major metabolic enzymes together with the up-regulation of glycogen metabolic enzymes suggest ammonia interferes with this bacterium's ability to generate energy, causing *P. russellii* to enter a limited growth state and stockpile energy reserves (glycogen) since the carbon source is non-limiting.
8. Transcriptional analysis showed that ammonia stress and sodium stress both induced two potassium/proton antiporters, one of which shares similarity with the trkAH potassium/proton (or sodium) transport system and a putative osmolyte transporter system, supporting the hypothesis that ammonia toxicity may in part be due to a hyperosmotic pressure effect.
9. EC processing of synthetic urine produced a maximum ammonium flux of 384 ± 8 g N m^{-2} d^{-1} with a 61 ± 1% current efficiency at a cost of 12 kWh kg^{-1} N.

10. EC processing of real urine produced similar performance, with an average NH_4^+ flux of 275 ± 5 g N m^{-2} d^{-1} sustained over 10 days with 55 ± 1% current efficiency at a cost of 13 kWh kg^{-1} N transferred.
11. Based on our data, it appears the electrochemical system is capable of a higher overall ammonia recovery than bioelectrochemical systems, due mainly to their ability to produce higher current densities, which deliver greater nitrogen flux.

7.2 Significance

We hypothesized that there might be some universal ammonia stress response in ammonia-tolerant microorganisms exposed to high concentrations of TAN. If a universal response was observed, such genes could be selected as biomarkers that could be used to monitor anaerobic digesters during dynamic operation, or could be detected in mixed microbial communities—thus indicating whether the community contained abundant ammonia-tolerant members. Such a set of biomarkers would be useful for designing feeding strategies for digesters (for example to lessen ammonia stress) or for monitoring microbial community enrichment in ammonia-tolerant microbes to ensure stable performance. The two putative transcriptional regulators that were found to be highly overexpressed uniquely under ammonia stress may be good candidates for such a biomarker, and further studies could be completed to further characterize the expression profiles of these proteins under a wider range of ammonia stressed conditions.

Previously, methanogens (*Methanosarcina thermophile* TM-1 and *Methanosarcina mazei* S-6) were shown to exhibit a dose dependent response in induction of *trkA* expression under ammonia stress (Hofman-Bang *et al.*, 1999; de Macario and Macario, 2003). The TrkA protein performs a regulatory role in K^+ efflux systems that function to maintain pH and osmotic homeostasis and its upregulation would appear to support the supposition that ammonia disrupts pH and/or osmotic homeostasis of cells. Here we observed a low level transcriptional response under both ammonia and sodium stress inducing the expression of two different potassium/proton transporters, including a putative *trkA* gene as was observed in the methanogen studies. Thus ammonia stress may induce a similar response in both bacteria and archaea.

This study has yielded valuable information about the adaptation of *P. russellii* to stress conditions—both sodium and ammonium. One clear response to ammonium stress in *P. russellii* is the initiation of glycogen synthesis. Since nutrient limitation is thought to result in carbon storage in microorganisms, we excluded the possibility that phosphorus could have been limiting by calculating the removal of phosphate through (theoretical) struvite and hydroxyapatite formation. The systems do not appear to have suffered from P limitation, and certainly N was not limiting. It cannot be excluded that other unknown trace elements limited growth and caused initiation of carbon storage. The down-regulation of metabolic enzymes and ribosomal enzymes indicates that ammonia stress has forced the cells into non-growth state where energy and carbon is stored for later use as glycogen. This

adaptation would be useful under conditions of intermittent carbon and/or energy availability, such as the animal gut. In the case of an anaerobic digester, competition for these resources will be high, and this adaptation will likely offer a competitive advantage to this bacterium.

Economic recovery of ammonia from HNOWs for use as a fertilizer is an attractive idea from an environmental perspective in that it could reduce the need for production of ammonia through the Haber-Bosch process, a process that has a high demand for fossil fuels. In the case of ammonia recovery from sewage wastewaters, economically viable recovery is not feasible in the current system (for the US) where the resource (urine) is diluted at the source and widely dispersed before reaching the treatment center. Source separation of urine could provide an ideal concentrated waste stream for nitrogen and phosphorus recovery.

Electrochemical extraction shows promise as a method for treatment and recovery of ammonia from highly concentrated HNOWs such as source separated human urine. This technology might be well suited for a decentralized treatment scenario whereby highly pure ammonia and hydrogen gas are recovered as valuable products against the cost of treatment. Discharge of anode effluent to the sewer system would still substantially reduce the nutrient load to wastewater treatment plants and thus reduce costs at these facilities. The cost of the recovery through EC ($\sim$ 13 kWh kg^{-1} N) is higher than the cost of ammonia production via Haber-Bosch ($\sim$10 kWh kg^{-1} N), but has the alternative benefits of decreased downstream wastewater treatment costs and lower emissions along the sewer line. Furthermore,

the Haber-Bosch process is lower cost because it utilizes fossil fuel as the hydrogen source and to fuel the reaction—a resource that would become more costly if climate change regulations are put into place.

7.3 Recommendations

Clostridiales, the order in which *P. russellii* is classified, have been identified as dominant members in some full-scale anaerobic digestion studies (Nagase and Matsuo, 1982; Werner *et al.*, 2011). Indeed, in a recent community analysis study of full-scale anaerobic digesters, members of the order Clostridiales were present at high relative abundances under prevailing digester conditions of higher total ammonia nitrogen (De Vrieze *et al.*, 2015), although it was not reported which genera were mainly present. The authors hypothesized that this increased abundance could be associated with an increase in anaerobic acetate oxidation since the organisms that carry out this function are also members of the Clostridiales. One avenue of exploration based on the work reported here, would be to investigate whether ammonia-stress related glycogen storage occurs in other Clostridiales, and whether this might offer protection to these organisms against ammonia-stress in anaerobic digesters.

Co-digestion after blending with lower nitrogen feedstocks is currently the most common method for digesting high nitrogen wastes such as animal manures. Feedstock blending is becoming more and more costly due to increasing value placed on low nitrogen organic wastes. An alternative might be to utilize a two stage digestion system where ammonia can be released from high nitrogen feedstocks

and recovered in the first stage, and the fermentation/hydrolysis products be fed to a second stage reactor that is methanogenic. This would eliminate the major inhibitor to methane formation from these wastes and would have the additional benefit of recovering the ammonia. In the case where an EC system was used for ammonia separation, added value from hydrogen recovery could also be introduced. Improvements to manure handling technologies are also necessary to reduce point source pollution through the transfer of ammonia to air and water at these facilities.

Bibliography

Abouelenien, F., Fujiwara, W., Namba, Y., Kosseva, M., Nishio, N., and Nakashimada, Y. (2010) Improved methane fermentation of chicken manure via ammonia removal by biogas recycle. *Bioresour. Technol.* **101**: 6368–6373.

Andreesen, J.R. (1994) Glycine metabolism in anaerobes. *Antonie Van Leeuwenhoek* **66**: 223–237.

Angelidaki, I. and Ahring, B.K. (1993) Thermophilic anaerobic digestion of livestock waste: the effect of ammonia. *Appl. Microbiol. Biotechnol.* **38**: 560–564.

Aziz, R.K., Bartels, D., Best, A.A., DeJongh, M., Disz, T., Edwards, R.A., et al. (2008) The RAST Server: rapid annotations using subsystems technology. *BMC Genomics* **9**: 75.

Babson, D.M., Bellman, K., Prakash, S., and Fennell, D.E. (2013) Anaerobic digestion for methane generation and ammonia reforming for hydrogen production: A thermodynamic energy balance of a model system to demonstrate net energy feasibility. *Biomass Bioenergy* **56**: 493–505.

Banks, C.J., Chesshire, M., Heaven, S., and Arnold, R. (2011) Anaerobic digestion of source-segregated domestic food waste: Performance assessment by mass and energy balance. *Bioresour. Technol.* **102**: 612–620.

Barker, H.A. (1981) Amino Acid Degradation by Anaerobic Bacteria. *Annu. Rev. Biochem.* **50**: 23–40.

Bates, R.G. and Pinching, G.D. (1950) Dissociation Constant of Aqueous Ammonia at 0 to 50° from E. m. f. Studies of the Ammonium Salt of a Weak Acid. *J. Am. Chem. Soc.* **72**: 1393–1396.

Beyenbach, K.W. and Wieczorek, H. (2006) The V-type H+ ATPase: molecular structure and function, physiological roles and regulation. *J. Exp. Biol.* **209**: 577–589.

Biegel, E. and Müller, V. (2010) Bacterial Na+-translocating ferredoxin:NAD+ oxidoreductase. *Proc. Natl. Acad. Sci. U. S. A.* **107**: 18138–18142.

Biegel, E., Schmidt, S., González, J.M., and Müller, V. (2010) Biochemistry, evolution and physiological function of the Rnf complex, a novel ion-motive electron transport complex in prokaryotes. *Cell. Mol. Life Sci.* **68**: 613–634.

Braun, E., United Nations Environment Programme., Division of Technology, I. and Economics., Woods Hole Research Center. (2007) Reactive nitrogen in the environment: too much or too little of a good thing. UNEP DTIE, Sustainable Consumption and Production Branch ; Woods Hole Research Center, Paris and Falmouth, MA.

Britto, D.T. and Kronzucker, H.J. (2002) NH4+ toxicity in higher plants: a critical review. *J. Plant Physiol.* **159**: 567–584.

Britto, D.T., Siddiqi, M.Y., Glass, A.D.M., and Kronzucker, H.J. (2001) Futile transmembrane NH4+ cycling: A cellular hypothesis to explain ammonium toxicity in plants. *Proc. Natl. Acad. Sci.* **98**: 4255–4258.

Buckel, W. (1980) The Reversible Dehydration of (R)-2-Hydroxyglutarate to (E)-Glutaconate. *Eur. J. Biochem.* **106**: 439–447.

Buckel, W. (2001) Unusual enzymes involved in five pathways of glutamate fermentation. *Appl. Microbiol. Biotechnol.* **57**: 263–273.

Calli, B., Mertoglu, B., Inanc, B., and Yenigun, O. (2005) Effects of high free ammonia concentrations on the performances of anaerobic bioreactors. *Process Biochem.* **40**: 1285–1292.

Carpenter, S.R., Caraco, N.F., Correll, D.L., Howarth, R.W., Sharpley, A.N., and Smith, V.H. (1998) Nonpoint pollution of surface waters with phosphorus and nitrogen. *Ecol. Appl.* **8**: 559–568.

Chen, Y., Cheng, J.J., and Creamer, K.S. (2008) Inhibition of anaerobic digestion process: A review. *Bioresour. Technol.* **99**: 4044–4064.

Clauwaert, P., Tolêdo, R., van der Ha, D., Crab, R., Verstraete, W., Hu, H., et al. (2008) Combining biocatalyzed electrolysis with anaerobic digestion. *Water Sci. Technol.* **57**: 575.

Clesceri, L.S., Greenberg, A.E., and Eaton, A.D. eds. (1998) Inorganic Nonmetallic Constituents, Part 4500-N. In, *Standard Methods for the Examination of Water and Wastewater*. American Public Health Association, American Water Works Association, Water Environment Federation, Baltimore, Maryland.

Csonka, L.N. (1989) Physiological and genetic responses of bacteria to osmotic stress. *Microbiol. Rev.* **53**: 121–147.

Demirel, B., Yenigun, O., and Onay, T.T. (2005) Anaerobic treatment of dairy wastewaters: a review. *Process Biochem.* **40**: 2583–2595.

De Baere, L.A., Devocht, M., Van Assche, P., and Verstraete, W. (1984) Influence of high NaCl and NH4Cl salt levels on methanogenic associations. *Water Res.* **18**: 543–548.

De Macario, E. and Macario, A. (2003) Molecular biology of stress genes in methanogens: potential for bioreactor technology. *Adv. Biochem. Eng. Biotechnol.* **81:** 95–150.

De Vrieze, J., Saunders, A.M., He, Y., Fang, J., Nielsen, P.H., Verstraete, W., and Boon, N. (2015) Ammonia and temperature determine potential clustering in the anaerobic digestion microbiome. *Water Res.* **75:** 312-323.

Desloover, J., Abate Woldeyohannis, A., Verstraete, W., Boon, N., and Rabaey, K. (2012) Electrochemical Resource Recovery from Digestate to Prevent Ammonia Toxicity during Anaerobic Digestion. *Environ. Sci. Technol.* **46**: 12209–12216.

Desloover, J., De Vrieze, J., Van de Vijver, M., Mortelmans, J., Rozendal, R., and Rabaey, K. (2015) Electrochemical Nutrient Recovery Enables Ammonia Toxicity Control and Biogas Desulfurization in Anaerobic Digestion. *Environ. Sci. Technol.* **49**: 948–955.

Dickert, S., Pierik, A.J., and Buckel, W. (2002) Molecular characterization of phenyllactate dehydratase and its initiator from Clostridium sporogenes. *Mol. Microbiol.* **44**: 49–60.

Doyle, J.D. and Parsons, S.A. (2002) Struvite formation, control and recovery. *Water Res.* **36**: 3925–3940.

Drennan, M.F. and DiStefano, T.D. (2014) High solids co-digestion of food and landscape waste and the potential for ammonia toxicity. *Waste Manag.* **34**: 1289–1298.

Erisman, J.W., Galloway, J.N., Seitzinger, S., Bleeker, A., Dise, N.B., Petrescu, A.M.R., et al. (2013) Consequences of human modification of the global nitrogen cycle. *Philos. Trans. R. Soc. Lond. B Biol. Sci.* **368**: 20130116.

Ezaki, T. and Suzuki, S. (1982) Achromopeptidase for lysis of anaerobic gram-positive cocci. *J. Clin. Microbiol.* **16**: 844–846.

Ferraz, F.M., Povinelli, J., and Vieira, E.M. (2013) Ammonia removal from landfill leachate by air stripping and absorption. *Environ. Technol.* **34**: 2317–2326.

Fonknechten, N., Chaussonnerie, S., Tricot, S., Lajus, A., Andreesen, J.R., Perchat, N., et al. (2010) Clostridium sticklandii, a specialist in amino acid degradation:revisiting its metabolism through its genome sequence. *BMC Genomics* **11**: 555.

Galloway, J., Dentener, F., Burke, M., Dumont, E., Bouwman, A.F., Kohn, R.A., Mooney, H.A., Seitzinger, S., Kroeze, C. (2010) The impact of animal production systems on the nitrogen cycle. In *Livestock in a changing landscape: drivers, consequences and responses*. Island Press, pp. 83–95.

Galloway, J.N., Townsend, A.R., Erisman, J.W., Bekunda, M., Cai, Z., Freney, J.R., et al. (2008) Transformation of the Nitrogen Cycle: Recent Trends, Questions, and Potential Solutions. *Science* **320**: 889–892.

García-Gen, S., Rodríguez, J., and Lema, J.M. (2014) Optimisation of substrate blends in anaerobic co-digestion using adaptive linear programming. *Bioresour. Technol.* **173**: 159–167.

Gildemyn, S., Luther, A.K., Andersen, S.J., Desloover, J., and Rabaey, K. (2015) Electrochemically and Bioelectrochemically Induced Ammonium Recovery. *J. Visualized. Experiments.* **95:** e52405, doi:10.3791/52405.

Graef, S.P. and Andrews, J.F. (1974) Stability and Control of Anaerobic Digestion. *J. Water Pollut. Control Fed.* **46**: 666–683.

Gray, D.M., Suto, P., and Peck, C. (2008) Anaerobic Digestion of Food Waste. *US EPA No. EPA-R9-WST-06*.

Gruber, N. and Galloway, J.N. (2008) An Earth-system perspective of the global nitrogen cycle. *Nature* **451**: 293–296.

Hafner, S.D. and Bisogni Jr., J.J. (2009) Modeling of ammonia speciation in anaerobic digesters. *Water Res.* **43**: 4105–4114.

Hansen, K.H., Angelidaki, I., and Ahring, B.K. (1998) Anaerobic digestion of swine manure: inhibition by ammonia. *Water Res.* **32**: 5–12.

Hofman-Bang, J., Lange, M., Conway de Macario, E., Macario, A.J.L., and Ahring, B.K. (1999) The genes coding for the hsp 70(dnaK) molecular chaperone machine occur in the moderate thermophilic archaeon Methanosarcina thermophila TM-1. *Gene* **238**: 387–395.

Hofmeister, A.E.M. and Buckel, W. (1992) (R)-Lactyl-CoA dehydratase from Clostridium propionicum. *Eur. J. Biochem.* **206**: 547–552.

Iannotti, E.L., Fischer, J.R., and Sievers, D.M. (1982) Characterization of Bacteria from a Swine Manure Digester. *Appl. Environ. Microbiol.* **43**: 136–143.

Jackins, H.C. and Barker, H.A. (1951) Fermentative Processes of the Fusiform Bacteria. *J. Bacteriol.* **61**: 101–114.

Jetten, M.S.M., Stams, A.J.M., and Zehnder, A.J.B. (1992) Methanogenesis from acetate: a comparison of the acetate metabolism in Methanothrix soehngenii and Methanosarcina spp. *FEMS Microbiol. Rev.* **8**: 181–197.

Kayhanian, M. (1999) Ammonia Inhibition in High-Solids Biogasification: An Overview and Practical Solutions. *Environ. Technol.* **20**: 355–365.

Kerkhof, L. and Ward, B.B. (1993) Comparison of Nucleic Acid Hybridization and Fluorometry for Measurement of the Relationship between RNA/DNA Ratio and Growth Rate in a Marine Bacterium. *Appl. Environ. Microbiol.* **59**: 1303–1309.

Kim, J., Darley, D., and Buckel, W. (2005) 2-Hydroxyisocaproyl-CoA dehydratase and its activator from Clostridium difficile. *FEBS J.* **272**: 550–561.

Kim, J., Hetzel, M., Boiangiu, C.D., and Buckel, W. (2004) Dehydration of (R)-2-hydroxyacyl-CoA to enoyl-CoA in the fermentation of α-amino acids by anaerobic bacteria. *FEMS Microbiol. Rev.* **28**: 455–468.

Kleiner, D. (1981) The transport of NH3 and NH4+ across biological membranes. *Biochim. Biophys. Acta* **639**: 41–52.

Koster, I.W. (1986) Characteristics of the pH-influenced adaptation of methanogenic sludge to ammonium toxicity. *J. Chem. Technol. Biotechnol.* **36**: 445–455.

Kugelman, I.J. and McCarty, P.L. (1965) Cation Toxicity and Stimulation in Anaerobic Waste Treatment. *J. Water Pollut. Control Fed.* **37**: 97–116.

Kuntke, P., Geleji, M., Bruning, H., Zeeman, G., Hamelers, H.V.M., and Buisman, C.J.N. (2011) Effects of ammonium concentration and charge exchange on

ammonium recovery from high strength wastewater using a microbial fuel cell. *Bioresour. Technol.* **102**: 4376–4382.

Kuntke, P., Sleutels, T.H.J.A., Saakes, M., and Buisman, C.J.N. (2014) Hydrogen production and ammonium recovery from urine by a Microbial Electrolysis Cell. *Int. J. Hydrog. Energy* **39**: 4771–4778.

Kuntke, P., Smiech, K.M., Bruning, H., Zeeman, G., Saakes, M., Sleutels, T.H.J.A., et al. (2012) Ammonium recovery and energy production from urine by a microbial fuel cell. *Water Res.* **46**: 2627–2636.

Kuntke, P., Śmiech, K.M., Bruning, H., Zeeman, G., Saakes, M., Sleutels, T.H.J.A., et al. (2012) Ammonium recovery and energy production from urine by a microbial fuel cell. *Water Res.* **46**: 2627–2636.

Kuntke, P., WUR Wageningen UR, Buisman, prof. dr. ir. C.J.N., Zeeman, Dr ir G., and Bruning, Dr ir H. (2013) Nutrient and energy recovery from urine.

Larsen, T.A. and Gujer, W. (1996) Separate management of anthropogenic nutrient solutions (human urine). *Water Sci. Technol.* **34**: 87–94.

Leejeerajumnean, A., Ames, J. m., and Owens, J. d. (2000) Effect of ammonia on the growth of Bacillus species and some other bacteria. *Lett. Appl. Microbiol.* **30**: 385–389.

Li, H., Dai, X., and Zhao, X. (2008) A nearest neighbor approach for automated transporter prediction and categorization from protein sequences. *Bioinformatics* **24**: 1129–1136.

Liu, W.-T., Mino, T., Nakamura, K., and Matsuo, T. (1996) Glycogen accumulating population and its anaerobic substrate uptake in anaerobic-aerobic activated sludge without biological phosphorus removal. *Water Res.* **30**: 75–82.

Locke, E. and Laquidara (2006) Three examples of wet weather mitigation evaluations. Presentation at the Water Environment Research Foundation workshop 05-CTS-1W, Nutrient removal: how low can we go and what is stopping us from going lower? Washington, DC.

Logan, B.E. and Rabaey, K. (2012) Conversion of Wastes into Bioelectricity and Chemicals by Using Microbial Electrochemical Technologies. *Science* **337**: 686–690.

Lou, J., Dawson, K.A., and Strobel, H.J. (1997) Glycogen Formation by the Ruminal Bacterium Prevotella ruminicola. *Appl. Environ. Microbiol.* **63**: 1483–1488.

Marshall, W.L. and Franck, E.U. (1981) Ion product of water substance, 0–1000 °C, 1–10,000 bars New International Formulation and its background. *J. Phys. Chem. Ref. Data* **10**: 295–304.

Martinelle, K. and Häggström, L. (1993) Mechanisms of ammonia and ammonium ion toxicity in animal cells: Transport across cell membranes. *J. Biotechnol.* **30**: 339–350.

Martinelle, K., Westlund, A., and Häggström, L. (1996) Ammonium ion transport—a cause of cell death. *Cytotechnology* **22**: 251–254.

Matassa, S., Batstone, D.J., Huelsen, T., Schnoor, J.L., and Verstraete, W. (2015) Can direct conversion of used nitrogen to new feed and protein help feed the world? *Environ. Sci. Technol.* **9:** 5247-5254.

Maurer, M., Pronk, W., and Larsen, T.A. (2006) Treatment processes for source-separated urine. *Water Res.* **40**: 3151–3166.

Maurer, M., Schwegler, P., and Larsen, T. (2003) Nutrients in urine: energetic aspects of removal and recovery. *Nutr. Remov. Recovery* **48**: 37–46.

McCarty, P.L. and McKinney, R.E. (1961) Salt toxicity in anaerobic digestion. *J. Water Pollut. Control Fed.* **33**: 399–415.

McLennan, A.G. (2005) The Nudix hydrolase superfamily. *Cell. Mol. Life Sci. CMLS* **63**: 123–143.

Mead, G.C. (1971) The Amino Acid-fermenting Clostridia. *J. Gen. Microbiol.* **67**: 47–56.

Mobley, H.L. and Hausinger, R.P. (1989) Microbial ureases: significance, regulation, and molecular characterization. *Microbiol. Rev.* **53**: 85–108.

Mook, W.T., Chakrabarti, M.H., Aroua, M.K., Khan, G.M.A., Ali, B.S., Islam, M.S., and Abu Hassan, M.A. (2012) Removal of total ammonia nitrogen (TAN), nitrate and total organic carbon (TOC) from aquaculture wastewater using electrochemical technology: A review. *Desalination* **285**: 1–13.

Mueller, D.K. and Gronberg, J.A.M. (2002) County-Level Estimates of Nitrogen and Phosphorus from Animal Manure for the Conterminous United States, Open-File Report 2013-1065, U.S. Geological Survey.

Müller, T., Walter, B., Wirtz, A., and Burkovski, A. (2006) Ammonium Toxicity in Bacteria. *Curr. Microbiol.* **52**: 400–406.

Murto, M., Björnsson, L., and Mattiasson, B. (2004) Impact of food industrial waste on anaerobic co-digestion of sewage sludge and pig manure. *J. Environ. Manage.* **70**: 101–107.

Nagase, M. and Matsuo, T. (1982) Interactions between amino-acid-degrading bacteria and methanogenic bacteria in anaerobic digestion. *Biotechnol. Bioeng.* **24**: 2227–2239.

Nahm, K. h. (2003) Evaluation of the nitrogen content in poultry manure. *Worlds Poult. Sci. J.* **59**: 77–88.

Nakashimada, Y., Ohshima, Y., Minami, H., Yabu, H., Namba, Y., and Nishio, N. (2008) Ammonia–methane two-stage anaerobic digestion of dehydrated waste-activated sludge. *Appl. Microbiol. Biotechnol.* **79**: 1061–1069.

Nisman, B. (1954) The Stickland reaction. *Bacteriol. Rev.* **18**(1): 16-42.

Natural Resource, Agriculture, and Engineering (NRAES) (1992) On-Farm Composting Handbook. In, *On-Farm Composting Handbook*, Appendix A: Characteristics of raw materials. Cornell University, Ithica, NY.

Oh, S.T. and Martin, A.D. (2014) Loss of thermodynamic spontaneity in methanogenic consortium with ammonia contents. *Chem. Eng. J.* **243**: 244–253.

Overbeek, R., Begley, T., Butler, R.M., Choudhuri, J.V., Chuang, H.-Y., Cohoon, M., et al. (2005) The subsystems approach to genome annotation and its use in the project to annotate 1000 genomes. *Nucleic Acids Res.* **33**: 5691–5702.

Parameswaran, P. and Rittmann, B.E. (2012) Feasibility of anaerobic co-digestion of pig waste and paper sludge. *Bioresour. Technol.* **124**: 163–168.

Pham, T.H., Rabaey, K., Aelterman, P., Clauwaert, P., De Schamphelaire, L., Boon, N., and Verstraete, W. (2006) Microbial Fuel Cells in Relation to Conventional Anaerobic Digestion Technology. *Eng. Life Sci.* **6**: 285–292.

Pohland, F.G. and Harper, S.R. (1985) Critical review and summary of leachate and gas production from landfills. Project Summary Report: EPA/600/S2-86/073, United States Environmental Protection Agency.

Preiss, J. (1984) Bacterial glycogen synthesis and its regulation. *Annu. Rev. Microbiol.* **38**: 419–458.

Rajagopal, R., Massé, D.I., and Singh, G. (2013) A critical review on inhibition of anaerobic digestion process by excess ammonia. *Bioresour. Technol.* **143**: 632–641.

Ramsay, I.R. and Pullammanappallil, P.C. (2001) Protein degradation during anaerobic wastewater treatment: derivation of stoichiometry. *Biodegradation* **12**: 247–256.

Reinhart, D.R. and Townsend, T.G. (1998) Landfill Bioreactor Design & Operation, Lewis Publishers, Boca Raton, FL.

Richardson, A.J., McKain, N., and Wallace, R.J. (2013) Ammonia production by human faecal bacteria, and the enumeration, isolation and characterization of bacteria capable of growth on peptides and amino acids. *BMC Microbiol.* **13**: 1-9.

Russell, J.B., Strobel, H.J., and Chen, G.J. (1988) Enrichment and Isolation of a Ruminal Bacterium with a Very High Specific Activity of Ammonia Production. *Appl. Environ. Microbiol.* **54**: 872–877.

Santiago-Sotelo, P. and Ramirez-Prado, J.H. (2012) prfectBLAST: a platform-independent portable front end for the command terminal BLAST+ stand-alone suite. *BioTechniques* **53**: 299–300.

Savijoki, K., Ingmer, H., and Varmanen, P. (2006) Proteolytic systems of lactic acid bacteria. *Appl. Microbiol. Biotechnol.* **71**: 394–406.

Schlösser, A., Meldorf, M., Stumpe, S., Bakker, E.P., and Epstein, W. (1995) TrkH and its homolog, TrkG, determine the specificity and kinetics of cation transport by the Trk system of Escherichia coli. *J. Bacteriol.* **177**: 1908–1910.

Schmidt, I., Sliekers, O., Schmid, M., Bock, E., Fuerst, J., Kuenen, J.G., et al. (2003) New concepts of microbial treatment processes for the nitrogen removal in wastewater. *FEMS Microbiol. Rev.* **27**: 481–492.

Schnürer, A., Houwen, F.P., and Svensson, B.H. (1994) Mesophilic syntrophic acetate oxidation during methane formation by a triculture at high ammonium concentration. *Arch. Microbiol.* **162**: 70–74.

Schnürer, A. and Nordberg, A. (2008) Ammonia, a selective agent for methane production by syntrophic acetate oxidation at mesophilic temperature. *Water Sci. Technol.* **57**: 735-740.

Selmer, T., Willanzheimer, A., and Hetzel, M. (2002) Propionate CoA-transferase from Clostridium propionicum. *Eur. J. Biochem.* **269**: 372–380.

Shibata, H., Branquinho, C., McDowell, W.H., Mitchell, M.J., Monteith, D.T., Tang, J., et al. (2014) Consequence of altered nitrogen cycles in the coupled human and ecological system under changing climate: The need for long-term and site-based research. *Ambio*. **44:** 178-193.

Siebert, M. and Toerien, D. (1969) The proteolytic bacteria present in the anaerobic digestion of raw sewage sludge. *Water Res.* **3**: 241–250.

Siegrist, H. (1996) Nitrogen removal from digester supernatant - comparison of chemical and biological methods. *Water Sci. Technol.* **34**: 399–406.

Sleator, R.D. and Hill, C. (2002) Bacterial osmoadaptation: the role of osmolytes in bacterial stress and virulence. *FEMS Microbiol. Rev.* **26**: 49–71.

Smith, E.A. and Macfarlane, G.T. (1997) Dissimilatory Amino Acid Metabolism in Human Colonic Bacteria. *Anaerobe* **3**: 327–337.

Sprott, G.D. and Patel, G.B. (1986) Ammonia toxicity in pure cultures of methanogenic bacteria. *Syst. Appl. Microbiol.* **7**: 358–363.

Sprott, G.D., Shaw, K.M., and Jarrell, K.F. (1984) Ammonia/potassium exchange in methanogenic bacteria. *J. Biol. Chem.* **259**: 12602–12608.

Sprott, G.D., Shaw, K.M., and Jarrell, K.F. (1985) Methanogenesis and the K+ transport system are activated by divalent cations in ammonia-treated cells of Methanospirillum hungatei. *J. Biol. Chem.* **260**: 9244–9250.

Stams, A.J.M. (1994) Metabolic interactions between anaerobic bacteria in methanogenic environments. *Antonie Van Leeuwenhoek* **66**: 271–294.

Stead, M.B., Agrawal, A., Bowden, K.E., Nasir, R., Mohanty, B.K., Meagher, R.B., and Kushner, S.R. (2012) RNAsnap™: a rapid, quantitative and inexpensive, method for isolating total RNA from bacteria. *Nucleic Acids Res.* **40**: e156.

Stickland, L.H. (1934) Studies in the metabolism of the strict anaerobes (genus Clostridium). *Biochem. J.* **28**: 1746–1759.

Stickland, L.H. (1935a) Studies in the metabolism of the strict anaerobes (Genus Clostridium). *Biochem. J.* **29**: 288–290.

Stickland, L.H. (1935b) Studies in the metabolism of the strict anaerobes (genus Clostridium). *Biochem. J.* **29**: 889–898.

Stinson, B. (2006) Alternatives to Mitigate the Impacto of Recycle Streams on Nitrogen Removal. Presentation at the Water Environment Research Foundation workshop 05-CTS-1W, Nutrient removal: how low can we go and what is stopping us from going lower? Washington, DC.

Talbot, G., Roy, C.S., Topp, E., Kalmokoff, M.L., Brooks, S.P.J., Beaulieu, C., et al. (2010) Spatial distribution of some microbial trophic groups in a plug-flow-type anaerobic bioreactor treating swine manure. *Water Sci. Technol. J. Int. Assoc. Water Pollut. Res.* **61**: 1147–1155.

Tu, Y. and Schuler, A.J. (2013) Low acetate concentrations favor polyphosphate-accumulating organisms over glycogen-accumulating organisms in enhanced biological phosphorus removal from wastewater. *Environ. Sci. Technol.* **47**: 3816–3824.

Udert, K.M., Larsen, T.A., and Gujer, W. (2003) Biologically induced precipitation in urine-collecting systems. *Water Sci. Technol. Water Supply* **3**: 71–78.

Udert, K.M., Larsen, T.A., and Gujer, W. (2006) Fate of major compounds in source-separated urine. *Water Sci. Technol. J. Int. Assoc. Water Pollut. Res.* **54**: 413–420.

US EPA (2012) Municipal Solid Waste Generation, Recycling, and Disposal in the United States: Facts and Figures for 2012. http://www2.epa.gov/learn-issues/learn-about-waste.

US EPA (2003) National Management Measures to Control Nonpoint Source Pollution from Agriculture, US EPA: EPA reference document 841-B-03-004.

US EPA (2010) Nutrient control design manual state of technology review report.

Van de Guchte, M., Serror, P., Chervaux, C., Smokvina, T., Ehrlich, S.D., and Maguin, E. (2002) Stress responses in lactic acid bacteria. *Antonie Van Leeuwenhoek* **82**: 187–216.

Verstraete, W. and Philips, S. (1998) Nitrification-denitrification processes and technologies in new contexts. *Environ. Pollut.* **102**: 717–726.

Vitousek, P.M., Aber, J.D., Howarth, R.W., Likens, G.E., Matson, P.A., Schindler, D.W., et al. (1997) Human alteration of the global nitrogen cycle: sources and consequences. *Ecol. Appl.* **7**: 737–750.

Werner, J.J., Knights, D., Garcia, M.L., Scalfone, N.B., Smith, S., Yarasheski, K., et al. (2011) Bacterial community structures are unique and resilient in full-scale bioenergy systems. *Proc. Natl. Acad. Sci.* **108**: 4158–4163.

White, D. (1995) The physiology and biochemistry of prokaryotes, 3rd edn., New York, USA: Oxford University Press.

Whitehead, T.R. and Cotta, M.A. (2004) Isolation and Identification of Hyper-Ammonia Producing Bacteria from Swine Manure Storage Pits. *Curr. Microbiol.* **48**: 20–26.

Whitehead, T.R., Cotta, M.A., Falsen, E., Moore, E., and Lawson, P.A. (2011) Peptostreptococcus Russellii Sp. Nov., Isolated from a Swine-Manure Storage Pit. *Int. J. Syst. Evol. Microbiol.* **61**: 1875–1879.

Worm, P., Müller, N., Plugge, C., Stams, A., and Schink, B. (2010) Syntrophy in Methanogenic Degradation. In (Endo)symbiotic Methanogenic Archaea, Microbiology Monographs **19:** 143-173. Springer-Verlag Berlin Heidelberg.

Yabu, H., Sakai, C., Fujiwara, T., Nishio, N., and Nakashimada, Y. (2011) Thermophilic two-stage dry anaerobic digestion of model garbage with ammonia stripping. *J. Biosci. Bioeng.* **111**: 312–319.

Yenigün, O. and Demirel, B. (2013) Ammonia inhibition in anaerobic digestion: A review. *Process Biochem.* **48**: 901–911.

Zhang, L., Lee, Y.-W., and Jahng, D. (2011) Anaerobic co-digestion of food waste and piggery wastewater: Focusing on the role of trace elements. *Bioresour. Technol.* **102**: 5048–5059.

Zhang, R., El-Mashad, H.M., Hartman, K., Wang, F., Liu, G., Choate, C., and Gamble, P. (2007) Characterization of food waste as feedstock for anaerobic digestion. *Bioresour. Technol.* **98**: 929–935.

Zhang, Y., Banks, C.J., and Heaven, S. (2012) Anaerobic digestion of two biodegradable municipal waste streams. *J. Environ. Manage.* **104**: 166–174.

Zhao, G. and Winkler, M.E. (1996) A novel alpha-ketoglutarate reductase activity of the serA-encoded 3-phosphoglycerate dehydrogenase of Escherichia coli K-12 and its possible implications for human 2-hydroxyglutaric aciduria. *J. Bacteriol.* **178**: 232–239.

Zinder, S.H. (1998) Methanogens. In, *Techniques in Microbial Ecology*. New York: Oxford University Press.

Zinder, S.H. and Koch, M. (1984) Non-aceticlastic methanogenesis from acetate: acetate oxidation by a thermophilic syntrophic coculture. *Arch. Microbiol.* **138**: 263–272.

Zlatkis, A. and Liebich, H.M. (1971) Profile of volatile metabolites in human urine. *Clin. Chem.* **17**: 592–594.